

HIGHER ORDER MICROFIELD EFFECTS ON  
SPECTRAL LINE BROADENING IN DENSE  
PLASMAS

By

DAVID PARKER KILCREASE

A DISSERTATION PRESENTED  
TO THE GRADUATE SCHOOL  
OF THE UNIVERSITY OF FLORIDA IN  
PARTIAL FULFILLMENT OF THE REQUIREMENTS  
FOR THE DEGREE OF DOCTOR OF PHILOSOPHY

UNIVERSITY OF FLORIDA

1991

All we know of the truth is that the absolute truth, such as it is, is beyond our reach.

Nicholas of Cusa, 1401-1464 A.D.

## ACKNOWLEDGEMENTS

I am extremely grateful to all of the people who have helped me in my scientific career; there are too many to enumerate them all. I am also most grateful to the taxpayers for making it possible for me to participate in the great enterprise of scientific research.

## TABLE OF CONTENTS

	<i>page</i>
ACKNOWLEDGEMENTS .....	iii
ABSTRACT .....	vi
CHAPTERS	
I. INTRODUCTION .....	1
1.1 The Big Picture .....	1
1.2 Focus of This Work .....	3
1.3 Outline .....	5
II. THEORETICAL BACKGROUND TO THE LINE BROADENING PROBLEM .....	8
2.1 Dense Plasma Fundamentals .....	9
2.2 Historical Background .....	17
2.3 Theoretical Formulation .....	18
III. HIGHER ORDER FIELD EFFECTS .....	39
3.1 The Ion-Quadrupole Effect .....	39
3.2 Atomic Data by Perturbation Theory Solution .....	54
3.3 Atomic Data by Numerical Solution .....	70
3.4 Electron Delocalization and Field Ionization .....	78
IV. RESULTS AND DISCUSSION .....	89
4.1 The Lyman $\alpha$ Line .....	91
4.2 The Lyman $\beta$ Line .....	92
4.3 Conclusions .....	99

## APPENDICES

A. SOME EXPRESSIONS IN USEFUL UNITS .....	123
B. THE APEX CONDITIONAL DISTRIBUTION FUNCTION .....	125
C. PARABOLIC COORDINATES .....	130
D. IMPORTANCE OF THE ION-QUADRUPOLE EFFECT .....	132
E. FINE STRUCTURE CORRECTIONS .....	138
F. COMPUTER CODE DOCUMENTATION .....	144
REFERENCES .....	149
BIOGRAPHICAL SKETCH .....	154

Abstract of Dissertation Presented to the Graduate School  
of the University of Florida in Partial Fulfillment of the  
Requirements for the Degree of Doctor of Philosophy

HIGHER ORDER MICROFIELD EFFECTS ON  
SPECTRAL LINE BROADENING IN DENSE  
PLASMAS

By

David Parker Kilcrease

May 1991

Chairman: Charles F. Hooper, Jr.

Major Department: Physics

Radiating atoms in dense plasmas are highly affected by their local plasma environment. We examine the effect of this environment on hydrogenic radiators by using an atomic wave function basis set that is itself a function of the plasma electric microfield for the calculation of spectral line profiles. Our theoretical development includes the effect of static ion perturbers up to the quadrupole term in the multipole expansion of the radiator-perturbing ion interaction, as well as dynamic electron broadening up to second order in the radiator-perturbing electron interaction. Effects due to the presence of the uniform ion-electric field are treated exactly within this framework, and the field gradient is then treated as a perturbation by inclusion of the ion-quadrupole term. We employ a basis set for the representation of the upper state of the transition that includes states of principal quantum number  $n$  as well as  $n+1$  to allow for the field mixing of these two manifolds. The ion-quadrupole effect is treated in a new way that includes ion correlations by using a renormalized

independent-particle model for the perturbing ions. We also present a preliminary assessment of the importance of field ionization on the spectral line shapes. Our results are compared with previously reported calculations using field independent matrix elements, neglect of possible field ionization and the independent-particle model of the ion-quadrupole effect. Hence, we are able to identify the most important effects that arise from the use of the field dependent basis set. These comparisons also allow us to examine the importance of ion correlations when determining the ion-quadrupole effect.

## CHAPTER I INTRODUCTION

In this dissertation we, that is you and I, will be examining the theory of spectral line radiation from highly ionized atoms in dense plasmas. Before we go into this in detail it will be helpful and illuminating to stand back and look at the relevance of this from a wider perspective; to take a look at the big picture.

### 1.1 The Big Picture

In general, a plasma can be defined as a statistical system containing mobile charges.<sup>1</sup> We will be concerned with a subcategory of this definition and will limit ourselves to discussing electrically neutral plasmas associated with hot highly ionized atoms. This is no great limitation since over 99 percent of the known universe is covered in this category.<sup>2</sup> With the aid of sophisticated astronomical detection equipment, most of what we see of the universe is electromagnetic radiation emanating from a variety of objects ranging from ordinary stars to extremely luminescent quasistellar objects located at the edge of the known universe. The matter in all of these entities exists almost entirely in the plasma state; plasmas whose constituents range from ordinary ionized atoms to exotic matter-antimatter electron pairs. The radiation reaching the earth from these distant bodies runs the gamut from radio waves, through the visible spectrum and into the realm of X-rays and  $\gamma$ -rays. It is easy to see that an understanding of the behavior of these plasmas can and will give us great insight into the structure and workings of the universe in which we live.

Of more mundane concerns are the plasmas encountered here on earth. These are evident in such natural phenomena as lightning and fire. Man-made plasmas are also numerous in example, ranging from ordinary fluorescent lighting to terrifying large scale thermonuclear explosions that result from the fusion of hydrogen isotopes. Since the early 1950s, one of the primary goals of plasma physics has been to bring under control these tremendous quantities of energy liberated by thermonuclear fusion. When this goal is achieved, we will have succeeded in obtaining access to a nearly unlimited supply of relatively clean and safe energy that will last into the foreseeable future.<sup>3</sup>

Due to the extremes of physical conditions under which many plasmas exist and due to their often ephemeral nature, making direct measurements of the composition, density, temperature and other physical parameters that are necessary for a clear understanding of their inner workings is often impossible. What is needed is an indirect nonintrusive probe of the plasma interior. The radiation emitted or absorbed by these plasmas is the ideal answer to this problem. Isolated, partially ionized atoms can emit or absorb radiation that results from atomic electrons passing from one energy level to another. This radiation is emitted or absorbed in discrete amounts leading to distinct and identifiable sharp spectral lines. These lines have a slight width, called the natural width, due to quantum fluctuations in the atom's own electromagnetic field. As long as the atoms remain isolated, the spectral lines remain relatively sharp. When linked to their plasma environment, however, the situation changes radically. The amounts of energy emitted or absorbed by the atoms are now affected by the plasma, often revealing pertinent information about this environment. Thus we may explore the atom's surroundings indirectly through changes in the profile of its spectral lines. This technique is employed

in many areas of science to reveal information about the internal structure of matter in a noninvasive way by examining emitted or absorbed radiation. Some examples of this application are nuclear magnetic resonance (NMR) and Mössbauer spectroscopy.<sup>4</sup> In this dissertation we will be concerned with spectral lines of emitted radiation from plasmas although the formalism applies equally well to spectral lines originating from the absorption of radiation. The line shapes will reveal information about the density and temperature in the vicinity of the radiating atoms, regardless of whether they are located in a simple laboratory experiment or in a distant star.

### 1.2 Focus of This Work

The main focus of this work will be on the shapes of line spectra from dense, high temperature plasmas consisting of atoms of moderate atomic number,  $Z$ . These terms "dense" and "high" are quite relative and historically have meant the densest and hottest plasmas obtainable in laboratory experiments for a particular element at that particular point in time. As an example, in the mid 1960's these terms referred to electron number densities,  $n_e$ , of around  $10^{17} \text{ cm}^{-3}$  and temperatures corresponding to a few eV for elements such as hydrogen and helium.<sup>5</sup> Today, high density refers to  $n_e = 10^{24}$  to  $10^{25} \text{ cm}^{-3}$  and temperatures corresponding to 600 to 1000 eV for elements such as argon and krypton with  $Z = 18$  and 36 respectively.<sup>6,7,8,9,10</sup> One method of creating these dense plasma conditions in the laboratory is by laser driven inertial confinement. Current experiments using this method have created conditions of many times solid density for periods of a few hundred picoseconds.<sup>9</sup> The mechanism of compression employs high intensity laser light to symmetrically irradiate spherical targets containing the material under investigation.<sup>11</sup> When

this energy is rapidly deposited in the outer layers of the target (mostly by inverse Bremsstrahlung), these layers are quickly vaporized and blown outwards away from the target. This propels the remainder of the target material inward. This is in close analogy to the way a rocket works by combusting fuel in an engine and expelling it in one direction in order to be propelled in the other direction. If our laser irradiation is sufficiently symmetrical, the target will be reduced in size many times as it is compressed, and resulting shock waves will heat the core to a high temperature. This compression and heating can produce the plasmas of high density and temperature that we wish to examine in this dissertation.

Approximate descriptions of spectral line shapes emitted from dense, hot plasmas are usually derived from theories that use an atomic physics description of atoms that are isolated from their environment. In reality, the atomic wave functions for the radiating atoms can be strongly perturbed by surrounding charged particles, and in extreme cases it is not realistic to think of the atoms as separate entities at all but rather as clusters of ions surrounded by clouds of electrons. Radiation from atoms in this highly interacting environment will run the gamut from continuum to discrete. Therefore, in order to construct a tractable method for the calculation of spectral line shapes, we must often, somewhat arbitrarily, distinguish between the radiator and its perturbers. However, the more influence of the surrounding particles that we can include in the description of our radiating atoms at the outset of our development, the better off we will be when considering further perturbations. Our goal in this work will be to include some of the higher order effects of the plasma microfield on atomic spectral line emission. To this end, we will use for our zero-order atomic wave functions, numerical solutions to Schrödinger's

equation for an atom in a uniform electric field. These field dependent solutions are supplemented by solutions obtained from a systematic perturbation theory treatment for small field values. The zero order atomic Hamiltonian will thus contain the perturbing ion-dipole interaction and higher order corrections will describe nonuniformities in the plasma electric field. We will include the first of these higher order corrections, the ion-quadrupole term, to account for the effects of the field gradient.<sup>12,13,14,15</sup> Griem<sup>16</sup> has pointed out as early as 1954 the possible importance of this field dependence, as well as the ion quadrupole effect, as a source of spectral line asymmetry.

The plasma electric microfield can produce additional effects on the radiating atoms beyond those given by the simple field dependence of their atomic wave functions and energy levels. Atomic bound state energies which were discrete in the absence of the plasma electric field now become resonance states with finite widths. The formerly bound electrons are now free to quantum mechanically tunnel through the potential barrier created by the electric field. Although atomic electrons that lie deep in the radiator potential well are little affected by the plasma electric field, high lying electron levels are perturbed to the point where they are, for all practical purposes, no longer bound to the atom. This field ionization phenomenon could have important consequences for the relative populations of the radiator excited states.

### 1.3 Outline

Chapter 2 focuses on the development of a general plasma line broadening theory and the accompanying approximations. We discuss fundamental length and time scales for the interactions of the two main components of the plasma with the radiator: the highly charged ions and the unbound plasma

electrons. We also discuss under what conditions and where in the line profile the phenomenon of perturber motion will be important (both ion and electron). Next follows a discussion of the strength and nature of the various interactions between the plasma particles. From this consideration, we decide which interactions are important and which can be ignored.

A brief account of the historical development of the main ideas of spectral line broadening theory is presented. We find the historical roots for the ideas of Stark, Doppler and electron broadening in the late 1800's and early 1900's.

Next follows a detailed derivation of a calculable form of the line shape function. We first present a general formalism appropriate for multi-electron radiators that includes field dependent wave functions, an exact treatment of the perturbing ion radiator-dipole interaction, field dependent NLTE level populations and field dependent electron broadening. This general formalism is then restricted to the case of hydrogenic radiators with no lower state broadening. We also discuss a method for approximately including field induced resonance widths in the line shape. Chapter 2 ends with a brief note about other line broadening phenomenon that may need to be included before comparisons with experiment can be carried out.

Chapter 3 begins with the development of a theory for the approximate evaluation of the ion-quadrupole effect. We present approximations for the probability function for the field gradient term as well as an approximation for the average field gradient constrained to have a given field value. These approximations include ion-ion correlations and represent an improvement over previous theories. We then compare our calculation of this field gradient with previous calculations and simple approximations. Next, we discuss the methods

of calculation of field dependent wave functions and matrix elements by perturbation theory and by direct numerical solution of Schrödinger's equation. The numerical solution technique is also used to calculate resonance widths that give an approximate measure of the lifetimes of the field dependent resonance states produced by the presence of the plasma microfield. These lifetimes are then used to study the effect of the resulting possible level depletion on the line shape. We discuss a simple population kinetics model for this purpose.

In chapter 4, we present some theoretical spectral line shapes resulting from our work. We calculate line shapes for the  $L_\alpha$  and  $L_\beta$  lines of hydrogenic argon at  $kT = 800$  eV and for an electron density range of  $1 \times 10^{24}$  to  $1 \times 10^{25}$  cm $^{-3}$ . We then examine the importance of the various effects studied in this dissertation on the spectral line shape, width and asymmetry. We close with some conclusions and suggestions for further work.

Appendices discuss several useful topics and give some details of calculations presented in the main text. We have a discussion of physical units, some details of the model used to calculate the average field gradient required for the treatment of the ion-quadrupole effect, a discussion of parabolic coordinates and the details of the perturbation theory calculation of the field dependent fine structure corrections to the radiator Hamiltonian.

## CHAPTER II

### THEORETICAL BACKGROUND TO THE LINE BROADENING PROBLEM

We will now develop a theory<sup>17,18</sup> for the description of spectral line shapes in dense plasmas. The physical conditions we will be interested in considering will be pertinent to inertial confinement fusion plasmas. These plasmas will be at, or near solid density and at relatively hot temperatures (i.e. hot enough that the plasma is not quantum mechanically degenerate). We will also be interested in systems where the plasma ions have much greater mass than the electrons. This difference will allow us to consider different domains: one defined by the fast moving or dynamic electrons and one appropriate for the description of slow moving or quasi-static ions. This will allow us to proceed with the development of a simplified formalism.

The physical systems and conditions that we will examine in this dissertation are restricted to argon radiators immersed in a pure argon plasma at a temperature corresponding to 800 eV and an electron number density ranging from  $10^{24} \text{ cm}^{-3}$  to  $10^{25} \text{ cm}^{-3}$ . These densities are high enough to bring out the higher order field effects but not high enough for the plasma to be in the degenerate electron regime. In local thermodynamic equilibrium (LTE), the line shape is not very sensitive to small variations in temperature. Consequently, we will not examine the temperature dependence of the line shape. These physical conditions are also relevant to current experiments<sup>9</sup> that employ argon radiators.

## 2.1 Dense Plasma Fundamentals

In dense plasmas there are several fundamental length and time scales that are important for understanding the interactions among the plasma particles. Since our plasmas are dynamic systems, the particles are in constant motion and travel, on the average, a characteristic distance in a given relevant time interval. This fact allows us to establish some relations between length and time scales. The use of these scales will allow us to classify the various plasma particles into categories that are governed by interactions of differing strengths. This will be important when deciding what approximations are suitable and consistent in our description of the plasma. Without approximations we would be hopelessly lost in a morass of  $\sim 10^{23}$  coupled equations of motion. A fate, preferably, to be avoided.

We will now discuss some relevant length scales<sup>1,19,2</sup> (see Appendix A). The ion-sphere radius  $r_o$  is an estimate of the average distance between two ions of species  $j$ . It is given by

$$r_{o,j} = \left( \frac{3}{4\pi n_j} \right)^{1/3}, \quad (2.1)$$

where  $n_j$  is the number density of species  $j$ .

Another important quantity is the Debye length  $\lambda_D$ . It is an indication of the distance from an ion beyond which screening of its charge becomes significant. It is given by

$$\lambda_{D,j} = \left( \frac{kT}{4\pi Z^2 e^2 n_j} \right)^{1/2}, \quad (2.2)$$

where  $k$  is Boltzmann's constant,  $T$  is the temperature and  $Ze$  is the charge of species  $j$  that forms the screening cloud. For more than one component, the

resultant screening length is  $\lambda_D^{-2} = \sum_j \lambda_{D,j}^{-2}$  where the sum is over the different species.

The thermal de Broglie wavelength  $\Lambda$  gives an estimate of the quantum mechanical wave nature of the plasma particles. It is given by

$$\Lambda = \left( \frac{2\pi\hbar^2}{mkT} \right)^{1/2}, \quad (2.3)$$

where  $m$  is the particle mass. Except for the factor of  $2\pi$  this is just the quantum mechanical wave length of plasma particles possessing average kinetic energy  $kT$ . It gives us an estimate of the spatial extent of the particle wave packet.

The radial dimension of an atomic ion can be estimated by considering the radius of the Bohr orbit for the most probable quantum state, and writing the radius as,

$$r_n = a_o n^2 / Z; \quad (2.4)$$

$n$  is the principal quantum number for the atomic ion,  $a_o$  is the radius of the first Bohr orbit for hydrogen and  $Z$  is the nuclear charge.

In order to relate time scales to characteristic lengths we need an estimate of the velocity for particles of species  $j$ . Using the magnitude of the most probable velocity for classical motion, we have

$$v_{mp,j} = \left( 2kT/m_j \right)^{1/2}. \quad (2.5)$$

We have now defined the basic quantities which will allow us to make estimates of several important time scales of interest. Additionally, the length

scales will be used in determining appropriate scale factors for perturbation expansions.

We will now look at the time scales relevant to motion of the plasma particles, specifically the perturbing electrons and ions. It will be shown in section 2.3 that the line shape function  $I(\Delta\omega)$  can be represented by the transform of a dipole autocorrelation function  $C(t)$  such that

$$I(\Delta\omega) = \int \exp(i\Delta\omega t)C(t)dt, \quad (2.6)$$

where  $\Delta\omega$  is the separation from line center and  $C(t)$  is a decreasing function of  $t$ . When  $t > 1/\Delta\omega$ , the exponential begins to oscillate rapidly causing the contribution to the integral from the integrand in that region to be small. So, for a given value of  $\Delta\omega$ , the integral is determined, for the most part, by  $C(t)$  such that  $0 \leq t \leq 1/\Delta\omega$ . Hence, we can define the time interval of interest for the line shape at the distance from line center  $\Delta\omega$  as  $\tau = 1/\Delta\omega$ . If the duration of a perturber's collision with the radiator is significantly greater than the time of interest  $\tau$  corresponding to the part of the spectral line  $\Delta\omega$ , we may regard the perturber as being stationary during the time of interest and treat its perturbation as static. This is known as the quasi-static approximation. If the duration of collision does not meet this criterion, we must regard its perturbation as dynamic and explicitly take its time dependence into account.

For a particular separation from line center  $\Delta\omega$ , the effect of perturbing ion motion will be negligibly small if<sup>17</sup>

$$\left| \frac{\dot{F}(t)}{F(t)} \right| \ll |\Delta\omega_{i,f}(F)|, \quad (2.7)$$

where  $F(t)$  is the perturbing ion electric field strength at the radiator,  $\dot{F}(t)$  is its time derivative and  $\Delta\omega_{i,f}(F)$  represents the separation from line center,  $\Delta\omega$ ,

due to the static linear Stark effect. Note that  $\Delta\omega_{i,f}(F) = \omega_{i,f}(F) - \omega_{i,f}(0)$ , where  $i$  and  $f$  refer to the initial and final state of the transition, respectively, and  $\omega_{i,f}$  is the transition energy  $\omega_{i,f} = \omega_i - \omega_f$ . The linear Stark shifted energy for level  $i$  is  $\omega_i(0) + \frac{3}{2}n_i q_i \hbar F / m_e$ . We use the parabolic representation (see Appendix C) and take  $F = Z_i e / r^2$  where  $r$  is the distance from the radiator to the perturbing ion, and obtain on substitution into Eq. (2.7)

$$\Delta\omega = \frac{3\hbar Z_i(n_i q_i - n_f q_f)}{2Z m_e r^2} \gg \frac{v}{r}, \quad (2.8)$$

where  $n_{i,f}$  and  $q_{i,f}$  are the parabolic quantum numbers for the initial and final states and  $v$  is the perturbing ion velocity. Eliminating  $r$  from both sides of the inequality gives

$$\Delta\omega \gg \frac{2m_e v^2 Z}{3\hbar Z_i(n_i q_i - n_f q_f)}. \quad (2.9)$$

We can use the most probable velocity as an estimate for  $v$  to obtain

$$\Delta\omega \gg \frac{4m_e k T Z}{\mu \hbar Z_i(n_i q_i - n_f q_f)} \equiv \Delta\omega_i, \quad (2.10)$$

where we have used the perturbing ion-radiator reduced mass  $\mu$  in the expression for  $v$  because we are only interested in the relative motion. Here, we have defined  $\Delta\omega_i$  as the characteristic shift from line center due to ion motion. The criterion for the quasistatic ion approximation to be valid is thus:  $\Delta\omega \gg \Delta\omega_i$ . For the Lyman  $\alpha$  line in pure argon plasma with  $kT = 800$  eV,  $q_i = 1$  and  $q_f = 0$  we have  $\hbar\Delta\omega_i = 0.044$  eV. For higher series members  $\hbar\Delta\omega_i$  will be less. We conclude that estimated shifts due to ion dynamics will be much smaller than the estimated shifts due to the static-ion Stark effect. The latter are on the order of tens to hundreds of electron volts for the physical conditions we

are interested in in this work. Consequently, we can confidently use the quasistatic approximation for the perturbing ions. For low mass perturbing ions the situation is quite different. In the case of proton perturbers  $\hbar\Delta\omega_i = 16$  eV and ion motion will become a significant component of the line width.

The story for the perturbing electrons is, however, another matter. Due to their much lighter mass, the electrons will be traveling much faster when they have the same kinetic energy; their dynamic influence on the radiator will need to be considered. If we treat the plasma ions as static, the plasma electrons will form shielding charge clouds around them, screening the ionic charge at a distance of roughly the Debye length.<sup>20</sup> This is given by  $\lambda_{D,e} = (kT/4\pi e^2 n_e)^{1/2}$ . If we regard the time of interest for the interaction of a perturbing electron with the screened radiator as roughly the time it takes to cross the Debye sphere radius  $\lambda_{D,e}$ , we have

$$\tau_e^{-1} = \frac{v_e}{\lambda_{D,e}} \approx \frac{v_{mp,e}}{\lambda_{D,e}} , \quad (2.11)$$

where we have estimated  $v_e$  by its most probable value. This gives us

$$\tau_e^{-1} = \sqrt{2} \omega_{p,e} , \quad (2.12)$$

where  $\omega_{p,e}$  is the electron plasma frequency given by

$$\omega_{p,e} = \left( \frac{4\pi n_e e^2}{m_e} \right)^{1/2} . \quad (2.13)$$

The portion of the line profile that corresponds to electron dynamics is then given by

$$\Delta\omega < \omega_{p,e} , \quad (2.14)$$

with a quasistatic electron approximation being applicable for  $\Delta\omega \gg \omega_{p,e}$ . For our physical conditions  $\omega_{p,e}$  is in the neighborhood of 10–150 eV. Examination of the statics and dynamics of the perturbing ions and electrons allows us to conclude that the quasistatic approximation for ions is good throughout the line profile except at the very center for  $\Delta\omega$  less than 1 eV while electrons behave dynamically inside  $\omega_{p,e}$ . This will allow us to separate the problem of plasma perturbations of the radiator into two regimes coupled only by the static plasma microfield: that of purely static screened ions and purely dynamic electrons. This will greatly simplify the line shape theory that we wish to formulate.

For our plasma particles to behave non-degenerately we require that the interparticle spacing be much greater than the quantum mechanical wavelength of the moving particles. For the plasma electrons this condition is

$$\Lambda_e \ll r_{o,e} . \quad (2.15)$$

This requirement, except for a slight difference in the numerical constant, is the same as  $E_F/kT \ll 1$ , where the electron Fermi energy,  $E_F$ , is given by

$$E_F = \frac{\hbar^2}{2m_e} (3\pi^2 n_e)^{2/3} . \quad (2.16)$$

For our plasma at  $kT_e = 800$  eV and  $n_e = 1 \times 10^{25} \text{ cm}^{-3}$  the above ratio is 0.21. However, for a density of  $n_e = 1 \times 10^{26} \text{ cm}^{-3}$  the ratio becomes 0.98 and it is no longer a reasonable approximation to treat the plasma electrons non-degenerately. We will take an electron density upper bound of  $n_e = 1 \times 10^{25} \text{ cm}^{-3}$  to avoid the problem of electron degeneracy in this work. The much heavier plasma ions, on the other hand, will behave classically under any conditions we will be considering here.

To judge the importance of correlations between particles in our system we can look at the Coulomb coupling constant  $\Gamma$ . This is the ratio of a particle's potential energy of interaction with a neighboring particle to its kinetic energy. If  $\Gamma > 1$  then interactions with other particles will dominate ideal gas behavior. If  $\Gamma < 1$  then the kinetic energy will be most important in describing the particle behavior.

First we look at the coupling between electrons. For the potential energy we use the potential produced by an electron at the average interparticle spacing  $r_{o,e}$ . For the kinetic energy we use  $kT$  to give

$$\Gamma_{e,e} = \frac{e^2}{r_{o,e} kT} . \quad (2.17)$$

For our highest density,  $n_e = 1 \times 10^{25} \text{ cm}^{-3}$ , this gives  $\Gamma_{e,e} = 0.063$ . We conclude that the plasma electrons are weakly coupled to each other and can be treated, in a first approximation, as an ideal Boltzmann electron gas. Correlations between electrons will be treated in an approximate way.<sup>21</sup>

For the ions we use  $r_{o,i}$  and obtain

$$\Gamma_{i,i} = \frac{e^2}{r_{o,i} kT} , \quad (2.18)$$

but since  $r_{o,i} = Z^{1/3} r_{o,e}$  we have  $\Gamma_{i,i} = Z^{5/3} \Gamma_{e,e}$ . For our fully stripped argon plasma,  $Z=18$  and for our highest density we have  $\Gamma_{i,i} = 7.8$ . Clearly, then, we must not ignore ion-ion correlations. In particular the calculation of the ion microfield will require a careful treatment of these correlations.

For ion-electron correlations we take as the interparticle spacing  $r_o = (r_{o,e} + r_{o,i})/2$  to give

$$\Gamma_{e,i} = \frac{Ze^2}{r_o kT} . \quad (2.19)$$

Noting that  $r_o = (Z^{1/3} + 1)r_{o,e}/2$ , we can write

$$\Gamma_{e,i} = \frac{2Z}{(Z^{1/3} + 1)} \Gamma_{e,e} . \quad (2.20)$$

For  $n_e = 1 \times 10^{25} \text{ cm}^{-3}$  this gives  $\Gamma_{e,i} = 0.62$ . So ion-electron coupling is of order one and, although not as strong as ion-ion correlations, will need to be taken into account. This will be accomplished by a mean field approximation using screened ion potentials.

In order to examine the effect of ion radiator interactions it will be useful to make a multipole expansion of the radiator-perturbing ion interaction potential. To do this we define an expansion parameter  $\delta$ , where

$$\delta = \frac{r_a}{r_{o,i}} . \quad (2.21)$$

Here,  $r_a = \langle \psi_n | r | \psi_n \rangle \sim a_o n^2 / Z$  is the most probable orbital radius for a radiator in the state with principal quantum number  $n$  and nuclear charge  $Z$ . So

$$\delta = \left( \frac{4\pi}{3} \right)^{1/3} \frac{a_o n^2 n_e^{1/3}}{Z^{4/3}} . \quad (2.22)$$

This is  $\delta = 8.531 \times 10^{-9} n^2 n_e^{1/3} / Z^{4/3}$  with  $n_e$  given in  $\text{cm}^{-3}$ . At  $n_e = 1 \times 10^{25} \text{ cm}^{-3}$  for  $n = 2$  we have  $\delta = 0.16$  and for  $n = 3$  we have  $\delta = 0.35$ . The dipole term of the multipole expansion is second order in  $\delta$  and the quadrupole term is third order in  $\delta$ . For  $n = 3$  this gives  $\delta^2 = 0.12$  and  $\delta^3 = 0.043$ . So our expansion is quite legitimate.

## 2.2 Historical Background

We will now take a brief look at the historical development of spectral line shape theory with the goal of identifying the origin of the main ideas of line broadening.<sup>22</sup>

In 1889, Lord Rayleigh<sup>23</sup> correctly explained the broadening of spectral lines due to the Doppler effect. He used the not completely accepted idea at that time, of a collection of randomly moving atomic radiators whose velocity was governed by Maxwell's distribution. Interest was such that by 1895 A. A. Michelson<sup>24</sup> was able to summarize the possible mechanisms of line broadening as he saw them. Among the proposed mechanisms were the following:

- 1) The change in the emitted radiator frequency due to neighboring molecules.

In those days the term "molecule" was used to refer to any atomic sized entity;<sup>22</sup>

- 2) Doppler broadening due to radiator motion;
- 3) Broadening of radiator emission lines due to radiation interrupting collisions.

Michelson developed a theory for this effect and showed that the resulting line shape was that of a Lorentzian. These early theories considered the radiators to be classical oscillators. We will see that collisional broadening is often proportional to the density, and hence, to the pressure, assuming the temperature is held constant. This is where the terminology pressure broadening originated;

- 4) The natural line width due to radiation damping which was viewed as the leaking away of the oscillator's energy to the environment.

In 1901 C. Godfrey<sup>25</sup> combined Doppler and collisional broadening in a unified description. At that time these two effects were viewed as the most significant causes of observed line broadening. With the advent of the quantum

theory the time was ripe for a reworking of the old classical line broadening theory. In 1924, W. Lenz<sup>26</sup> applied some elements of the new quantum theory to collisional broadening but still considered the radiator as a classical oscillator. Returning to the problem in 1933<sup>27</sup>, Lenz incorporated line shifts and asymmetries into his collisional line broadening theory by using finite collision times. Previously all radiation interrupting collisions had been assumed to occur instantaneously.

Michelson's point about the radiation from atoms being affected by atoms in their vicinity was taken up by Holtsmark<sup>28,29</sup> in 1919 and developed into the theory of statistical Stark broadening. Holtsmark considered the effect of a particular configuration of static perturbers surrounding the radiator on the shift of the radiator's characteristic frequency. He then averaged over the possible configurations to produce a broadened line profile. If the perturbers are electric monopoles this theory is referred to as Stark broadening theory after an idea originally suggested by J. Stark<sup>30</sup> in 1914. Holtsmark also developed similar theories for perturbing dipoles and quadrupoles.

This brings us to a point in the historical development of line broadening theory where we see the emergence of the primary theoretical points of view as to the physical causes of line broadening in plasmas. These are Doppler broadening, collisional broadening and statistical Stark broadening. Many further developments and refinements<sup>17,18</sup> have occurred since these "early days" of line broadening physics but we will not follow the historical development further. We will jump to the point of present day developments.

### 2.3 Theoretical Formulation

In order to examine the line radiation from a plasma, we must look at the power emitted by dipole radiation from an emitter immersed in the plasma. At the outset we assume that the plasma consists of ionic emitters surrounded by a plasma consisting of perturbing ions and electrons. This will allow us to model the plasma line radiation by examining the radiation from one of the emitters and averaging over all possible configurations of the surrounding plasma. This is equivalent to looking at a large number of plasma radiators in differing environmental conditions.

The resulting power radiated by dipole radiation from an emitter immersed in a plasma, as a function of the frequency, is given by<sup>31,32</sup>

$$P(\omega) = \frac{4\omega^4}{3c^3} I(\omega) \quad (2.23)$$

where  $I(\omega)$ , the line shape function, is defined by

$$I(\omega) \equiv \sum_{a,b} \delta(\omega - \omega_{ab}) \left| \langle b | \vec{d} e^{-i\vec{k} \cdot \vec{R}} | a \rangle \right|^2 \rho_a \quad (2.24)$$

Here,  $a$  and  $b$  refer to the initial and final states of the total radiator-plasma system, respectively. The energy difference between these initial and final states can be written as  $\omega_{ab} = (E_a - E_b)/\hbar$ . The dipole moment of the radiator is given by  $\vec{d}$ , and the population of the initial states is given by  $\rho_a$  which is an eigenvalue of the density matrix  $\rho$ , where  $\rho = \sum_i \rho_i |i\rangle \langle i|$ . The radiator center-of-mass coordinate is given by  $\vec{R}$  and the wave vector of the emitted radiation is given by  $\vec{k}$  where  $k = \omega/c$ . The eigenvectors  $|i\rangle$  are eigenfunctions of the system Hamiltonian  $H$ . Free-free and free-bound transitions will not be examined in this dissertation so we consider only dipole radiation from atomic ions.

Since a similar formalism can be used to describe absorption line profiles, we will concern ourselves only with the line shape function  $I(\omega)$ . Our system will consist of plasma electrons, ions and the radiator which will always be referred to in this section by the subscripts “ $e$ ”, “ $i$ ”, and “ $r$ ”, respectively. For simplicity, we also set  $\hbar = 1$  for the remainder of this section.

We can express the Dirac delta function as an integral representation that will allow us to incorporate the time development of the system into the dipole moment operators (i.e. the Heisenberg representation). If we work with this representation, we have the advantage that all of our approximations must be made explicitly on the system Hamiltonian which will be contained in the expression for  $I(\omega)$ . This gives

$$\begin{aligned} I(\omega) &= \sum_{a,b} \frac{1}{2\pi} \int_{-\infty}^{\infty} dt e^{i(\omega - (\omega_a - \omega_b))t} \left| \langle b | \vec{d} e^{-i\vec{k} \cdot \vec{R}} | a \rangle \right|^2 \rho_a \\ &= \frac{1}{\pi} \text{Re} \int_0^{\infty} dt e^{i\omega t} \phi(t) , \end{aligned} \quad (2.25)$$

where

$$\begin{aligned} \phi(t) &= \sum_{a,b} \langle a | e^{i\vec{k} \cdot \vec{R}} \vec{d} | b \rangle \cdot \langle b | e^{i\omega_b t} \vec{d} e^{-i\vec{k} \cdot \vec{R}} e^{-i\omega_a t} \rho_a | a \rangle \\ &= \sum_{a,b} \langle a | \vec{d}_k(0) | b \rangle \cdot \langle b | \vec{d}_{-k}(t) \rho | a \rangle . \end{aligned} \quad (2.26)$$

Here we have used the fact that  $\rho |a\rangle = \rho_a |a\rangle$  and  $e^{-iHt} |a\rangle = e^{-i\omega_a t} |a\rangle$  and the definition of the time development of the dipole and radiator position operator,

$$\vec{d}_{-k}(t) = e^{iHt} \vec{d}(0) e^{-i\vec{k} \cdot \vec{R}} e^{-iHt} . \quad (2.27)$$

It follows that  $\vec{d}_k = \vec{d} e^{i\vec{k} \cdot \vec{R}}$ . We will consider our sum over states  $a$  and  $b$  to now be a sum over a complete set of states and replace the sum with a trace.

We are free to do this at the outset and only look at the elements of the sum that correspond to the spectral transitions we are interested in. Now we have

$$\begin{aligned}\phi(t) &= Tr_{r,e,i} \left[ \vec{d}_k(0) \cdot \vec{d}_{-k}(t) \rho \right] \\ &= \langle \vec{d}_k(0) \cdot \vec{d}_{-k}(t) \rangle\end{aligned}\quad (2.28)$$

and thus

$$I(\omega) = \frac{1}{\pi} Re \int_0^\infty dt e^{i\omega t} \langle \vec{d}_k(0) \cdot \vec{d}_{-k}(t) \rangle. \quad (2.29)$$

To address the problem of radiator motion, we will assume that the radiator velocity is statistically independent of perturbing ion and electron effects as well as of the internal state of the radiator. Consequently, we can factor the radiator translational motion from the density matrix. This gives

$$\rho = \rho_{tr} \rho_{r,i,e}. \quad (2.30)$$

Here,  $\rho_{tr}$  is the density matrix for the radiator translational motion. Assuming ideal gas behavior for the radiators, we have

$$\rho_{tr} = \left( \frac{m_r}{2\pi k T} \right)^{3/2} e^{-\frac{m_r v^2}{2kT}}, \quad (2.31)$$

where  $m_r$  is the radiator mass and  $v$  is its velocity. We may now separate out the radiator's translational motion to give

$$I(\omega) = \frac{1}{\pi} Re \int_0^\infty dt e^{i\omega t} \int d\vec{v} \rho_{tr} e^{i\vec{k} \cdot (\vec{R} - \vec{R}(t))} \langle \vec{d} \cdot \vec{d}(t) \rangle. \quad (2.32)$$

If we assume that the radiator's motion is constant during the time of interest, then we can write

$$\vec{R}(t) = \vec{R} + \vec{v}t. \quad (2.33)$$

This gives

$$I(\omega) = \frac{1}{\pi} \text{Re} \int_0^\infty dt e^{i\omega t} \int d\vec{v} \rho_{tr} e^{-i\vec{k} \cdot \vec{v} t} \langle \vec{d} \cdot \vec{d}(t) \rangle . \quad (2.34)$$

The integral over  $\vec{v}$  may be performed to give

$$I(\omega) = \frac{1}{\pi} \text{Re} \int_0^\infty dt e^{i\omega t} e^{-\left(\frac{\omega}{c}\right)^2 \frac{2kT}{m_r} t^2} \langle \vec{d} \cdot \vec{d}(t) \rangle . \quad (2.35)$$

It can be shown with the aid of the Fourier convolution theorem<sup>33</sup> that this expression is equivalent to

$$I(\omega) = \int_{-\infty}^\infty d\omega' I_D(\omega - \omega') I_S(\omega') , \quad (2.36)$$

where  $I_D(\omega - \omega')$  is the Doppler distribution given by

$$I_D(\omega - \omega') = \frac{1}{\sqrt{2\pi}\sigma} \exp\left(-\frac{(\omega - \omega')^2}{2\sigma^2}\right) , \quad (2.37)$$

where<sup>34</sup>

$$2\sigma^2 = \frac{\omega'^2}{c^2} \left( \frac{2kT}{m_r} \right) . \quad (2.38)$$

Here,  $m_r$  is the mass of the radiator and  $c$  is the speed of light. The line shape function for the static radiator is given by

$$I_S(\omega) = \frac{1}{\pi} \text{Re} \int_0^\infty dt e^{i\omega t} \langle \vec{d} \cdot \vec{d}(t) \rangle . \quad (2.39)$$

This result is the usual method for treating the Doppler effect but we see that it follows, with suitable approximations, directly from the expression for the power emitted by a radiator. The interaction of radiator motion with plasma perturbations can be treated<sup>32,35</sup> as an extension of the above development by not making the approximation:  $\vec{R}(t) = \vec{R} + \vec{v}t$ . We will employ

the Doppler convolution given by Eq. (2.36) to account for radiator motion and continue with the development of  $I_S(\omega)$ . We will drop the subscript from  $I_S(\omega)$  for convenience in what follows. This gives

$$I(\omega) = \frac{1}{\pi} \text{Re} \int_0^\infty dt e^{i\omega t} \langle \vec{d}(0) \cdot \vec{d}(t) \rangle . \quad (2.40)$$

We see that the line shape problem is reduced to the calculation of the system's dipole-dipole autocorrelation function. This is the starting point for some numerical simulation approaches.<sup>36</sup> We, however, will continue with the formal development of the theory along the general lines of the work of Smith and Hooper.<sup>37</sup>

We will see below that it is possible to approximately factor the density matrix into product form so that

$$\rho = \rho_i \rho_e \rho_r . \quad (2.41)$$

Here the individual density matrices are for the three subsystems: the plasma ions, the plasma electrons and the radiator. We will examine the LTE case where the density matrix becomes the simple Boltzmann factor  $\rho = e^{-\beta H} / \text{Tr } e^{-\beta H}$ .

Consider our system Hamiltonian

$$H = H_i^0 + H_r^0 + H_e^0 + V_{i,r} + V_{i,e} + V_{r,e} . \quad (2.42)$$

Here the  $H^0$ 's refer to the kinetic and potential energies of the respective subsystems so that  $H_i^0 = T_i + V_i$  and  $H_e^0 = T_e + V_e$ . The  $V_{j,k}$ 's refer to the potential energy of interaction between the subsystems  $j$  and  $k$ . We make the quasistatic approximation for the ions so we assume that they do not move appreciatively during the atomic radiation time. The use of the quasistatic

approximation allows the interaction of perturbing ions with the radiator to be statistically screened by the rapidly moving plasma electrons. Consequently, we will replace  $V_{i,e} + V_i$  with a screened ionic potential and as an approximation obtain

$$V'_i \approx V_i + V_{i,e} . \quad (2.43)$$

This gives us the effective ionic Hamiltonian  $H_i^{0'} = T_i + V'_i$ . What precise form this screened potential should take has been the subject of considerable work.<sup>38,39,40</sup> Here, we will use the lowest order screening approximation for  $V'_i$ : the Debye-Hückel potential.<sup>20</sup> In order to make the density matrix factorization, we will neglect  $V_{r,e}$ , but only in the density matrix. This amounts to neglecting radiator-perturbing electron correlations at the initial time. This is a reasonable approximation as long as  $kT > V_{r,e}$ . Now we have

$$H \approx H_i^{0'} + H_r^0 + H_e^0 + V_{i,r} . \quad (2.44)$$

The ion-radiator interaction,  $V_{i,r}$ , will be expressed as a multipole expansion which we will truncate. For the density matrix we will keep only terms through the dipole. The monopole term has only ion coordinates and is incorporated into  $H_i^{0'}$  to give  $H'_i$ . The dipole term contains both ion and radiator coordinates but we will use a mathematical device to eliminate those of the ions and combine it with  $H_r^0$  to give  $H_r(\vec{\epsilon})$ . Here  $\vec{\epsilon}$  is the plasma microfield to be discussed below. If we assume that the remaining effective Hamiltonians for the three subsystems commute amongst themselves the density matrix is now factorable with the Hamiltonian  $H \approx H'_i + H_r(\vec{\epsilon}) + H_e^0$ . We will see what these terms are in detail shortly.

Turning from the approximate form for the Hamiltonian in the density matrix, we consider the terms in the Hamiltonian of the dipole moment time development operator. We make a multipole expansion<sup>41</sup> of the radiator-ion interaction

$$V_{r,i} = \chi\phi(0) - \vec{d} \cdot \vec{E}(0) - \frac{1}{6} \sum_{i,j} Q_{i,j} \frac{\partial E_i(0)}{\partial x_j} + \dots \quad (2.45)$$

The electric fields and potentials refer to those produced by the plasma ions at the radiator which we take to be at the origin. The effective charge of the radiator is given by  $\chi = Z - \alpha$  where  $Z$  is the radiator charge and  $\alpha$  is the number of bound radiator electrons. The radiator dipole moment operator is given by  $\vec{d}$  and the components of the radiator quadrupole moment tensor are given by  $Q_{i,j}$ . One effect of the quadrupole term is the production of an asymmetry in the line by intensification of the blue portion of the line relative to the red.<sup>12</sup> The octupole term is fourth order in the expansion parameter  $\delta$  compared to the third order of the quadrupole term. For the special case of hydrogen-like ions, Joyce<sup>42</sup> has shown that the octupole term, to first order in perturbation theory, produces symmetric shifts of the hydrogenic energy levels and thus will not contribute significantly to the asymmetry of the spectral line. Since we are using a basis set for this calculation that is made up of eigenfunctions of the radiator Hamiltonian that includes the field dependent dipole term, we take the quadrupole term as the first order correction to this Hamiltonian, and neglect all higher order terms.

We will symbolically represent all field gradient terms  $\partial E_i(0)/\partial x_j$  by the generic term  $E_{\mu\nu} = \partial_\mu E_\nu$ . Whenever we use this term we will mean all relevant partial derivatives. Our device for removing the ion coordinates from the interaction potential  $V_{i,r}$  involves the introduction of a delta function in the

manner shown below. This will allow us to separate the ion coordinates from the radiator-perturbing electron subsystem and proceed with the development as shown below. Introducing the delta functions into Eq. (2.28) gives

$$\phi(t) = \int d\vec{\epsilon} \int d\epsilon_{\mu\nu} Tr_{r,e,i} \left[ \rho_i \delta(\vec{\epsilon} - \vec{E}) \delta(\epsilon_{\mu\nu} - E_{\mu\nu}) \vec{d}(0) \cdot \vec{d}(t) \rho_{re} \right] . \quad (2.46)$$

Here, the integration variable  $\epsilon_{\mu\nu}$  is used in the same way as  $E_{\mu\nu}$  above.

The time dependence of the radiator dipole operator is given in terms of the total system Hamiltonian  $H$ . The ion coordinates in  $H$  that are not removed by the delta function will commute with  $\vec{d}(0)$  in the static ion approximation and cancel.<sup>43,44</sup> This leaves the Hamiltonian  $H_{e,r}$  that has only radiator and perturbing electron coordinates. This is illustrated by

$$\vec{d}(t) = e^{iH_{er}t} \vec{d}(0) e^{-iH_{er}t} = e^{iLt} \vec{d}(0) , \quad (2.47)$$

where

$$H_{er} = H_e^0 + V_{e,r} + H_r(\vec{\epsilon}) - \frac{1}{6} \sum_{i,j} Q_{i,j} \frac{\partial \epsilon_i}{\partial x_j} , \quad (2.48)$$

and  $L$  is the Liouville superoperator expressed in terms of a commutator acting on an arbitrary operator  $\mathcal{O}$  as

$$L\mathcal{O} \equiv [H_{er}, \mathcal{O}] . \quad (2.49)$$

We have now successfully separated the system ion coordinates from the radiator and perturbing electron subsystems. This is expressed by

$$I(\omega) = \int d\vec{\epsilon} \int d\epsilon_{\mu\nu} W(\vec{\epsilon}, \epsilon_{\mu\nu}) J(\omega, \vec{\epsilon}, \epsilon_{\mu\nu}) , \quad (2.50)$$

where  $W(\vec{\epsilon}, \epsilon_{\mu\nu})$  is the ion probability function, and

$$\begin{aligned}
J(\omega, \vec{\epsilon}, \epsilon_{\mu\nu}) &= \frac{1}{\pi} \text{Re} \int_0^\infty dt e^{i\omega t} \langle \vec{d}(0) \cdot \vec{d}(t) \rangle_{e,r} \\
&= \frac{1}{\pi} \text{Re} \int_0^\infty dt e^{i\omega t} \text{Tr}_{e,r} \left[ \vec{d} \cdot e^{-iLt} (\rho_{e,r} \vec{d}) \right] \\
&= -\frac{1}{\pi} \text{Im} \text{Tr}_{e,r} \left[ \vec{d} \cdot R_{e,r}(\omega) (\rho_{e,r} \vec{d}) \right] .
\end{aligned} \tag{2.51}$$

We have defined the resolvent operator as

$$R_{e,r}(\omega) \equiv -i \int_0^\infty dt e^{i\omega t} e^{-iLt} = [\omega - L]^{-1} . \tag{2.52}$$

$\text{Re}$  and  $\text{Im}$  refer to the real and imaginary parts respectively. The ion probability function  $W(\vec{\epsilon}, \epsilon_{\mu\nu})$  is given by

$$\begin{aligned}
W(\vec{\epsilon}, \epsilon_{\mu\nu}) &= \text{Tr}_i \left[ \rho_i \delta(\vec{\epsilon} - \vec{E}) \delta(\epsilon_{\mu\nu} - E_{\mu\nu}) \right] \\
&\equiv \langle \delta(\vec{\epsilon} - \vec{E}) \delta(\epsilon_{\mu\nu} - E_{\mu\nu}) \rangle_i .
\end{aligned} \tag{2.53}$$

The field  $\vec{E}$  and field gradient  $E_{\mu\nu}$  are sums of contributions from all of the individual system ions. We will return to the evaluation of  $W(\vec{\epsilon}, \epsilon_{\mu\nu})$  in chapter 3. Recalling that  $\rho_{e,r} = \rho_e \rho_r$ , we can perform the trace over plasma electron coordinates to give

$$J(\omega, \vec{\epsilon}, \epsilon_{\mu\nu}) = -\frac{1}{\pi} \text{Im} \text{Tr}_r \left[ \vec{d} \cdot \langle R_{er}(\omega) \rangle_e (\rho_r \vec{d}) \right] . \tag{2.54}$$

We see that the effects due to the perturbing electrons have been isolated in  $R_r(\omega) \equiv \langle R_{er}(\omega) \rangle_e$ . Note that  $L = L(\vec{\epsilon}, \epsilon_{\mu\nu})$ .

Next, we proceed with the evaluation of the operator  $R_r(\omega)$ . We now introduce a coupling constant  $\lambda$  as an expansion parameter. Write

$$L = L_0 + \lambda L_I , \tag{2.55}$$

where  $L$  corresponds to the Hamiltonian:

$$H_{e,r} = H_0 + \lambda V_I = H_{e,r}^0 + \lambda \left( V_{e,r} - \frac{1}{6} \sum_{i,j} Q_{i,j} \frac{\partial \epsilon_i}{\partial x_j} \right). \quad (2.56)$$

The  $H_{e,r}^0$  corresponds to  $L_0$  and  $V_{e,r} + V_{i,r}^Q$  corresponds to  $L_I$ . Here,  $Q_{i,j}$  is a function of the radiator's electron coordinates (for single or multielectron radiators),  $V_{e,r}$  is the radiator and plasma-electron interaction,  $V_{i,r}^Q$  is the ion-quadrupole interaction, and  $H_{e,r}^0 = H_r(\vec{\epsilon}) + H_e^0$  is the combined non-interacting radiator plasma-electron Hamiltonian containing the ion-dipole term. We will now implicitly define an electron broadening operator  $M(\omega)$ , by setting

$$R_r(\omega) \equiv [\omega - L_r(\vec{\epsilon}, \epsilon_{\mu\nu}) - M(\omega)]^{-1}, \quad (2.57)$$

where  $L_r(\vec{\epsilon}, \epsilon_{\mu\nu})$  is the Liouville operator corresponds to the Hamiltonian:

$$H_r(\vec{\epsilon}, \epsilon_{\mu\nu}) = H_r(\vec{\epsilon}) - \frac{1}{6} \sum_{i,j} Q_{i,j} \partial_i \epsilon_j. \quad (2.58)$$

Here,  $H_r(\vec{\epsilon})$  is the Hamiltonian of the field-free radiator with the ion-dipole term, and we have used the quadrupole approximation for the remainder of the interaction of the plasma ions with the radiator. Specifically,

$$H_r(\vec{\epsilon}) = H_r^0 - \vec{d} \cdot \vec{\epsilon}. \quad (2.59)$$

Note that  $H_r(\vec{\epsilon}) = H_r(\vec{\epsilon}, 0)$ .

So, using Eqs. (2.52),(2.55) and (2.57), we can write,

$$[\omega - L_r(\vec{\epsilon}, \epsilon_{\mu\nu}) - M(\omega)]^{-1} = \langle [\omega - L_0 - \lambda L_I]^{-1} \rangle_e. \quad (2.60)$$

Next, we expand  $M(\omega)$  in powers of the coupling constant, expand both sides of Eq. (2.60), equate coefficients of equal powers of  $\lambda$ , and thus identify the terms of the  $M(\omega)$  expansion.

The right-hand side of Eq. (2.60) can be expanded in a Lippmann-Schwinger expansion and the left-hand side can be expanded in a Taylor series in  $\lambda$ . First, we will expand the right-hand side. For simplicity in notation we will denote the full resolvent operator by  $R_{e,r}(\omega) \equiv R$ , and define a zero order resolvent operator as

$$R_0 \equiv [\omega - L_0]^{-1} . \quad (2.61)$$

We can construct an iterative equation for  $R$  by noting that

$$R - R_0 = R_0 \left[ R_0^{-1} - R^{-1} \right] R \quad (2.62)$$

or explicitly,

$$\frac{1}{\omega - L} - \frac{1}{\omega - L_0} = \frac{1}{\omega - L_0} [\omega - L_0 - (\omega - L)] \frac{1}{\omega - L} . \quad (2.63)$$

This can be written equivalently as,

$$\frac{1}{\omega - L} = \frac{1}{\omega - L_0} + \frac{1}{\omega - L_0} \lambda L_I \frac{1}{\omega - L} , \quad (2.64)$$

or simply as just

$$R = R_0 + \lambda R_0 L_I R . \quad (2.65)$$

This is the Dyson equation for this system in Liouville space. This implicit equation for  $R$  can be iterated to give a series expansion for  $R$  in powers of  $\lambda$ :

$$R = \sum_{n=0}^{\infty} \lambda^n R_0 (L_I R_0)^n . \quad (2.66)$$

To second order in  $\lambda$  we have

$$R = R_0 + \lambda R_0 L_I R_0 + \lambda^2 R_0 L_I R_0 L_I R_0 . \quad (2.67)$$

In order to examine what  $\langle \cdots \rangle_e$  does to this, look at

$$R_r(\omega) = \langle R \rangle_e . \quad (2.68)$$

To second order in the interaction Liouville operator this is

$$R_r(\omega) = \langle R_0 \rangle_e + \lambda \langle R_0 L_I R_0 \rangle_e + \lambda^2 \langle R_0 L_I R_0 L_I R_0 \rangle_e . \quad (2.69)$$

Here  $R_0$  is a function of  $L_r$  and  $L_e$ , the zero-order-radiator and perturbing-electron Liouville operators with  $L_r$  corresponding to  $H_r(\vec{\epsilon})$  and  $L_e$  to  $H_e^0$ . Tighe<sup>44</sup> has shown that when  $L_0$  operates on objects of the form  $B = \rho_e b$ , where  $b$  operates on radiator coordinates only, then

$$\langle L_0^n \rangle_e = L_r^n . \quad (2.70)$$

On expanding  $R_0$  this leads to

$$\langle R_0 \rangle_e = [\omega - L_r]^{-1} \equiv R_r^0(\omega) . \quad (2.71)$$

For combinations of  $R_0$  with a general operator  $\mathcal{L}$  in Liouville space Tighe<sup>44</sup> has shown that

$$\langle R_0 \mathcal{L} \rangle_e = R_r^0 \langle \mathcal{L} \rangle_e, \quad (2.72)$$

and

$$\langle \mathcal{L} R_0 \rangle_e = \langle \mathcal{L} \rangle R_r^0 . \quad (2.73)$$

These identities allow us to simplify the expression for the resolvent. We obtain

$$\langle R \rangle_e = R_r^0 + \lambda R_r^0 \langle L_I \rangle_e R_r^0 + \lambda^2 R_r^0 \langle L_I R_0 L_I \rangle_e R_r^0 . \quad (2.74)$$

For the left-hand side of Eq. (2.60) we postulated an equivalent form for the resolvent that contains all of the perturbing electron statistics in an implicitly defined operator  $M(\lambda, \omega)$  which is analytic in the coupling constant  $\lambda$ . Restating this we have

$$\langle R \rangle_e \equiv [\omega - L_r(\vec{\epsilon}, \epsilon_{\mu\nu}) - M(\lambda, \omega)]^{-1} , \quad (2.75)$$

where  $L_r$  is defined above. Expanding  $M(\lambda, \omega)$  in powers of  $\lambda$  we have

$$M(\lambda, \omega) = M^{(0)}(\omega) + \lambda M^{(1)}(\omega) + \lambda^2 M^{(2)}(\omega) + \dots . \quad (2.76)$$

To expand the right-hand side of Eq. (2.75) about  $\lambda = 0$  we will need the following easily proved operator identity for some operator  $A$  in Liouville space:

$$\frac{\partial A^{-1}}{\partial \lambda} = -A^{-1} \frac{\partial A}{\partial \lambda} A^{-1} . \quad (2.77)$$

Expanding  $A^{-1}(\lambda)$  about  $\lambda = 0$  we have

$$A^{-1}(\lambda) = A^{-1}(0) + \lambda \frac{\partial A^{-1}(0)}{\partial \lambda} + \frac{1}{2} \lambda^2 \frac{\partial^2 A^{-1}(0)}{\partial \lambda^2} + O(\lambda^3) . \quad (2.78)$$

In this case we have

$$A(\lambda) = [\omega - L_r(\vec{\epsilon}, 0) - \lambda L_{r,i}(\epsilon_{\mu\nu}) - M(\lambda, \omega)] , \quad (2.79)$$

with  $L_{r,i}(\epsilon_{\mu\nu})$  corresponding to  $V_{r,i}^Q$ . Using the identity of Eq. (2.77), along with

$$\frac{\partial A(0)}{\partial \lambda} = L_{r,i}(\epsilon_{\mu\nu}) - M^{(1)}(\omega) , \quad (2.80)$$

$$\frac{\partial^2 A(0)}{\partial \lambda^2} = -2M^{(2)}(\omega) \quad (2.81)$$

and

$$A^{-1}(0) = \left[ \omega - L_r(\vec{\epsilon}, 0) - M^{(0)}(\omega) \right]^{-1} , \quad (2.82)$$

we can evaluate the expansion of  $A^{-1}$  about  $\lambda = 0$ . We obtain

$$\begin{aligned} \langle R \rangle_e = A^{-1} &= A^{-1}(0) + \lambda A^{-1}(0) \left[ L_{r,i}(\epsilon_{\mu\nu}) + M^{(1)}(\omega) \right] A^{-1}(0) \\ &- \lambda^2 \left\{ A^{-1}(0) \left[ L_{r,i}(\epsilon_{\mu\nu}) + M^{(1)}(\omega) \right] A^{-1}(0) \left[ L_{r,i}(\epsilon_{\mu\nu}) + M^{(1)}(\omega) \right] A^{-1}(0) \right. \\ &\left. - A^{-1}(0) M^{(2)}(\omega) A^{-1}(0) \right\} + O(\lambda^3) . \end{aligned} \quad (2.83)$$

Comparison of the two expansions for  $\langle R \rangle_e$ , term by term in powers of  $\lambda$  up to second order, allows us to make the following identifications for the terms in the expansion of  $M(\lambda, \omega)$ :

$\lambda^{(0)}$  term

$$M^{(0)}(\omega) = 0 , \quad (2.84)$$

$\lambda^{(1)}$  term

$$M^{(1)}(\omega) = \langle L_{r,e} \rangle_e , \quad (2.85)$$

$\lambda^{(2)}$  term

$$M^{(2)}(\omega) = \langle L_I R_0 L_I \rangle - \langle L_I \rangle_e R_r^0 \langle L_I \rangle_e . \quad (2.86)$$

This last expression for  $M^{(2)}(\omega)$  can be further simplified if we expand  $L_I$ . Recall that  $L_I = L_{e,r} + L_{i,r}$  with  $L_{e,r}$  corresponding to  $V_{e,r}$  and  $L_{i,r}$  to  $V_{i,r}^Q$ . This gives

$$\begin{aligned} M^{(2)}(\omega) &= \langle L_{r,e} R_0 L_{r,e} \rangle_e - \langle L_{r,e} \rangle_e R_r^0 \langle L_{r,e} \rangle_e \\ &\quad + L_{r,i} \langle (R_0 - R_r^0) L_{r,e} \rangle_e + \langle L_{r,e} (R_0 - R_r^0) \rangle_e L_{r,i} . \end{aligned} \quad (2.87)$$

With the use of Eqs. (2.72) and (2.73) the last two terms cancel to give

$$M^{(2)}(\omega) = \langle L_{r,e} R_0 L_{r,e} \rangle_e - \langle L_{r,e} \rangle_e R_r^0 \langle L_{r,e} \rangle_e . \quad (2.88)$$

If the dipole approximation is made for  $V_{e,r}$ , we will find for the corresponding Liouville operator,  $\langle L_{e,r} \rangle_e = 0$ . This is easy to see by noting that in order to evaluate this expression we need to calculate  $\langle \vec{E}_e \rangle_e$  which must average to zero since there is no preferred direction in the plasma. This holds true for the case of hydrogenic or multielectron radiators. The first surviving term in the  $M(\omega)$  expansion will then be to second order. So to lowest order in  $\lambda$ ,

$$M(\omega) = M^{(2)}(\omega) = \langle L_{e,r} R_0(\omega) L_{e,r} \rangle_e , \quad (2.89)$$

where  $R_0(\omega) = [\omega - L_0]^{-1}$ . This gives us

$$M(\omega) = -i \int_0^\infty dt e^{i\omega t} \langle L_{e,r} e^{-iL_0 t} L_{e,r} \rangle_e . \quad (2.90)$$

This operator is tetradic<sup>37</sup> because of the use of the Liouville operators and, when evaluated as a matrix element, will give<sup>45</sup>

$$\begin{aligned}
M(\omega)_{ab,a'b'} = & -\frac{i}{3} \left[ \delta_{bb'} \sum_{a''} \vec{d}_{aa''} \cdot \vec{d}_{a''a'} G(\Delta\omega_{a''b}) \right. \\
& + \delta_{aa'} \sum_{b''} \vec{d}_{b'b''} \cdot \vec{d}_{b''b} G(-\Delta\omega_{ab''}) \\
& \left. - \vec{d}_{aa'} \cdot \vec{d}_{b'b} \{G(\Delta\omega_{ab'}) + G(-\Delta\omega_{a'b})\} \right], \tag{2.91}
\end{aligned}$$

where the first term represents electron broadening of the upper state, the second term represents electron broadening of the lower state and the third term represents interference effects.

The many-body electron broadening function  $G(\Delta\omega_{ab})$  is given by

$$G(\Delta\omega_{ab}) = \int_0^\infty dt e^{i\Delta\omega_{ab}t} \langle \vec{E}_e \cdot \vec{E}_e(t) \rangle_e, \tag{2.92}$$

with  $\vec{E}_e(t) = e^{iH_e^0 t} \vec{E}_e(0) e^{-iH_e^0 t}$  and  $\Delta\omega_{ab} = \omega - (\omega_a - \omega_b)$ . Thus the electron perturber effects are given in terms of an autocorrelation function for the plasma electric field at the radiator due to the plasma electrons. We have calculated only the imaginary part of  $M(\omega)$  which corresponds to line width operator. The real part corresponds to the line shift operator and yields only a small shift<sup>44</sup> which is ignored here.

In our approach to this calculation we approximate the effects of correlations among the perturbing electrons by the use of  $G(\Delta\omega) = G(\omega_p)$  for  $|\Delta\omega| \leq \omega_p$ , where  $\omega_p$  is the electron plasma frequency. This procedure has been shown to be a good approximation by a detailed treatment of dynamic electron correlations.<sup>21</sup> This handling of electron correlations allows us to use single particle Coulomb waves in taking the trace over perturbing electron coordinates. The Coulomb waves are single particle solutions to Schrödinger's equation with a central  $1/r$  potential with effective radiator charge  $\chi$ , where  $\chi = Z - \alpha_N$ ;  $\alpha_N$  being the number of bound radiator electrons.  $G(\Delta\omega)$  is

then evaluated using the method of Tighe and Hooper.<sup>46</sup> Other theories<sup>47</sup> also exist for the evaluation of  $G(\Delta\omega)$ . It is instructive to point out, however, that we can relate this electric field autocorrelation function to the charge density autocorrelation function<sup>48</sup> which gives us,

$$\langle \vec{E}_e \cdot \vec{E}_e(t) \rangle_e = \int d^3x \int d^3x' \frac{\vec{x} \cdot \vec{x}'}{x^3 x'^3} \langle \rho(\vec{x}) \rho(\vec{x}', t) \rangle_e . \quad (2.93)$$

This illustrates the relationship of the plasma charge-density fluctuations to the spectral line-broadening problem. Note that this charge density correlation function is not translationally invariant for ionic radiators as is sometimes assumed.<sup>49</sup> Translational invariance would imply a uniform perturbing electron gas; for highly charged radiators, this assumption would ignore aspects of the radiator-perturbing electron correlations.

Altogether, our approach leads to a line shape function of the following form:

$$I(\omega) = \int d\vec{\epsilon} \int d\epsilon_{\mu\nu} W(\vec{\epsilon}, \epsilon_{\mu\nu}) J(\omega, \vec{\epsilon}, \epsilon_{\mu\nu}) ,$$

where

$$J(\omega, \vec{\epsilon}, \epsilon_{\mu\nu}) = -\frac{1}{\pi} \text{Im} \text{Tr}_r \left\{ \vec{d} \cdot [\omega - L_r(\vec{\epsilon}, \epsilon_{\mu\nu}) - M(\omega)]^{-1} \rho_r \vec{d} \right\} \quad (2.94)$$

or in matrix element form

$$J(\omega, \vec{\epsilon}, \epsilon_{\mu\nu}) = -\frac{1}{\pi} \text{Im} \sum_{a a' b b'} \rho_a \vec{d}_{b' a'} \cdot \vec{d}_{a b} [\omega - L_r(\vec{\epsilon}, \epsilon_{\mu\nu}) - M(\omega)]_{a' b', a b}^{-1} , \quad (2.95)$$

where  $a$  and  $b$  refer to initial and final radiator states respectively.

The above equations for the line intensity  $I(\omega)$  are valid for the general case of multielectron radiators with combined upper and lower state electron broadening effects and Stark shifts. In this work we will be considering hydrogenic ion resonance lines which have the ground state as the lower state. For hydrogenic ions the ground state is not subject to electron broadening and only very weakly affected by the plasma electric microfield. Therefore we will ignore lower state broadening and interference effects. This will leave only the upper state term of the three terms in the matrix element expression for the electron broadening operator  $M(\omega)$  given by Eq. (2.91). This gives

$$M(\omega)_{aa'} = -\frac{i}{3} \sum_{a''} \vec{d}_{aa''} \cdot \vec{d}_{a''a'} G(\Delta\omega_{a''f}) , \quad (2.96)$$

where subscript  $f$  refers to the single lower radiator state.

Since lower state ion produced Stark shifts are unimportant here, the radiator Liouville operator  $L_r(\vec{\epsilon}, \epsilon_{\mu\nu})$  in Eq. (2.95) can be evaluated to give

$$J(\omega, \vec{\epsilon}, \epsilon_{\mu\nu}) = -\frac{1}{\pi} \text{Im} \sum_{aa'} \rho_a \vec{d}_{af} \cdot \vec{d}_{fa'} [\omega - (H_r(\vec{\epsilon}, \epsilon_{\mu\nu}) - \omega_f) - M(\omega)]_{aa'}^{-1} \quad (2.97)$$

where  $\omega_f$  is the lower state energy of the radiator. We note that since there is only one lower state the sum over  $b$  is absent.

For our case, the dipole and quadrupole operators become single electron quantities with

$$\begin{aligned} \vec{d} &= -e\vec{r} \\ Q_{i,j} &= -e(3x_i x_j - r^2 \delta_{i,j}) \end{aligned} \quad (2.98)$$

Here  $\vec{r}$  and  $x_i$  refer to radiator electron coordinates. The corresponding multielectron quantities are just sums of terms similar to these for each radiator electron.

Any intrinsic line width, such as the resonance width induced by the presence of an electric field (see Chapter 3), can be approximately included in the line profile formalism by replacing the affected level energy  $E$  by a complex resonance energy<sup>50</sup>  $\tilde{E}$ . For level  $j$  this gives

$$\tilde{E}_j \approx E_j - i \frac{\Gamma_j}{2} , \quad (2.99)$$

where  $E_j$  is the energy at the center of the resonance and the presence of  $i\Gamma_j/2$  assumes a Lorentzian shape for the resonance.  $\Gamma_j$  is the full width at half maximum of resonance  $j$ . We have chosen the minus sign in Eq. (2.99) to be consistent with the fact that the electron broadening operator  $M(\omega)$  is proportional to  $-i$ . A choice of  $E_j - i\frac{\Gamma_j}{2}$  would correspond to a proportionality factor of  $+i$ . The use of this complex energy is only an approximation since we are attempting to describe the time dependent behavior of a resonant state in a stationary state formalism. We use this procedure to approximately include the field induced resonance width for the upper states of the Lyman series in hydrogenic argon.

When considering the comparison of theoretical line profiles to experimental results, it is important to remember the factor  $\omega^4$  in the relation for the total power,  $P(\omega) = \text{Const. } \omega^4 I(\omega)$ . If the radiation energy is high enough and the line shape is broad enough, this factor will not be approximately constant across the line shape and  $I(\omega)$  must be redefined to include it. Otherwise an

additional source of line asymmetry will be neglected. For experimental comparison, it is also important to include instrumental broadening<sup>5</sup> as well as opacity effects<sup>51</sup> if significant.

## CHAPTER III HIGHER ORDER FIELD EFFECTS

In the preceding chapter we have reviewed some fundamentals of dense plasmas and formulated a theory of spectral line shapes. We will now examine some of the processes and effects that can make important contributions to these line shapes in the high density regime.

### 3.1 The Ion-Quadrupole Effect

Previously we introduced the ion coordinate joint probability function  $W(\vec{\epsilon}, \epsilon_{\mu\nu})$  to describe the joint probability distribution for the microfield  $\vec{\epsilon}$  together with the field gradients  $\epsilon_{\mu\nu}$ . Recall that for notational convenience,  $\epsilon_{\mu\nu}$  represents all of the field gradient terms. Writing out this probability function explicitly we have

$$\begin{aligned}
 W(\vec{\epsilon}, \epsilon_{\mu\nu}) &= \langle \delta(\vec{\epsilon} - \vec{E}) \delta(\epsilon_{xx} - E_{xx}) \delta(\epsilon_{yy} - E_{yy}) \delta(\epsilon_{zz} - E_{zz}) \\
 &\quad \times \delta(\epsilon_{xy} - E_{xy}) \delta(\epsilon_{yz} - E_{yz}) \delta(\epsilon_{zx} - E_{zx}) \rangle_i \\
 &= \frac{1}{Z_c} \int e^{-\beta V} \delta(\vec{\epsilon} - \vec{E}) \delta(\epsilon_{xx} - E_{xx}) \cdots d^{3N} r ,
 \end{aligned} \tag{3.1}$$

where  $\langle \cdots \rangle_i$  is the ensemble average over ion coordinates,  $Z_c$  is the configurational partition function for the ion subsystem,  $N$  is the number of ions, and  $V$  is the potential energy of the ion subsystem in the presence of the charged radiator. The quantities  $\vec{E}$  and  $E_{ij}$  are the many particle electric field and field gradients at the radiator and are functions of the perturbing ion coordinates. Using an integral representation of the field gradient delta function,

$$\delta(\epsilon_{xx} - E_{xx}) = \frac{1}{2\pi} \int d\sigma_{xx} e^{-i\sigma_{xx}(\epsilon_{xx} - E_{xx})} , \quad (3.2)$$

gives

$$\begin{aligned} W(\vec{\epsilon}, \epsilon_{\mu\nu}) &= \frac{1}{(2\pi)^6 Z_c} \int d^6\sigma e^{-i(\sigma_{xx}\epsilon_{xx} + \dots)} \int d^{3N}r e^{\beta V} \delta(\vec{\epsilon} - \vec{E}) e^{i(\sigma_{xx}E_{xx} + \dots)} \\ &= \frac{1}{(2\pi)^6 Z_c} \int d^{3N}r \delta(\vec{\epsilon} - \vec{E}) e^{\beta V} \int d^6\sigma e^{-i(\sigma_{xx}\epsilon_{xx} + \dots)} \langle e^{i\Theta} \rangle_\epsilon \\ &= \frac{1}{(2\pi)^6} Q(\vec{\epsilon}) \int d^6\sigma e^{-i(\sigma_{xx}\epsilon_{xx} + \sigma_{yy}\epsilon_{yy} + \dots)} \langle e^{i\Theta} \rangle_\epsilon \\ &= Q(\vec{\epsilon}) P(\vec{\epsilon} | \epsilon_{\mu\nu}) , \end{aligned} \quad (3.3)$$

where

$$\Theta = \sigma_{xx}E_{xx} + \sigma_{yy}E_{yy} + \sigma_{zz}E_{zz} + \sigma_{xy}E_{xy} + \sigma_{yz}E_{yz} + \sigma_{zx}E_{zx} . \quad (3.4)$$

We have defined the conditional averaged quantity

$$\langle e^{i\Theta} \rangle_\epsilon \equiv \frac{\int d^{3N}r e^{-\beta V} \delta(\vec{\epsilon} - \vec{E}) e^{i\Theta}}{\int d^{3N}r e^{-\beta V} \delta(\vec{\epsilon} - \vec{E})} . \quad (3.5)$$

This is the ensemble average of  $e^{i\Theta}$  where all included ion configurations are constrained to have the microfield value  $\vec{\epsilon}$ . It is normalized to give one if  $\Theta = 0$ . By defining the average in this way we have retained the benefits of using the ordinary plasma microfield function  $Q(\vec{\epsilon})$  to describe the uniform field at the radiator and we are now free to approximate the higher order field gradients if we choose. The function  $P(\vec{\epsilon} | \epsilon_{\mu\nu})$  is the conditional probability for  $\epsilon_{\mu\nu}$  given  $\vec{\epsilon}$ . We take the field to be in the  $z$  direction for simplicity and without loss of generality.

Direct evaluation of this constrained average is quite difficult if we wish to retain all of the ion interactions. Consequently, we will make a simple approximation to this function in order to proceed. We will expand the exponential in a cumulant expansion<sup>52</sup> by taking

$$\langle e^{i\Theta} \rangle_\epsilon = \exp \left( \sum_{n=1}^{\infty} \frac{(i)^n}{n!} C_n \right), \quad (3.6)$$

where

$$\begin{aligned} C_1 &= \langle \Theta \rangle_\epsilon \\ C_2 &= \langle (\Theta - \langle \Theta \rangle_\epsilon)^2 \rangle_\epsilon \\ C_3 &= \langle (\Theta - \langle \Theta \rangle_\epsilon)^3 \rangle_\epsilon. \end{aligned} \quad (3.7)$$

Higher order terms are more complicated. In terms of the expansion parameter  $\delta$ , which we introduced in the multipole expansion (see Eq. (2.22)), we have  $C_1 \sim \delta^3$  and  $C_2 \sim \delta^6$ . We see this by noting that  $\Theta$  goes as  $\partial E_i / \partial x_j$  which goes as  $1/r^3$  and  $1/r$  is of order  $\delta$ . For our highest density of  $n_e = 1 \times 10^{25} \text{ cm}^{-3}$ , this gives  $C_1 \sim 0.043$  and  $C_2 \sim 0.0018$  for the  $n = 3$  level. The  $C_2$  term, which is actually the variance of the quantity *Theta*, is therefore in the neighborhood of 4% of the lower order term  $C_1$ . Here, we will keep only the  $C_1$  term in our approximation. This gives us

$$\langle e^{i\Theta} \rangle_\epsilon \approx e^{i\langle \Theta \rangle_\epsilon}. \quad (3.8)$$

Inserting this into Eq. (3.3) gives

$$\begin{aligned} W(\vec{\epsilon}, \epsilon_{\mu\nu}) &= \frac{1}{(2\pi)^6} Q(\vec{\epsilon}) \int d^6 \sigma e^{-i(\sigma_{xx}\epsilon_{xx} + \dots)} e^{i\langle \Theta \rangle_\epsilon} \\ &= Q(\vec{\epsilon}) \delta(\epsilon_{xx} - \langle E_{xx} \rangle_\epsilon) \delta(\epsilon_{yy} - \langle E_{yy} \rangle_\epsilon) \dots \\ &= Q(\vec{\epsilon}) \delta(\epsilon_{\mu\nu} - \langle E_{\mu\nu} \rangle_\epsilon). \end{aligned} \quad (3.9)$$

This gives us for the approximation of the conditional probability:

$$P(\vec{\epsilon}|\epsilon_{\mu\nu}) \approx \delta(\epsilon_{\mu\nu} - \langle E_{\mu\nu} \rangle_{\epsilon}) . \quad (3.10)$$

We have developed a systematic expansion for the conditional probability function and have examined the magnitude of the expansion terms. We can identify the first term of this expansion as the approximation used by Joyce.<sup>12</sup> Returning to the expression for the spectral line intensity, Eq. (2.50) now gives

$$I(\omega) = \int d\vec{\epsilon} \int d\epsilon_{\mu\nu} Q(\vec{\epsilon}) P(\vec{\epsilon}|\epsilon_{\mu\nu}) J(\omega, \vec{\epsilon}, \epsilon_{\mu\nu}) . \quad (3.11)$$

The microfield function  $Q(\vec{\epsilon})$  does not depend on the direction of  $\vec{\epsilon}$  but only on its magnitude,  $\epsilon$ . We can therefore preform the angular integration and define a new microfield distribution function as

$$P(\epsilon) \equiv 4\pi\epsilon^2 Q(\vec{\epsilon}) . \quad (3.12)$$

Now, the intensity becomes

$$I(\omega) = \int d\epsilon \int d\epsilon_{\mu\nu} P(\epsilon) P(\epsilon|\epsilon_{\mu\nu}) J(\omega, \epsilon, \epsilon_{\mu\nu}) . \quad (3.13)$$

Using our approximation for  $P(\epsilon|\epsilon_{\mu\nu})$  we can carry out the  $\epsilon_{\mu\nu}$  integrations to obtain

$$I(\omega) = \int d\epsilon P(\epsilon) J(\omega, \epsilon, \langle E_{\mu\nu} \rangle_{\epsilon}) . \quad (3.14)$$

The field gradient terms in  $J(\omega, \epsilon, \epsilon_{\mu\nu})$  have now been replaced with their constrained averages that depend only on  $\epsilon$  so we can write  $J(\omega, \epsilon, \langle E_{\mu\nu} \rangle_{\epsilon}) = J'(\omega, \epsilon)$ , where the prime indicates the replacement of the field gradient by its constrained average. For the remainder of this work, we will drop the

prime with the understanding that we actually mean  $J'(\omega, \epsilon)$ . Our use of the approximation for  $P(\epsilon|\epsilon_{\mu\nu})$  has lead to a significant simplification of the line shape formula that still retains the approximate effect of the field gradients.

In order to proceed we will need to evaluate this constrained average of the field gradient. From the ensemble of all possible ion configurations in the presence of the radiator we choose only those configurations that give a certain field magnitude  $\epsilon$  at the origin. If we average a quantity  $F$  over this subset of configurations, we have constructed the constrained field average that we introduced above. We denote this average by

$$\langle F \rangle_\epsilon = \frac{\langle F \delta(\vec{\epsilon} - \vec{E}) \rangle}{Q(\vec{\epsilon})} , \quad (3.15)$$

where  $Q(\vec{\epsilon})$  is the plasma microfield function and  $\langle \dots \rangle$  is the complete ion subsystem ensemble average. This average, as we have said, is such that for  $F = 1$ ,  $\langle F \rangle_\epsilon = 1$ . We will show that it is possible to relate this constrained average to a functional derivative of the plasma microfield function. This will allow us to evaluate the constrained average in terms of available simplified models for the microfield function  $Q(\vec{\epsilon})$ .

For our purposes we will take  $F$  to be an additive function of the ion coordinates,

$$F = \sum_i f(\vec{r}_i) = \int d\vec{r} f(\vec{r}) n(\vec{r}) , \quad (3.16)$$

where

$$n(\vec{r}) = \sum_i \delta(\vec{r} - \vec{r}_i) . \quad (3.17)$$

Note that  $\int d\vec{r} n(\vec{r}) = N_i$ , the total number of ions in the system. So we can now write

$$\begin{aligned}\langle F \rangle_\epsilon &= \frac{1}{Q(\vec{\epsilon})} \int d\vec{r} f(\vec{r}) \langle n(\vec{r}) \delta(\vec{\epsilon} - \vec{E}) \rangle \\ &= \int d\vec{r} f(\vec{r}) n_i g(\vec{r}; \vec{\epsilon}) ,\end{aligned}\tag{3.18}$$

where we have defined

$$n_i g(\vec{r}; \vec{\epsilon}) \equiv \frac{\langle n(\vec{r}) \delta(\vec{\epsilon} - \vec{E}) \rangle}{Q(\vec{\epsilon})} .\tag{3.19}$$

On expanding the delta function we have

$$n_i g(\vec{r}; \vec{\epsilon}) = \frac{1}{Q(\vec{\epsilon})} \int \frac{d\vec{\lambda}}{(2\pi)^3} e^{-i\vec{\lambda} \cdot \vec{\epsilon}} \langle n(\vec{r}) e^{i\vec{\lambda} \cdot \vec{E}} \rangle .\tag{3.20}$$

We would like to relate the average on the right-hand side of Eq. (3.20) to a functional derivative of the plasma microfield function. To do this we introduce  $G(\vec{\lambda})$ , the generating function of the microfield distribution, where

$$G(\vec{\lambda}) = \ln \tilde{Q}(\vec{\lambda}) = \ln \langle e^{i\vec{\lambda} \cdot \vec{E}} \rangle .\tag{3.21}$$

If we define a function  $\phi$ , such that

$$\phi = i\vec{\lambda} \cdot \vec{E}(\vec{r}) ,\tag{3.22}$$

then  $G(\vec{\lambda})$  becomes a functional of  $\phi$ , or

$$G(\vec{\lambda}) = G[\phi] .\tag{3.23}$$

Now we can cast  $G(\vec{\lambda})$  in the form of a functional derivative, where

$$\begin{aligned}
G(\vec{\lambda}) &= \int_0^\lambda dl \frac{\partial G(\vec{l})}{\partial l} \\
&= \int_0^\lambda dl \int d\vec{r} \frac{\partial \phi}{\partial l} \frac{\delta G[\phi]}{\delta \phi} \\
&= \int_0^\lambda dl \int d\vec{r} i\vec{l} \cdot \vec{E}(\vec{r}) \frac{\delta G[\phi]}{\delta(i\vec{l} \cdot \vec{E}(\vec{r}))},
\end{aligned} \tag{3.24}$$

where  $\vec{l} = l\hat{\lambda}$  and  $\hat{\lambda}$  is the unit vector in the direction of  $\vec{\lambda}$ .

Alternately, from the definition of  $G(\vec{\lambda})$  in Eq. (3.21), we have

$$\begin{aligned}
G(\vec{\lambda}) &= \int_0^\lambda dl \frac{\partial \ln \tilde{Q}(\vec{l})}{\partial l} \\
&= \int_0^\lambda dl \frac{\langle i\hat{\lambda} \cdot \vec{E} e^{i\vec{l} \cdot \vec{E}} \rangle}{\langle e^{i\vec{l} \cdot \vec{E}} \rangle} \\
&= \int_0^\lambda dl \frac{i\hat{\lambda} \cdot \langle \vec{E} e^{i\vec{l} \cdot \vec{E}} \rangle}{\langle e^{i\vec{l} \cdot \vec{E}} \rangle}.
\end{aligned} \tag{3.25}$$

Note that we can write,

$$\begin{aligned}
i\hat{\lambda} \cdot \vec{E} &= \int d\vec{r} i\hat{\lambda} \cdot \vec{E}(\vec{r}) \sum_{i=1}^N \delta(\vec{r} - \vec{r}_i) \\
&= \int d\vec{r} i\hat{\lambda} \cdot \vec{E}(\vec{r}) n(\vec{r}).
\end{aligned} \tag{3.26}$$

Using Eqs. (3.25) with (3.26) gives

$$\ln \tilde{Q}(\vec{\lambda}) = \int_0^\lambda dl \int d\vec{r} i\hat{\lambda} \cdot \vec{E}(\vec{r}) \frac{\langle n(\vec{r}) e^{i\vec{l} \cdot \vec{E}} \rangle}{\langle e^{i\vec{l} \cdot \vec{E}} \rangle}. \tag{3.27}$$

Comparison of Eqs. (3.24) and (3.27) gives us the connection between the constrained average considered here,  $\langle F \rangle_\epsilon$ , and a functional derivative of the microfield generating functional  $G[\phi]$ :

$$\frac{\langle n(\vec{r}) e^{i\vec{l} \cdot \vec{E}} \rangle}{\langle e^{i\vec{l} \cdot \vec{E}} \rangle} = \frac{\delta G[\phi]}{\delta(i\vec{l} \cdot \vec{E}(\vec{r}))}; \tag{3.28}$$

which on substitution into Eq. (3.20) above, gives

$$n_i g(\vec{r}; \vec{\epsilon}) = \frac{1}{Q(\vec{\epsilon})} \int \frac{d\vec{\lambda}}{(2\pi)^3} e^{-i\vec{\lambda} \cdot \vec{\epsilon}} \tilde{Q}(\vec{\lambda}) \frac{\delta G[\phi]}{\delta(i\vec{\lambda} \cdot \vec{E}(\vec{r}))}. \quad (3.29)$$

Substitution into Eq. (3.18) above gives us the relationship we want:

$$\langle F \rangle_\epsilon = \frac{1}{Q(\vec{\epsilon})} \int d\vec{r} f(\vec{r}) \int \frac{d\vec{\lambda}}{(2\pi)^3} e^{-i\vec{\lambda} \cdot \vec{\epsilon}} \tilde{Q}(\vec{\lambda}) \frac{\delta G[\phi]}{\delta(i\vec{\lambda} \cdot \vec{E}(\vec{r}))}. \quad (3.30)$$

This explicitly shows that we can relate the constrained average to a functional derivative of a microfield generating function  $G(\vec{\lambda}) = \ln \tilde{Q}(\vec{\lambda})$ . We are free to use whatever functional model we choose for  $\tilde{Q}(\vec{\lambda})$ .

As an aid in evaluating these constrained averages we define the transform of  $g(\vec{r}; \vec{\epsilon})$  by

$$\tilde{g}(\vec{r}; \vec{\lambda}) \equiv \frac{1}{n_i} \frac{\delta G[\phi]}{\delta(i\vec{\lambda} \cdot \vec{E}(\vec{r}))}. \quad (3.31)$$

From Eqs. (3.20) and (3.28) we see that the transforms are related by

$$g(\vec{r}; \vec{\epsilon}) = \frac{1}{Q(\vec{\epsilon})} \int \frac{d\vec{\lambda}}{(2\pi)^3} e^{-i\vec{\lambda} \cdot \vec{\epsilon}} \tilde{Q}(\vec{\lambda}) \tilde{g}(\vec{r}; \vec{\lambda}). \quad (3.32)$$

Thus a knowledge of  $\tilde{g}(\vec{r}; \vec{\lambda})$  obtained from  $\tilde{Q}(\vec{\lambda})$  will lead to  $g(\vec{r}; \vec{\epsilon})$  through the transform and then to  $\langle F \rangle_\epsilon$  through Eq. (3.18).

To evaluate the ion-quadrupole term recall that the perturbed radiator Hamiltonian is

$$H_r(\epsilon, \langle E_{\mu\nu} \rangle_\epsilon) = H_r(\epsilon) - \frac{1}{6} \sum_{i,j} Q_{i,j} \langle E_{ij} \rangle_\epsilon, \quad (3.33)$$

where the ion-quadrupole term is just  $V_{r,i}$ . To evaluate the  $\langle E_{ij} \rangle_\epsilon$  terms note that when the angular integrations are performed, the  $\varphi$ , or azimuthal, integrals lead explicitly to<sup>42</sup>

$$\langle E_{xy} \rangle_\epsilon = \langle E_{yz} \rangle_\epsilon = \langle E_{zx} \rangle_\epsilon = 0 . \quad (3.34)$$

Together with the property  $\partial_j E_i = \partial_i E_j$ , this leads to the simplification

$$\sum_{i,j} Q_{i,j} \langle E_{ij} \rangle_\epsilon = \sum_i Q_{ii} \langle E_{ii} \rangle_\epsilon . \quad (3.35)$$

With the field in the  $z$  direction there is no difference between the  $x$  and  $y$  directions so  $\langle E_{xx} \rangle_\epsilon = \langle E_{yy} \rangle_\epsilon$ . Additionally, with the tracelessness of the quadrupole tensor<sup>41</sup> we have

$$\begin{aligned} \sum_{i,j} Q_{i,j} \langle E_{ij} \rangle_\epsilon &= Q_{zz} (\langle E_{zz} \rangle_\epsilon - \langle E_{xx} \rangle_\epsilon) \\ &= -\frac{3}{2} Q_{zz} \left( \langle E_{zz} \rangle_\epsilon - \frac{1}{3} \langle \vec{\nabla} \cdot \vec{E} \rangle_\epsilon \right) . \end{aligned} \quad (3.36)$$

If the ion interaction potentials are screened we have  $\vec{\nabla} \cdot \vec{E} \neq 0$  due to the continuous charge distribution. However, the form of the multipole expansion we have employed made use of  $\vec{\nabla} \cdot \vec{E} = 0$  at the origin which is not strictly true for our screened ion potentials. We reconcile these two facts by noting that if we restrict the screening charge density of the perturbing ions to lie outside the Bohr orbit of the radiator's bound electron, we will have  $\vec{\nabla} \cdot \vec{E} = 0$  at the origin. Tests of the computation of the field gradient term show that its value upon taking  $\vec{\nabla} \cdot \vec{E} = 0$  is approximately 20% less than that obtained on taking  $\vec{\nabla} \cdot \vec{E} \neq 0$  at a field value corresponding to the maximum of the microfield probability function at  $n_e = 1 \times 10^{25} \text{ cm}^{-3}$  and  $kT = 800 \text{ eV}$ . The difference is less for lower densities. In light of the uncertain nature of the actual form of the ion potential, this does not seem unreasonable. Consequently, we will take  $\vec{\nabla} \cdot \vec{E} = 0$  in the evaluation of the field gradient term in agreement with the form of our multipole expansion. This amounts to requiring that we have

no penetration of the radiator by the perturbing ions or their screening charge density. For the ion-quadrupole term this gives us

$$V_{r,i} = -\frac{1}{4}Q_{zz}\langle E_{zz}\rangle_\epsilon, \quad (3.37)$$

with the radiator Hamiltonian given by  $H_r(\epsilon) + V_{r,i}$ . To evaluate  $V_{r,i}$  we must calculate the constrained average term  $\langle E_{zz}\rangle_\epsilon$ , and to do this we must pick a model for the microfield function  $Q(\epsilon)$ .

In this dissertation we choose the adjustable parameter exponential approximation (APEX)<sup>53,54,55,56</sup> for the microfield. It has the advantage of incorporating correlations between the perturbing ions while retaining the functional simplicity of the independent particle (IP) model<sup>42</sup> of the microfield. Joyce<sup>42,12</sup> used the IP model to evaluate the ion-quadrupole effect which we will see leads to an overestimate of its magnitude due to the neglect of the inter-ion correlations. We will compare these two models along with a nearest neighbor (NN) approximation for the field gradient.

The APEX model for the microfield is based on the independent particle model but with an effective inverse screening length,  $\alpha$ . The field is effectively renormalized in this way by requiring that two conditions<sup>54</sup> be met: the so called second moment condition and the local field condition (see Appendix B). The transformed conditional distribution function  $\tilde{g}(\vec{r}; \vec{\lambda})$  for the APEX microfield distribution is given by (see Appendix B)

$$\tilde{g}(\vec{r}; \vec{\lambda}) = g(r)e^{i\vec{\lambda} \cdot \vec{E}^*(\vec{r})}, \quad (3.38)$$

where  $g(r)$  is the equilibrium radial distribution function and  $\vec{E}^*(\vec{r})$  is the APEX renormalized field. This field is given by

$$\vec{E}^*(\vec{r}) = \vec{E}(\vec{r})(1 + \alpha r)e^{-\alpha r}, \quad (3.39)$$

where  $\alpha$  is determined by the second moment of  $Q(\vec{\epsilon})$ , and  $\vec{E}(\vec{r})$  is the screened field produced by the plasma ions. We calculate the radial distribution function  $g(r)$  by integral equation methods due to Rogers.<sup>39</sup> Lado and Dufty<sup>57</sup> have shown that this method of calculating  $g(\vec{r}; \vec{\epsilon})$  by using the APEX microfield underestimates the inter-ion correlations in some cases. In particular, for the case of a hydrogen plasma with  $\Gamma_{ii} = 10$  at a field value of  $\epsilon/\epsilon_o = 0.4$  ( $\epsilon_o = e/r_{o,i}^2$ ), the APEX calculation underestimates the maximum value of  $g(\vec{r}; \vec{\epsilon})$  by a factor of two. We retain the APEX model, however, because of its simplicity and significant improvement over the IP model of Joyce<sup>12,42</sup> which ignores ion-ion correlations entirely.

With the APEX model for  $g(\vec{r}; \vec{\epsilon})$  obtained from Eqs. (3.32) and (3.38) we can evaluate the constrained average by using Eq. (3.18) to obtain

$$\langle F \rangle_\epsilon = \frac{n_i}{Q(\vec{\epsilon})} \int d\vec{r} f(\vec{r}) g(r) Q\left(\vec{\epsilon} - \vec{E}^*(\vec{r})\right), \quad (3.40)$$

where it is understood that the microfield distributions,  $Q(\vec{\epsilon})$ , are in the APEX approximation.

For the ion-quadrupole effect, the constrained average we need to evaluate is  $\langle E_{zz} \rangle_\epsilon$ . In particular, we have

$$F = E_{zz} = \sum_i \epsilon_{zz}(r_i). \quad (3.41)$$

In general, the one perturber derivative term is given by

$$\epsilon_{\mu\nu}(r) = Z e \frac{e^{-r/\lambda}}{r^3} \left(1 + \frac{r}{\lambda}\right) \left(\delta_{\mu,\nu} - 3 \frac{x_\mu x_\nu}{r^2}\right), \quad (3.42)$$

so for our case we have

$$\varepsilon_{zz}(r) = Ze \frac{e^{r/\lambda}}{r^3} \left(1 + \frac{r}{\lambda}\right) \left(1 - 3 \cos^2 \theta\right). \quad (3.43)$$

The microfield function in the APEX approximation is<sup>54</sup>

$$Q_{APEX}(\vec{\epsilon}) = \frac{1}{2\pi^2 \epsilon} \int_0^\infty dk k \sin(k\epsilon) e^{n_i h_1(k)}, \quad (3.44)$$

with

$$h_1(k) = 4\pi \int_0^\infty dr r^2 g(r) \frac{E(r)}{E^*(r)} (j_0(kE^*(r)) - 1), \quad (3.45)$$

where  $j_0(x) = \sin(x)/x$  is the zero order spherical Bessel function of the first kind. From now on when we speak of  $Q(\vec{\epsilon})$  we will implicitly assume the APEX approximation and suppress the subscript. Using this approximation we can evaluate Eq. (3.40) for the case of  $F = E_{zz}$  to obtain

$$\langle E_{zz} \rangle_\epsilon = \frac{Zen_i}{2\pi^2 Q(\vec{\epsilon})} \int_0^\infty dk k^2 e^{n_i h_1(k)} \int_0^\infty dr r^2 g(r) \frac{e^{-r/\lambda}}{r^3} (1 - r/\lambda) I_\Omega(r). \quad (3.46)$$

The angular integral  $I_\Omega$  has been evaluated by Joyce<sup>42</sup> and is given by

$$\begin{aligned} I_\Omega(r) &\equiv \int d\Omega (1 - 3 \cos^2 \theta) j_0 \left( k \left| \vec{\epsilon} - \vec{E}^*(r) \right| \right) \\ &= -8\pi j_2(k\epsilon) j_2(kE^*(r)), \end{aligned} \quad (3.47)$$

with  $d\Omega = d\varphi d(\cos \theta)$ .

To evaluate  $\langle E_{zz} \rangle_\epsilon$  numerically, we cast its variables in unitless form by taking

$$\begin{aligned}
\tilde{\epsilon} &= \epsilon/\epsilon_o \\
\tilde{k} &= \epsilon_o k \\
a &= r_{o,i}/\lambda \\
x &= r/r_{o,i} ,
\end{aligned} \tag{3.48}$$

where

$$\epsilon_o = \frac{e}{r_{o,i}^2} . \tag{3.49}$$

We obtain

$$\langle E_{zz} \rangle_\epsilon = -6\tilde{\epsilon} \left( \frac{e}{r_{o,i}^3} \right) \frac{\int_0^\infty d\tilde{k} \tilde{k}^2 e^{n_i h_1(\tilde{k})} j_2(\tilde{k}\tilde{\epsilon}) \int_0^\infty dx g(x) \frac{e^{-ax}}{x} (1+ax) j_2(\tilde{k}\tilde{E}^*(x))}{\int_0^\infty d\tilde{k} \tilde{k} e^{n_i h_1(\tilde{k})} \sin(\tilde{k}\tilde{\epsilon})} , \tag{3.50}$$

with

$$h_1(\tilde{k}) = \frac{3}{n_i} \int_0^\infty dx x^2 g(x) \frac{E(x)}{E^*(x)} \left( j_0(\tilde{k}\tilde{E}^*(x)) - 1 \right) . \tag{3.51}$$

In this form, the equation for  $\langle E_{zz} \rangle_\epsilon$  can be directly evaluated numerically. Following Joyce<sup>42</sup> we implement this function in the line shape calculation by the use of a Padé approximate. For a particular case,  $\langle E_{zz} \rangle_\epsilon$  is calculated for a mesh of  $\tilde{\epsilon}$  values. The Padé function is then fit to the calculated values by minimizing the squared difference between the two while varying the coefficients of the Padé function. The resulting approximation then yields  $\langle E_{zz} \rangle_\epsilon$  for any value of the scaled field up to  $\tilde{\epsilon} = 20$  with an accuracy of about 5% compared with the values calculated from Eq. (3.50). This is quite sufficient for calculating most line shapes. If more accurate values of the field gradient are required, the directly calculated values can be used.

We would like to examine the behavior of the field gradient term  $\langle E_{zz} \rangle_\epsilon$  in the limit of large and small values of  $\epsilon$ . For  $\epsilon \rightarrow 0$  it is easy to show that the field dependence follows the limit of  $j_2(k\epsilon)$  to lowest order in  $\epsilon$ . This will give

$$\lim_{\epsilon \rightarrow 0} \langle E_{zz} \rangle_\epsilon = -C \tilde{\epsilon}^2, \quad (3.52)$$

where  $C$  is a constant that depends on  $n_e$ ,  $T$  and  $Z_i$ . Thus, the zero field limit is zero. This is easy to see physically. If  $\epsilon = 0$  there will be no preferred direction about the radiator and the fluctuations in the field gradient  $E_{zz}$  will sum to zero upon averaging over the ensemble of ion configurations. The  $\epsilon \rightarrow \infty$  limit is somewhat more complicated so we will examine the behavior of a simple nearest neighbor model for  $\langle E_{zz} \rangle_\epsilon$ . The large field behavior of the microfield at a charged radiator is governed by a single nearest neighbor ion.<sup>58,59</sup> For the strongest fields, the nearest neighbor will be significantly inside the screening length  $\lambda_{D,e}$  so screening will be negligible. To approximate  $\langle E_{zz} \rangle_\epsilon$  let the field gradient at the radiator be that produced by a single ion located at the distance from the radiator sufficient to give a field value at the radiator of  $\epsilon$ . This gives us the nearest neighbor approximation of

$$\langle E_{zz} \rangle_{\epsilon,NN} = -\frac{2}{\sqrt{Z_i}} \left( \frac{e}{r_{o,i}^3} \right) \tilde{\epsilon}^{3/2}, \quad (3.53)$$

for large  $\epsilon$ .

In Fig. (3.1) we compare three different models for  $\langle E_{zz} \rangle_\epsilon$ . For purposes of comparison, we take  $(e/r_{o,i}^3) = 1$ . We look at the APEX model which includes ion-ion correlations, the independent particle model of Joyce<sup>42</sup> which ignores ion-ion correlations and the nearest neighbor model for large fields as discussed above. We see that the APEX model gives a field gradient whose magnitude is consistently smaller than that of the other two. This is to be expected since the

ion-ion correlations tend to cause the plasma ions to repel each other and thus to be less likely to converge on the radiator and create a large gradient. The ion-ion correlations will, in general, lessen plasma ion microfields by causing a rough ordering of plasma ions. The nearest neighbor model produces the largest gradient due to its assumption of all charge located on the  $z$  axis. It also includes no correlation effects. The IP model of Joyce falls in between because it includes radiator-ion correlations but no ion-ion correlations.

In Fig. (3.2) we examine the behavior of the APEX model for the field gradient at several values of the electron number density. For  $n_e = 1 \times 10^{24} \text{ cm}^{-3}$  the average  $E_{zz}$  gradient's magnitude is less than that of the nearest neighbor model as was pointed out above. As the density increases the APEX field gradient approaches that of the nearest neighbor model for all relevant values of the field (in this case we refer to a range of field values of  $\epsilon/\epsilon_0 = 0$  to 5). For a particular density, we can see that the gradient also approaches the nearest neighbor value as the field increases. This behavior can be explained by recalling that the presence of large fields at the radiator is generally due to the location of a nearest neighbor perturbing ion close to the radiator. The large field behavior at constant density should be due to a nearest neighbor ion and ion-ion correlations play little role in the interaction of two nearest neighbors at these densities. The probability is small for having a positively charged perturbing ion close to the positively charged radiator. It is even less probable to have two ions close to a positively charged radiator; and we need two for ion-ion correlations to be important. The approach of  $\langle E_{zz} \rangle_\epsilon$  toward the nearest neighbor value as density increases should be due, simply, to the ions being forced closer to the radiator. With decreased interparticle spacing the field gradient naturally increases.

### 3.2 Atomic Data by Perturbation Theory Solution

To evaluate the radiator subsystem matrix elements necessary for the calculation of the spectral line shape  $I(\omega)$ , we are free to use any complete set of basis states that spans the Hilbert space of the system. A true representation of an operator in this basis will thus consist of a matrix whose dimension is the same as the number of basis vectors necessary to span the particular Hilbert space. For our case this dimension is a nondenumerable infinity. However, a reasonable representation of the operator can be obtained by using a truncated set of basis vectors. For weak fields, a reasonable representation of the Hamiltonian for a radiator in the state with principal quantum number  $n$  can be obtained by using eigenvectors of the field-free radiator Hamiltonian for states  $n$  and  $n + 1$  as basis vectors.<sup>60</sup> For stronger fields, the need to include other states, including positive energy states, will be necessary. In fact, the resonance nature of the strong-field states can not be described without including positive energy states to account for the unbound character of field dependent solutions that allow for the possibility of tunneling. In order to include these effects we will employ an alternative method using a basis set that consists of the eigenvectors of a radiator Hamiltonian that includes the ion-dipole term from the perturbing-ion multipole expansion. This Hamiltonian is

$$H_r(\vec{\epsilon}) = H_r^0 - \vec{d} \cdot \vec{\epsilon}. \quad (3.54)$$

$H_r(\vec{\epsilon})$  is diagonal in this field dependent basis set. By using this Hamiltonian, we will automatically incorporate the characteristics of the resonate nature of the states into our basis. Specifically, we will use  $H_r(\vec{\epsilon})$  as our zero order radiator Hamiltonian. The first order correction to this will be the next term in the perturbing-ion multipole expansion, the ion-quadrupole term  $V_{r,i}$ .

To calculate our field dependent basis we solve Schrödinger's equation in the position representation with the Hamiltonian  $H_r(\vec{\epsilon})$ . The equation is

$$H_r(\vec{\epsilon})\psi(\vec{r}) = E\psi(\vec{r}) . \quad (3.55)$$

The natural coordinates to use for this Hamiltonian are parabolic coordinates.<sup>61,62</sup> The wave equation will then be separable. Assuming the plasma microfield to be in the  $z$  direction, we write Eq. (3.55) in atomic units (see Appendix A) and scaled to  $Z = 1$  as

$$\left( \nabla^2 + \frac{2}{r} + 2E - 2Fz \right) \psi(\vec{r}) = 0 , \quad (3.56)$$

where  $F$  is the magnitude of the plasma ion microfield. In parabolic coordinates (see Appendix C), Schrödinger's equation becomes

$$\begin{aligned} & \frac{4}{\xi + \eta} \frac{\partial}{\partial \xi} \left( \xi \frac{\partial \psi}{\partial \xi} \right) + \frac{4}{\xi + \eta} \frac{\partial}{\partial \eta} \left( \eta \frac{\partial \psi}{\partial \eta} \right) + \frac{1}{\xi \eta} \frac{\partial^2 \psi}{\partial \varphi^2} \\ & + \left\{ \frac{4}{(\xi + \eta)} + 2E - F(\xi - \eta) \right\} \psi = 0 . \end{aligned} \quad (3.57)$$

We exploit the separability of the equation by looking for a solution of the form:

$$\psi(\vec{r}) = f(\xi)g(\eta) \frac{e^{\pm im\varphi}}{\sqrt{2\pi}} . \quad (3.58)$$

We define new scaled variables and transform the two resulting separated equations. We take

$$\begin{aligned} x & \equiv \xi/n \\ y & \equiv \eta/n \\ \lambda & \equiv (1/4)n^3 F , \end{aligned} \quad (3.59)$$

and obtain the system of equations

$$\left\{ \frac{d}{dx}x \frac{d}{dx} - \frac{m^2}{4x} + \frac{n^2}{2}Ex - \lambda x^2 + A \right\} f(x) = 0 , \quad (3.60)$$

and

$$\left\{ \frac{d}{dy}y \frac{d}{dy} - \frac{m^2}{4y} + \frac{n^2}{2}Ey + \lambda y^2 + B \right\} g(y) = 0 , \quad (3.61)$$

with

$$A + B = n . \quad (3.62)$$

### Field-Free Solution

For the field-free case we take  $\lambda = 0$  and obtain the solutions (in  $Z = 1$  atomic units)

$$\begin{aligned} E_0 &= -\frac{1}{2n^2} \\ A_0 &= n_1 + \frac{m+1}{2} \\ B_0 &= n_2 + \frac{m+1}{2} , \end{aligned} \quad (3.63)$$

with

$$n = n_1 + n_2 + m + 1 . \quad (3.64)$$

Here  $n_1$  and  $n_2$  are the integer valued parabolic quantum numbers.<sup>61</sup> The field-free eigenfunctions are

$$\begin{aligned} f_0(x) &= u(n_1, m, x) \\ g_0(y) &= u(n_2, m, y) . \end{aligned} \quad (3.65)$$

where

$$u(n_1, m, x) = \frac{\sqrt{n_1!}x^{m/2}}{[(n_1 + m)!]^{3/2}} e^{-x/2} L_{n_1}^m(x) . \quad (3.66)$$

$L_{n_1}^m(x)$  is an associated Laguerre polynomial given by<sup>63</sup>

$$L_{n_1}^m(x) = [(n_1 + m)!]^2 \sum_{p=0}^{n_1} \frac{(-x)^p}{(m + p)! (n_1 - p)! p!} . \quad (3.67)$$

For our case  $m$  is restricted to integers for which  $m \geq 0$ . Other definitions of  $L_{n_1}^m(x)$  are quite common.<sup>33</sup>

### Field Dependent Solution

In order to solve Eqs. (3.60) and (3.61) for  $\lambda \neq 0$  we will expand the unknowns  $f(x)$ ,  $g(y)$ ,  $A$ ,  $B$  and  $E$  in powers of  $\lambda$ . The zero order terms will be given by the  $\lambda = 0$  results above. This perturbation expansion technique closely follows the work of Hoe et al.<sup>64,65</sup> The expansions are

$$\begin{aligned} E &= -\frac{1}{2n^2} \left[ 1 + 4 \sum_{p \geq 1} \nu_p \lambda^p \right] \\ A &= \sum_{p \geq 0} A_p \lambda^p \\ B &= \sum_{p \geq 0} B_p \lambda^p \\ f(x) &= \sum_{p \geq 0} \lambda^p \sum_{h \geq -n_1} a_p^h u(n_1 + h, m, x) \\ g(y) &= \sum_{p \geq 0} \lambda^p \sum_{h \geq -n_2} b_p^h u(n_2 + h, m, y) . \end{aligned} \quad (3.68)$$

The sums for index  $h$  are over all possible values of  $n_1$  and  $n_2$ . Upon evaluation of the coefficients  $a_p^h$  and  $b_p^h$ , however, we will find that all terms in the sum are zero except for  $\max(-n_1, -2p) \leq h \leq 2p$ . This is also true for the sum involving  $n_2$ . We immediately see that because of the condition  $A + B = n$ , we have

$$A_0 + B_0 = n \quad (3.69)$$

and

$$B_p = -A_p \quad \text{for } p > 0 . \quad (3.70)$$

The other coefficients in the expansion can be obtained by solving for the  $p$ 'th coefficients in terms of the  $p-1$  and lower coefficients. Thus, a knowledge of the zero order terms will allow us to construct all higher order terms iteratively. To accomplish this we substitute the expansions for  $f(x)$  and  $g(y)$  into Eqs. (3.60) and (3.61), multiply by  $u(x)$  and  $u(y)$  and integrate over  $x$  and  $y$ , respectively. For the  $x$  coordinate we obtain

$$\int_0^\infty dx u(n_1 + k, m, x) \left\{ H_0(x) + A + \frac{x}{4}(1 + 2n^2 E) - \lambda x^2 \right\} f(x) = 0 , \quad (3.71)$$

where

$$H_0(x) = \frac{d}{dx} x \frac{d}{dx} - \frac{m^2}{4x} - \frac{x}{4} . \quad (3.72)$$

Following Hoe et al<sup>64,65</sup> we call  $H_0(x)$  the field-free effective Hamiltonian for the  $x$  coordinate. It gives

$$H_0(x)u(n_1 + h, m, x) = -A_0 u(n_1 + h, m, x) , \quad (3.73)$$

with

$$A_0 = n_1 + h + \frac{m + 1}{2} . \quad (3.74)$$

Carrying out the integration gives

$$\begin{aligned} \sum_{p \geq 0} \lambda^p \sum_{\max(-n_1, -2p)}^{2p} a_p^h \left\{ \int_0^\infty dx u(n_1 + k, m, x) H_0(x) u(n_1 + h, m, x) \right. \\ \left. + A \delta_{k,h} + (1/4)(1 + 2n^2 E)(x)_{k,h} - \lambda (x^2)_{k,h} \right\} = 0 , \end{aligned} \quad (3.75)$$

where

$$(x^n)_{k,h} \equiv \int_0^\infty dx x^n u(n_1 + k, m, x) u(n_1 + h, m, x) \quad (3.76)$$

and

$$\int_0^\infty dx u(n_1 + k, m, x) u(n_1 + h, m, x) = \delta_{k,h} . \quad (3.77)$$

Upon expanding  $E$  and  $A$  in powers of  $\lambda$ , we see that the  $p$ 'th coefficient is given by

$$ka_p^k = \sum_{i=0}^{p-1} A_{p-i} a_i^k - \sum_{h \geq \max(-n_1, -2p)}^{2p} \left\{ (x^2)_{k,h} a_{p-1}^h + (x)_{k,h} \sum_{i=0}^{p-1} \nu_{p-i} a_i^h \right\} . \quad (3.78)$$

If the maximum value of the sum index is less than the starting value of the index, then the sum is defined to be zero. We will return to the special case of  $k = 0$  below.

Likewise, we obtain for the  $y$  coordinate

$$kb_p^k = \sum_{i=0}^{p-1} B_{p-i} b_i^k + \sum_{h \geq \max(-n_2, -2p)}^{2p} \left\{ (y^2)_{k,h} b_{p-1}^h - (y)_{k,h} \sum_{i=0}^{p-1} \nu_{p-i} b_i^h \right\} . \quad (3.79)$$

For  $p = 0$  we must have

$$a_0^h = b_0^h = \delta_{0,h} . \quad (3.80)$$

To obtain the energy coefficients  $\nu_p$  we take the  $k = 0$  case of Eqs. (3.78) and (3.79). We obtain two equations for  $A_p$ . Equating these and solving for  $\nu_p$  gives

$$\begin{aligned} \nu_p = & \frac{1}{2n} \sum_{i=1}^{p-1} A_{p-i} \left( a_i^0 - b_i^0 \right) \\ & + \frac{1}{2n} \sum_h \left\{ (y^2)_{0,h} b_{p-1}^h - (x^2)_{0,h} a_{p-1}^h - \sum_{i=1}^{p-1} \nu_{p-i} \left[ (x)_{0,h} a_i^h + (y)_{0,h} b_i^h \right] \right\} . \end{aligned} \quad (3.81)$$

The sum over  $h$  is indexed from  $\max(-n_1, -2p)$  or  $\max(-n_2, -2p)$  to  $2p$  as appropriate.

We still need to evaluate the coefficients  $a_p^k$  and  $b_p^k$  for  $k = 0$ . To accomplish this note that

$$\int_0^\infty dx f^2(x) = 1 , \quad (3.82)$$

and

$$\int_0^\infty dy g^2(y) = 1 . \quad (3.83)$$

Evaluating these by using the series expansions for  $f(x)$  and  $g(y)$  and examining the coefficients of a particular term of order  $\lambda^p$  will give

$$a_p^0 = -\frac{1}{2} \sum_{h \geq \max(-n_1, -2p)}^{2p} \sum_{i=1}^{p-1} a_i^h a_{p-i}^h , \quad (3.84)$$

and

$$b_p^0 = -\frac{1}{2} \sum_{h \geq \max(-n_2, -2p)}^{2p} \sum_{i=1}^{p-1} b_i^h b_{p-i}^h . \quad (3.85)$$

We now have the coefficients for calculating the energy  $E$  and the components of the wavefunctions  $f(x)$  and  $g(y)$ . To evaluate these we need the integrals  $(x)_{k,h}$  and  $(x^2)_{k,h}$  as well as those for  $(y)_{k,h}$  and  $(y^2)_{k,h}$ . These can be straightforwardly evaluated to give

$$\begin{aligned}
(x)_{k,h} &= (2n_1 + 2k + m + 1)\delta_{k,h} \\
&\quad - \sqrt{(n_1 + k + 1)(n_1 + k + m + 1)}\delta_{k+1,h} \\
&\quad - \sqrt{(n_1 + k)(n_1 + k + m)}\delta_{k-1,h},
\end{aligned} \tag{3.86}$$

and

$$\begin{aligned}
(x^2)_{k,h} &= \{6(n_1 + k)(n_1 + k + m + 1) + (m + 1)(m + 2)\}\delta_{k,h} \\
&\quad - 2\sqrt{(n_1 + k + 1)(n_1 + k + m + 1)}(2n_1 + 2k + m + 2)\delta_{k+1,h} \\
&\quad - 2\sqrt{(n_1 + k)(n_1 + k + m)}(2n_1 + 2k + m)\delta_{k-1,h} \\
&\quad + \sqrt{(n_1 + k + 2)(n_1 + k + m + 1)(n_1 + k + 1)(n_1 + k + m + 2)}\delta_{k+2,h} \\
&\quad + \sqrt{(n_1 + k)(n_1 + k + m - 1)(n_1 + k + m)(n_1 + k - 1)}\delta_{k-2,h} .
\end{aligned} \tag{3.87}$$

The relations for  $(y)_{k,h}$  and  $(y^2)_{k,h}$  are obtained from these formulae by taking  $x \rightarrow y$  and  $n_1 \rightarrow n_2$ .

### Normalization

In order to compute matrix elements from the field dependent wave functions given in Eq. (3.58), we also need to determine their normalization. We take the normalization constant to be

$$N(n_1, n_2, m, \lambda) \equiv \frac{n^3}{4} \int_0^\infty \int_0^\infty dx dy (x + y)[f(x)g(y)]^2 . \tag{3.88}$$

Expanding  $N(n_1, n_2, m, \lambda)$  in powers of  $\lambda$  we have

$$N(n_1, n_2, m, \lambda) = \sum_{p \geq 0} N_p \lambda^p . \tag{3.89}$$

To evaluate the coefficients  $N_p$ , we expand the functions  $f(x)$  and  $g(y)$  in powers of  $\lambda$ , matching terms on the right- and left-hand sides to obtain

$$N_p = \frac{n^3}{4} \sum_{i=0}^p \sum_{h,k} \left[ a_i^h a_{p-i}^k(x)_{h,k} + b_i^h b_{p-i}^k(y)_{h,k} \right] . \quad (3.90)$$

The second sum is indexed from  $\max(-n_1, -2p)$  or  $\max(-n_2, -2p)$  to  $2p$  as appropriate. Note that

$$N_0 = \frac{1}{2} n^4 . \quad (3.91)$$

### Dipole Matrix Elements

Now that we have developed the formulae for the perturbation solution of the Schrödinger equation for a radiator in the presence of a uniform electric field, we can go on to calculate the dipole and quadrupole matrix elements needed for the calculation of the spectral line shape  $I(\omega)$ . Since we know the wave functions only in terms of their perturbation expansions, it will be necessary to develop perturbation expansions for the matrix elements as well.

We will follow the calculation of the atomic matrix element of the coordinate  $z$  as an example. The matrix elements for  $x$  and  $y$ , as well as the quadrupole matrix elements are calculated in the same way and only the results are presented here. Further details concerning the technique can be found in the references of Hoe et al.<sup>64,65</sup>

We wish to calculate the atomic matrix element

$$\langle \psi(n'_1, n'_2, m', \lambda') | z | \psi(n_1, n_2, m, \lambda) \rangle .$$

The normalized wave function is given by

$$\psi = \psi(n_1, n_2, m, \lambda) = \frac{1}{\sqrt{2\pi N(n_1, n_2, m, \lambda)}} f_{n_1 m \lambda}(\xi) g_{n_2 m \lambda}(\eta) e^{im\varphi} , \quad (3.92)$$

so the matrix element of the  $z$  coordinate of the radiator's bound electron is

$$\begin{aligned}
 \langle \psi' | z | \psi \rangle &= \frac{1}{2} \int d^3x (\xi - \eta) \psi^*(n'_1, n'_2, m', \lambda') \psi(n_1, n_2, m, \lambda) \\
 &= \frac{1}{8} \int_0^\infty \int_0^\infty \int_0^{2\pi} d\xi d\eta d\varphi (\xi^2 - \eta^2) \psi^*(n'_1, n'_2, m', \lambda') \psi(n_1, n_2, m, \lambda) \\
 &= \frac{\delta_{mm'}}{8\Phi} \int_0^\infty \int_0^\infty d\xi d\eta (\xi^2 - \eta^2) \\
 &\quad \times f_{n'_1 m' \lambda'}(\xi/n') f_{n_1 m \lambda}(\xi/n) g_{n'_2 m' \lambda'}(\eta/n') g_{n_2 m \lambda}(\eta/n) ,
 \end{aligned} \tag{3.93}$$

where

$$\Phi \equiv \sqrt{N(n'_1 n'_2 m' \lambda') N(n_1 n_2 m \lambda)} . \tag{3.94}$$

As a notational simplification, take

$$Z_{n_1 n_2 m}^{n'_1 n'_2 m'} \equiv \langle \psi' | z | \psi \rangle . \tag{3.95}$$

In order to evaluate  $\Phi$ , consider

$$\begin{aligned}
 \mathcal{N} &= N(n'_1, n'_2, m', \lambda') N(n_1, n_2, m, \lambda) \\
 &= \sum_{p' \geq 0} N'_{p'} \left( \frac{1}{4} n'^3 F \right)^{p'} \sum_{p \geq 0} \left( \frac{1}{4} n^3 F \right)^p \\
 &= \sum_{p' \geq 0} \sum_{p \geq 0} Q'_{p'} Q_p F^{p'+p} \\
 &= \sum_{p \geq 0} \sum_{i=0}^p Q'_i Q_{p-i} F^p \\
 &= \sum_{p \geq 0} \mathcal{N}_p F^p .
 \end{aligned} \tag{3.96}$$

We have defined

$$Q_p \equiv \left( \frac{n^3}{4} \right)^p N_p , \tag{3.97}$$

and

$$\mathcal{N}_p \equiv \sum_{i=0}^p Q'_i Q_{p-i} . \quad (3.98)$$

This gives us an expansion for  $\mathcal{N}$  in powers of the field  $F$ . Next, we use this to obtain the expansion of  $\Phi$ . Since  $\Phi = \sqrt{\mathcal{N}}$ , we have

$$\Phi^2 = \mathcal{N} . \quad (3.99)$$

If we expand  $\Phi$  and  $\mathcal{N}$  in powers of  $\lambda$  and multiply it out, we obtain

$$\sum_{p \geq 0} \sum_{i=0}^p \Phi_i \Phi_{p-i} F^p = \sum_{p \geq 0} \mathcal{N}_p F^p . \quad (3.100)$$

So,

$$\begin{aligned} \mathcal{N}_p &= \sum_{i=0}^p \Phi_i \Phi_{p-i} \\ &= \sum_{i=1}^{p-1} \Phi_i \Phi_{p-i} + 2\Phi_0 \Phi_p . \end{aligned} \quad (3.101)$$

Note that  $p = 0$  gives

$$\Phi_0 = \sqrt{\mathcal{N}_0} = \sqrt{N'_0 N_0} . \quad (3.102)$$

Solving for  $\Phi_p$  gives

$$\Phi_p = \frac{\mathcal{N}_p - \sum_{i=1}^{p-1} \Phi_i \Phi_{p-i}}{2\sqrt{\mathcal{N}_p}} \quad \text{for } p \geq 1 , \quad (3.103)$$

or in terms of the more basic quantities

$$\Phi_p = \frac{1}{n'^2 n^2} \left\{ \frac{1}{4^p} \sum_{i=0}^p (n'^3)^i (n^3)^{p-i} N'_i N_{p-i} - \sum_{i=1}^{p-1} \Phi_i \Phi_{p-i} \right\} , \quad (3.104)$$

for  $p \geq 1$ . For the  $p = 0$  case, we have

$$\Phi_0 = \frac{1}{2} n'^2 n^2. \quad (3.105)$$

To proceed with the evaluation of  $Z_{n_1 n_2 m}^{n'_1 n'_2 m'}$ , return to Eq. (3.93). We can separate the functions of the two coordinates to obtain

$$Z_{n_1 n_2 m}^{n'_1 n'_2 m'} = \frac{\delta_{m, m'}}{8\Phi} \left\{ F^{(2)} G^{(0)} - F^{(0)} G^{(2)} \right\}, \quad (3.106)$$

where

$$F^{(\alpha)} \equiv \int_0^\infty d\xi \xi^\alpha f_{n'_1 m' \lambda'}(\xi/n') f_{n_1 m \lambda}(\xi/n), \quad (3.107)$$

and

$$G^{(\alpha)} \equiv \int_0^\infty d\eta \eta^\alpha g_{n'_2 m' \lambda'}(\eta/n') g_{n_2 m \lambda}(\eta/n). \quad (3.108)$$

The orthogonality condition will not apply since we are dealing with integrals of the form  $\int_0^\infty d\xi f'(\xi/n') f(\xi/n)$  and in general  $n' \neq n$ .

To evaluate Eqs. (3.107) and (3.108), we expand their left-hand sides in powers of  $F$  to obtain

$$\begin{aligned} F^{(\alpha)} &= \sum_{p \geq 0} F_p^{(\alpha)} F^p \\ G^{(\alpha)} &= \sum_{p \geq 0} G_p^{(\alpha)} F^p. \end{aligned} \quad (3.109)$$

Expanding the right-hand sides of the integrals and rearranging as a series in increasing powers of  $F$  allows us to equate terms of like powers in  $F$  from both sides to obtain

$$\begin{aligned} F_p^{(\alpha)} &= \frac{1}{4^p} \sum_{h,k} I_{k,h}^{(\alpha)} \sum_{i=0}^p n'^{3i} n^{3(p-i)} a_i^h a_{p-i}^k \\ G_p^{(\alpha)} &= \frac{1}{4^p} \sum_{h,k} J_{k,h}^{(\alpha)} \sum_{i=0}^p n'^{3i} n^{3(p-i)} b_i^h b_{p-i}^k, \end{aligned} \quad (3.110)$$

where the sums over  $h$  and  $k$  are as before, and where

$$I_{k,h}^{(\alpha)} \equiv \int_0^\infty d\xi \xi^\alpha u(n_1 + k, m, \xi/n) u(n'_1 + h, m', \xi/n') , \quad (3.111)$$

and

$$J_{k,h}^{(\alpha)} \equiv \int_0^\infty d\eta \eta^\alpha u(n_2 + k, m, \eta/n) u(n'_2 + h, m', \eta/n') . \quad (3.111)$$

$I_{k,h}^{(\alpha)}$  can be evaluated from the definition of  $u(n_1, m, \eta/n)$  to obtain

$$\begin{aligned} I_{k,h}^{(l)} &= \left( \frac{2nn'}{n+n'} \right)^{l+1} \sqrt{(n_1+k)!(n_1+k+m)!(n'_1+h)(n'_1+h+m)!} \\ &\times \left( \frac{2n'}{n+n'} \right)^{\frac{m}{2}} \left( \frac{2n}{n+n'} \right)^{\frac{m'}{2}} \sum_{q=0}^{n_1+k} \sum_{s=0}^{n'_1+h} \left( \frac{-2n'}{n+n'} \right)^q \left( \frac{-2n}{n+n'} \right)^s \\ &\times \frac{\left( l + \frac{m+m'}{2} + q + s \right)!}{(m+q)!(n_1+k-q)!q!(m'+s)!(n'_1+h-s)!s!} . \end{aligned} \quad (3.112)$$

For  $J_{k,h}^{(l)}$ , just take  $n_1 \rightarrow n_2$  in Eq. (3.112).

To evaluate  $Z_{n_1 n_2 m}^{n'_1 n'_2 m'}$  we use the expansions for  $F^{(\alpha)}$  and  $G^{(\alpha)}$ . We obtain

$$Z_{n_1 n_2 m}^{n'_1 n'_2 m'} = \frac{T_{n_1 n_2 m}^{n'_1 n'_2 m'}}{\Phi}, \quad (3.113)$$

with

$$T_{n_1 n_2 m}^{n'_1 n'_2 m'} = \sum_{p \geq 0} T_p F^p , \quad (3.114)$$

where

$$T_p \equiv \frac{1}{8} \delta_{m, m'} \sum_{i=0}^p \left( F_i^{(2)} G_{p-i}^{(0)} - F_i^{(0)} G_{p-i}^{(2)} \right) . \quad (3.115)$$

We can also introduce the expansion

$$Z_{n_1 n_2 m}^{n'_1 n'_2 m'} = \sum_{p \geq 0} Z_p F^p . \quad (3.116)$$

Rewriting Eq. (3.113) as

$$T_{n_1 n_2 m}^{n'_1 n'_2 m'} = \Phi Z_{n_1 n_2 m}^{n'_1 n'_2 m'} , \quad (3.117)$$

and using the expansions for each side gives

$$T_p = \sum_{i=0}^p Z_i \Phi_{p-i} . \quad (3.118)$$

Solving this for  $Z_p$  gives

$$Z_p = \frac{T_p - \sum_{i=0}^{p-1} Z_i \Phi_{p-i}}{\Phi_0} . \quad (3.119)$$

If  $p = 0$  we take the sum to be zero. This expression gives the terms in the expansion for  $\langle \psi' | z | \psi \rangle$  given by Eq. (3.116). We have therefore successfully calculated the perturbation expansion for the atomic matrix element of the radiator's  $z$  coordinate.

We have followed the calculation of the  $z$  matrix element in detail in order to demonstrate the perturbation theory method. For the remaining matrix elements we present only the final results. The matrix elements for  $x$  and  $y$

are calculated by the same procedure except for the angular integrals which we evaluate explicitly. For  $x = \sqrt{\xi\eta} \cos \varphi$  we have

$$\begin{aligned} \int_0^{2\pi} d\varphi \cos \varphi e^{-i(m'-m)\varphi} &= \frac{2\pi}{2} [\delta_{m+1,m'} + \delta_{m-1,m'}] \\ &= \frac{2\pi}{2} \Delta_{m,m'}^{(+)} . \end{aligned} \quad (3.120)$$

For  $y = \sqrt{\xi\eta} \sin \varphi$  we have

$$\begin{aligned} \int_0^{2\pi} d\varphi \sin \varphi e^{-i(m'-m)\varphi} &= \frac{2\pi}{2i} [\delta_{m+1,m'} - \delta_{m-1,m'}] \\ &= \frac{2\pi}{i2} \Delta_{m,m'}^{(-)} . \end{aligned} \quad (3.121)$$

The factor of  $2\pi$  will cancel with a similar factor from the wave function normalization.

The  $x$  matrix element is given by

$$X_{n_1 n_2 m}^{n'_1 n'_2 m'} = \sum_{p \geq 0} X_p F^p , \quad (3.122)$$

where

$$X_p = \frac{R_p - \sum_{i=0}^{p-1} X_i \Phi_{p-i}}{\Phi_0} , \quad (3.123)$$

with

$$R_p \equiv \frac{1}{8} \Delta_{m,m'}^{(+)} \sum_{i=0}^p \left( F_i^{(3/2)} G_{p-i}^{(1/2)} + F_i^{(1/2)} G_{p-i}^{(3/2)} \right) . \quad (3.124)$$

The  $y$  matrix element is given by

$$Y_{n_1 n_2 m}^{n'_1 n'_2 m'} = -i \sum_{p \geq 0} Y_p F^p , \quad (3.125)$$

where

$$Y_p = \frac{K_p - \sum_{i=0}^{p-1} Y_i \Phi_{p-i}}{\Phi_0} , \quad (3.126)$$

with

$$K_p \equiv \frac{1}{8} \Delta_{m,m'}^{(-)} \sum_{i=0}^p \left( F_i^{(3/2)} G_{p-i}^{(1/2)} + F_i^{(1/2)} G_{p-i}^{(3/2)} \right) . \quad (3.127)$$

### Quadrupole Matrix Elements

The last atomic matrix element we need is the quadrupole moment tensor component  $Q_{zz}$ . Its operator in terms of radiator electron coordinates is given by (taking  $e = 1$ )

$$\begin{aligned} Q_{zz} &= - \left( 3z^2 - r^2 \right) \\ &= -\frac{1}{2} \left( \xi^2 + \eta^2 - 4\xi\eta \right) . \end{aligned} \quad (3.128)$$

The matrix elements of  $Q_{zz}$  are then given by

$$(Q_{zz})_{n_1 n_2 m}^{n'_1 n'_2 m'} = \sum_{p \geq 0} Q_p F^p , \quad (3.129)$$

where

$$Q_p = \frac{S_p - \sum_{i=0}^{p-i} Q_i \Phi_{p-i}}{\Phi_0} , \quad (3.130)$$

with

$$S_p \equiv -\frac{1}{8} \delta_{m,m'} \sum_{i=0}^p \left( F_i^{(3)} G_{p-i}^{(0)} + F_i^{(0)} G_{p-i}^{(3)} - 3F_i^{(2)} G_{p-i}^{(1)} - 3F_i^{(1)} G_{p-i}^{(2)} \right) . \quad (3.131)$$

The calculation of  $Q_{zz}$  goes beyond the work of Hoe et al<sup>64,65</sup> but the method is the same and is as outlined above in the calculation of the  $z$  matrix element.

For the perturbation theory calculations in this work, we will go to sixth order, taking  $p = 6$ . This will be more than sufficient for our purposes.

### 3.3 Atomic Data by Numerical Solution

Next, we give a qualitative discussion of the numerical solution of Schrödinger's equation for a hydrogenic radiator in a uniform electric field. We have already developed the perturbation solution useful for relatively small field values. Direct numerical solution is applicable, in principal, for fields of any magnitude, though, in practice, it turns out to be inconvenient for very small field values because it is difficult to numerically handle the resultant extremely sharp resonances. We will discuss this point further below. Consequently, the perturbation and numerical solution techniques are complementary and additionally should serve as consistency checks since they should produce matching results for a suitable intermediate range of fields. For large field values, the resonance nature of the radiator states becomes an essential part of their description and the perturbation theory used here is no longer useful for finding the field dependent eigenvalues and eigenfunctions of Schrödinger's equation. We also discuss the calculation of the width of these resonances and the numerical evaluation of the necessary atomic matrix elements.

The presence of the uniform field at the radiator changes the very nature of bound atomic states by turning each discrete energy level into a shape resonance; in other words, there will be a solution for a particular set of quantum numbers that includes a continuum of energy values.<sup>66,67</sup> For a field strength given by  $\lambda$ , the states can be characterised uniquely by the quantum numbers  $m_l$ ,  $A$  and the energy  $E$ . The quantum numbers  $m_l$  and  $A$  remain discrete but  $E$  now has a continuous spectrum. For weak field values, the density of

states is greatest for a radiator electron with an energy that closely corresponds to the discrete states given by the perturbation theory solution to the problem. As the field value increases, however, the density of states broadens and the probability of finding the electron with an energy more widely spaced from the resonance center increases. This is a result of the field induced broadening of the resonance. The width,  $\Gamma$ , of the resonance is also roughly inversely proportional to the lifetime of the electron inside the radiator. This is most easily seen from the time-energy uncertainty principle but also follows from a detailed WKB treatment of resonance decay.<sup>68</sup> In fact, the WKB treatment<sup>68,69</sup> of the field ionization problem leads to a probability of finding the quasibound electron inside the potential barrier given by the time dependence factor  $e^{-\Gamma t}$ . Thus, when  $t = 1/\Gamma$  the probability has decreased from one at  $t = 0$  to  $1/e = 0.37$ . The presence of the field lowers the Coulomb potential along the upfield direction thus producing a potential well defined by a finite-size potential barrier. The electron is then able to tunnel out of the radiator. Indeed, in the presence of the field, there are now no truly bound states in the sense of the electron being permanently associated with a particular atom baring radiative or collisional ionization. However, if the lifetime of the electron inside the radiator potential barrier is long compared to the time of interest for the radiator, it is effectively bound to the radiator. For even larger field values, the plasma electric field potential will exceed the attractive central Coulomb potential; the energy level will be above the top of the potential barrier. In this case, if the energy level is close to the top of the barrier, the electron can still spend a significant amount of time in the vicinity of the radiator nucleus and will retain some of the character of a bound state. As the field is increased further this bound character will gradually be reduced. This

phenomenon results in the smooth broadening of the resonances as the field increases until they overlap. At that point the resonances have merged into a relatively smooth background continuum.

We need to numerically solve the system of coupled second order ordinary differential equations (ODE's) given by Eqs. (3.60) and (3.61). In order to employ the solutions of these equations for the calculation of the matrix elements and line shapes, and since the eigenvalues are not discrete, we will use the Breit-Wigner<sup>62</sup> Lorentzian parameterization of resonances and take the eigenfunctions and eigenvalues at the center of each resonance as a representative value over the entire resonance. As long as the resonance is fairly narrow and remains distinct, this is a reasonable approximation. It breaks down for strong fields where the resonance becomes strongly asymmetric. Fig. (3.3) gives an example of this phenomenon. The reason for this asymmetry lies in the shape of the potential barrier; as the energy level goes higher it sees a thinner potential barrier. The thinner the potential barrier, the shorter the lifetime of the state and the greater the uncertainty in its energy. Consequently, the broader width on the high energy side of the resonance is due to the greater uncertainty in the energy value at that point. These resonance asymmetries have been investigated experimentally by Harmin.<sup>70</sup> We do not need to describe this behavior in detail since its contribution to the line shape is greatly attenuated due to the low probability of occurrence of the relevant high field values as reflected in a small value of the microfield probability function.

We employ the numerical solutions of Eqs. (3.60) and (3.61) by R. Mancini and C. Hooper<sup>71</sup> who follow the method of E. Luc-Koenig and A. Bachelier.<sup>66,67</sup>

We give here a general qualitative procedural description of the solution technique (see the above references for further details). The solutions for the equation in the scaled variable  $x$  are effectively bound and, therefore for large  $x$  are exponentially damped. The number of nodes in the wavefunction's  $x$  component is given by the parabolic quantum number  $n_1$ . The solutions for the equation in the scaled variable  $y$  are effectively unbound; that is, the solutions for large  $y$  outside the potential well are oscillatory in nature. On the other hand, for  $x$  and  $y \rightarrow 0$  we have  $f(0) = g(0) = 0$ .

To solve the the two equations, Eq. (3.60) and Eq. (3.61) consistently, first, we solve the effectively bound equation in  $x$  for a particular case given by specific values of  $F$ ,  $E$ ,  $n_1$  and  $m_l$ . This will give a value for the constant  $A$  by imposing the exponentially damped behavior of  $\mathcal{F}(x)$  for large  $x$  (this is an eigenvalue problem for A). We use this to determine the constant  $B$  and proceed with the solution of the effectively unbound equation in  $y$ . We change Eqs. (3.60) and (3.61) into a form more convenient for numerical solution by eliminating the first order derivative with the transformations

$$\mathcal{F}(x) \equiv \sqrt{x} f(x) , \quad (3.132)$$

and

$$\mathcal{G}(y) \equiv \sqrt{y} g(y) . \quad (3.133)$$

Our two equations will then be transform to

$$\frac{d^2 \mathcal{F}(x)}{dx^2} + T_x \mathcal{F}(x) = 0 , \quad (3.134)$$

and

$$\frac{d^2\mathcal{G}(y)}{dy^2} + T_y\mathcal{G}(y) = 0 , \quad (3.135)$$

where

$$T_x = \frac{A}{x} + \frac{n^2}{2}E - \frac{m^2 - 1}{4x^2} - \lambda x , \quad (3.136)$$

and

$$T_y = \frac{B}{y} + \frac{n^2}{2}E - \frac{m^2 - 1}{4y^2} + \lambda y . \quad (3.137)$$

The motivation for making this transformation is that now we have to deal with second order ODE's with missing first derivatives which can be efficiently integrated using the Numerov algorithm.

To solve Eq. (3.134) for an energy value  $E$ , a scaled field value  $\lambda$ , a value for the  $z$  component of the orbital angular momentum  $m_l$  and a value for the parabolic quantum number  $n_1$ , we pick a trial value for  $A$ . We solve the differential equation starting at  $x = 0$  using a power series expansion; this is used to initialize an outward numerical integration using a fourth order Numerov algorithm.<sup>66,72</sup> This numerical integration is continued up to the outer turning point of the effective potential barrier. (If the energy level is above the top of the potential barrier so that there is no outward turning point, we use the maximum of the potential barrier.) For suitable large  $x$  values, an exponentially damped asymptotic solution is used to begin an inward numerical integration, again using the Numerov method. The two solutions overlap at the outer turning point of the potential barrier (or the potential barrier maximum if the energy level is above it). At the meeting point, we match  $\mathcal{F}(x)$  by adjusting a multiplicative constant, and from the matching

condition for  $d\mathcal{F}(x)/dx$  we compute a correction to our initial guess for  $A$ . This defines an iterative procedure which is continued until the initial guess for  $A$  agrees within a given tolerance with the value found from matching the derivatives.<sup>73</sup>

To solve Eq. (3.135), the unbound equation in the scaled variable  $y$ , we note that once we have the value of the constant  $A$  we have  $B = n - A$ . This gives us  $E$ ,  $\lambda$ ,  $n_1$ ,  $m_l$ ,  $A$  and  $B$ ; therefore, it is not necessary to make any initial guesses. We start the outward integration as we have done for the variable  $x$  using a power series solution, and then switch to the numerical integration using the Numerov method as before. Since the constant  $B$  has already been determined, we continue the integration outward to large  $y$  beyond the effective potential barrier where we fit a large- $y$  analytic oscillatory asymptotic solution to the numerical results. This will give the value of the amplitude of  $\mathcal{G}(y)$  for large  $y$ . By studying the distribution of amplitudes with respect to the energy, the width and center-location of the resonance can be estimated.

Since the values of the energy can have a continuous spectrum, we have the normalization condition per unit energy given by

$$\frac{1}{4} \int_0^{2\pi} d\varphi \int_0^\infty d\xi \int_0^\infty d\eta (\xi + \eta) \psi_{m_l, A, E}^* \psi_{m'_l, A', E'} = \delta_{m_l, m'_l} \delta_{A, A'} \delta(E - E') . \quad (3.138)$$

it can be shown<sup>62</sup> this is equivalent to the condition  $I_{out} = 1/2\pi$ , where  $I_{out}$  is the outward flux in the  $\eta$  direction at large  $\eta$ . The outward flux  $I_{out}$  can be given in terms of the outgoing wave  $\psi_{out}$  where we have decomposed the stationary wavefunctions into outgoing and incoming components in the  $\eta$  direction.

The density of states can be obtained by studying the behavior of the electron probability density near the nucleus for the component of the wavefunction associated with a constant value of the outward flux. As stated before, we can approximate the density of states for a particular resonance using the Breit-Wigner parameterization.<sup>62</sup> We obtain

$$\mathcal{D}_{n_1}^m(E) = \mathcal{D}_{n_1}^m(E_r) \frac{\frac{1}{4}\Gamma^2}{(E - E_r)^2 + \frac{1}{4}\Gamma^2}, \quad (3.139)$$

where  $E_r$  corresponds to the energy value at the maximum of the density of states of the resonance, and  $\Gamma$  is the full resonance width at half maximum. This is a reasonable parameterization as long as the resonance remains distinct. The average lifetime  $\tau_{res}$ , of the resonance can be associated with the resonance width through<sup>65</sup>

$$\tau_{res} \approx \hbar/\Gamma. \quad (3.140)$$

This is just a manifestation of the time-energy uncertainty principal.

Once we have numerically evaluated  $\mathcal{F}(x)$  and  $\mathcal{G}(y)$ , we are free to calculate the matrix elements needed for the line shape. By straight forward numerical integration we evaluate matrix elements for  $x$ ,  $z$  and  $Q_{zz}$ . We cut-off the integration over the scaled variable  $y$  at the outer turning point of the effective potential barrier for energy values below the maximum of the potential barrier. (For energies greater than the maximum of the potential barrier, we stop the integration at the value of  $y$  corresponding to the maximum of the potential barrier.) Due to their resonance nature, the wavefunctions extend overall space but we are only interested in the portion located near the radiator. The numerical values of the matrix elements are not significantly sensitive to small changes in the location of this integration cut-off. Since we now have properly

normalized wavefunctions, we can evaluate the field dependent matrix element of a real operator  $\mathcal{O}$  between two resonance states denoted by subscripts "i" and "j" by integrating over the energy range of each resonance. The square of the matrix element for an operator  $\mathcal{O}$  can be written as,

$$|\mathcal{O}_{i,j}(F)|^2 = \int dE_i \int dE_j |\langle \psi_i(E_i, F) | \mathcal{O} | \psi_j(E_j, F) \rangle|^2 . \quad (3.141)$$

For narrow resonances we can approximate this results by

$$\mathcal{O}_{i,j} \approx \left(\frac{\pi\Gamma_i}{2}\right)^{\frac{1}{2}} \left(\frac{\pi\Gamma_j}{2}\right)^{\frac{1}{2}} \langle \psi_i(E_{r,i}, F) | \mathcal{O} | \psi_j(E_{r,j}, F) \rangle , \quad (3.142)$$

where we have used the value of the eigenfunctions at resonance center. This is a reasonable approximation because the main field dependence of the wave functions, for narrow resonances, is contained in the normalization factor which is a function of the square root of the density of states. Our evaluation of the square of the matrix element allows us to integrate over the density of states to obtain the  $\pi\Gamma_i/2$  factors. Since these factors are always positive and real, the sign (and any factors of  $i$ ) of  $\mathcal{O}_{i,j}$  is reliably given by the evaluation of  $\langle \psi_i(E_i, F) | \mathcal{O} | \psi_j(E_j, F) \rangle$  at  $E_i = E_{r,i}$ . Fig. 3.4 gives an example of the calculation of atomic matrix elements by both perturbation theory and direct numerical solution of Schrödinger's equation. We see that the two solutions join smoothly for intermediate field values and diverge for larger field values as the accuracy of the perturbation theory solution breaks down.

As the field  $F$  goes to zero, Eq. (3.141) will reduce to the usual no field limit where

$$\mathcal{O}_{i,j}(0) = \langle \psi_i^0 | \mathcal{O} | \psi_j^0 \rangle . \quad (3.143)$$

Here,

$$\psi_i^0 = u(n_1, m_l, \xi) u(n_2, m_l, \eta) \frac{e^{im_l\varphi}}{\sqrt{2\pi}}, \quad (3.144)$$

which, as expected, is just the solution to Schrödinger's equation for the field free case. Here, the state "i" is specified by  $E$ ,  $n_1$ ,  $m_l$  and  $F$ . Since for a solution with a discrete values of  $E$  there is a unique value of the principal quantum number  $n$ , we can obtain  $n_2$  through the relation  $n = n_1 + n_2 + |m_l| + 1$  and our limiting state can be characterized by  $n_1$ ,  $n_2$  and  $m_l$  as expected.

### 3.4 Electron Delocalization and Field Ionization

We have been using, as a model for the radiator-plasma interaction, the picture of a radiator in the presence of a uniform plasma microfield produced by the averaging of the fields from all the plasma particles. We have added the ion-quadrupole correction to account for a relatively small field gradient at the radiator. This picture is only a model, of course. As the plasma density increases, it becomes unreasonable to ignore the presence of highly charged nuclei close to the radiator. This fact creates a qualitatively different picture. In the uniform field case, a quasibound electron will tunnel out of the radiator and continue to accelerate toward the field source at infinity. In reality, large fields are produced primarily by nearby charges. The quasibound electron will then orbit about the ensuing multicenter ionic potential in a molecular orbital<sup>74</sup> instead of tunneling into the interparticle space; the electrons will become delocalized. A complication to this molecular orbital picture is the large number of free plasma electrons in the internuclear volume. It is unreasonable to assume that the quasibound electrons will not strongly interact with these free electrons as they resonate between various nuclei. Perhaps a more accurate picture for these conditions would be the self consistent treatment of

both bound and free electrons in the presence of the multicenter potentials. Some work has been done along these lines from an analytic point of view by Rogers,<sup>75</sup> and from a numerical simulation point of view by Younger et al.<sup>76</sup> Additionally, a model consisting of a cluster of nuclei with bound electrons has been considered by Collins and Merts<sup>77</sup> but for  $T_e = 0$ . Much work remains to be done before these models are capable of accurately treating spectral line transitions for plasmas of high density and temperature.

In addition to the question of whether field induced ionization or resonance exchange of electrons between nuclei is a better description of what strong fields do to quasibound electrons, there is the question of the level broadening produced by these two mechanisms. The field ionization picture contains level broadening due to the resonance character of the energy levels in the presence of the nearly uniform electric field. This is most easily seen from the uncertainty principle where the width is related to the resonance lifetime by  $\Delta E \approx \hbar/\tau_{res}$ . In the molecular orbital picture, an electron bound to two nuclei will still have a discrete energy. However, as the number of nuclei in the molecule or cluster increases, splitting is induced. If each level is  $m$ -fold degenerate and there are  $N$  nuclei in the cluster, the splitting will be on the order of  $mN$ -fold.<sup>77</sup> This large degree of splitting will be qualitatively similar to the intrinsic level broadening produced in the field ionization case. We see, therefore, that the level broadening from the two different models should produce similar results under similar conditions, at least as far as the level width is concerned.

At this point, it appears that the molecular orbital picture may be the most capable of describing our dense plasma since it is a truly many-body theory. However, there is the complicating factor of the intercollision of free and bound electrons. As the bound electrons exchange between the nuclei,

they will be subject to collisions with the free plasma electrons. If they are then thermalized into the plasma, the situation will be more like the field ionization case. A realistic picture probably lies somewhere between the two over simplified models.

In the molecular orbital model, radiator levels are not depopulated. On the other hand, in the field ionization model, all levels will be depopulated on time scales relevant to radiative decay, for sufficiently strong fields. If the actual phenomenon lies somewhere between these two pictures, then the resultant effect will range somewhere between no change in the line shape due to no level depopulation, to a substantial decrease in line radiation for large fields due to level depletion from field ionization. The levels will not be completely depopulated, of course, due to collisional and radiative repopulation. What effect could these two models have on the spectral line shape?

In order to estimate the importance of this possible ionization effect on level populations, we will examine the limiting case of field ionization due to tunneling with no reverse process to repopulate the radiator level except the usual collisional and radiative processes. We will construct a simple kinetic population model to describe the influence of field induced ionization on the relative population of the energy levels of hydrogen-like argon. We will present only the extreme case of no back tunneling in order to ascertain the maximum possible population depletion. As outlined above, the real situation could lead to results ranging somewhere from no tunneling depletion at all (the pure molecular orbital picture) to maximum depletion due to one way tunneling (the field ionization picture). We will not look for departures from absolute LTE populations but only relative departures from LTE among the upper states

involved in the spectral transitions; relative population differences are all we will be able to observe from experimental line spectra.

We will examine the relative distribution of populations of the  $n = 3$  and 4 levels of hydrogenic argon. The model includes connections between the hydrogenic excited state levels to the ground state and the fully stripped ion while omitting the  $n = 2$  levels which are little affected by field ionization. At the high densities we are concerned with in this work, collisional processes will dominate the other population altering processes and relative LTE populations will be very probable if we do not include the field ionization. We consider only these few levels because we are mainly interested in the question of whether the field ionization effect can depopulate the levels enough to produce a significant change in the line shape.

We will incorporate into the kinetic model collisional excitation, collisional de-excitation, collisional ionization, three body recombination, spontaneous emission, radiative recombination and field ionization. We can easily formulate a rate equation for the population  $N_i$  of a level denoted by the subscript "i". The number of excited quasibound levels is denoted by  $N$ , the fully stripped ion by the subscript "N+1" and the ground state level by "0". Our rate equation is

$$\begin{aligned} \frac{dN_i}{dt} = & \sum_{j=0}^{i-1} N_j n_e C_{j,i}^e + \sum_{j=i+1}^{N+1} N_j n_e C_{j,i}^d \\ & - \sum_{j=i+1}^{N+1} N_i n_e C_{i,j}^e - \sum_{j=0}^{i-1} N_i n_e C_{i,j}^d \\ & + \sum_{j=i+1}^{N+1} N_j A_{j,i} - \sum_{j=0}^{i-1} N_i A_{i,j} - N_i \Gamma_i , \end{aligned} \quad (3.145)$$

for  $i = 1$  to  $N + 1$ . Note that since the fully stripped ion has no electron to escape,  $\Gamma_{N+1} = 0$ . We will take the populations to be relative to the ground state population,  $N_0$ . This will give  $N_j \rightarrow N_j/N_0$  and  $N_0 \rightarrow 1$  for  $j = 1$  to  $N + 1$ . Since we are only interested in the steady state solution to these kinetic equations, we examine the case with

$$\frac{dN_i}{dt} = 0 , \quad (3.146)$$

for all  $i$ . Next, we define the rate coefficients in Eq. (3.145):

The collisional excitation rate is given by  $C_{i,j}^e$ , where<sup>78</sup>

$$C_{i,j}^e = 3.75 \times 10^{-5} T^{-1/2} |\langle i | \vec{r} | j \rangle|^2 e^{-\Delta E_{i,j}/kT} \text{ cm}^3 \text{ sec}^{-1} . \quad (3.147)$$

Here,  $T$  is in degrees K,  $\Delta E_{i,j}$  is the energy difference between levels  $i$  and  $j$ , and  $\langle i | \vec{r} | j \rangle$  is the atomic matrix element of  $\vec{r}$  in atomic units.

The collisional de-excitation rate is given by  $C_{i,j}^d$ . This can be related to the collisional excitation rate by the principle of detail balance.<sup>79</sup> This gives

$$C_{i,j}^d = C_{j,i}^e e^{-\Delta E_{i,j}/kT} , \quad (3.148)$$

for states of equal statistical weight.

The collisional ionization rate is given by  $C_{i,N+1}^e$ , where<sup>80</sup>

$$C_{i,N+1}^e = 3.46 \times 10^{-5} \left( \frac{13.606}{I_i} \right) T^{-1/2} e^{-x_i} \{1 - x_i e^{x_i} E_1(x_i)\} \text{ cm}^3 \text{ sec}^{-1} . \quad (3.149)$$

Here,  $T$  is in degrees K,  $I_i$  is the ionization potential of level  $i$  in eV and

$$x_i = I_i/kT , \quad (3.150)$$

and

$$E_1(x) = \int_1^\infty dt \frac{e^{-xt}}{t} \quad (3.151)$$

is the first order exponential integral.

The three body recombination rate is given by  $C_{N+1,i}^d$ . This can be related to the collisional ionization rate by the principle of detail balance.

The spontaneous emission rate is given by the Einstein coefficient  $A_{i,j}$ , where<sup>79</sup>

$$A_{i,j} = 2.142 \times 10^{10} (\Delta E_{i,j})^3 |\langle i | \vec{r} | j \rangle|^2 \text{ sec}^{-1} . \quad (3.152)$$

Here,  $\Delta E_{i,j}$  and  $\langle i | \vec{r} | j \rangle$  are in atomic units.

The radiative recombination rate is given by  $A_{N+1,i}$ , where<sup>81</sup>

$$A_{N+1,i} = 5.197 \times 10^{-14} n_e Z x_i^{3/2} e^{x_i} E_1(x_i) \text{ sec}^{-1} . \quad (3.153)$$

Here,  $Z$  is the radiator charge,  $n_e$  is the plasma electron number density given in  $\text{cm}^{-3}$  and  $x_i$  is given by Eq. (3.150).

For the steady state case and because we have taken  $N_0 = 1$ , we can write all of the  $N + 1$  rate equations in the form

$$a_0 + a_1 N_1 + a_2 N_2 + \cdots + a_N N_N + a_{N+1} N_{N+1} = 0 , \quad (3.154)$$

where the coefficients  $a_i$  do not depend on the level populations. These equations may be cast in matrix form to obtain

$$C = R N . \quad (3.155)$$

Here,  $C$  is a column vector of dimension  $N + 1$  containing the  $a_0$  rate coefficients,  $N$  is a column vector of dimension  $N + 1$  containing the level populations  $N_i$  and  $R$  is a  $N + 1 \times N + 1$  matrix containing the remaining rate constants. This equation is easily solved to give the  $N + 1$  relative populations  $N_i$ . We have

$$N = R^{-1}C . \quad (3.156)$$

This effectively solves the relative populations problem for the  $N$  quasi-bound excited state levels plus the the fully stripped ion. For the total number of quasibound levels, we use the  $n = 3$  and  $n = 4$  levels of a hydrogen-like ion. This gives a total of  $N = 3^2 + 4^2 = 25$  levels. The effect of the lack of inclusion of the  $n = 2$  levels was examined by comparison with a more detailed kinetic population model.<sup>82</sup> This showed no significant change in the relative populations upon inclusion of these levels.

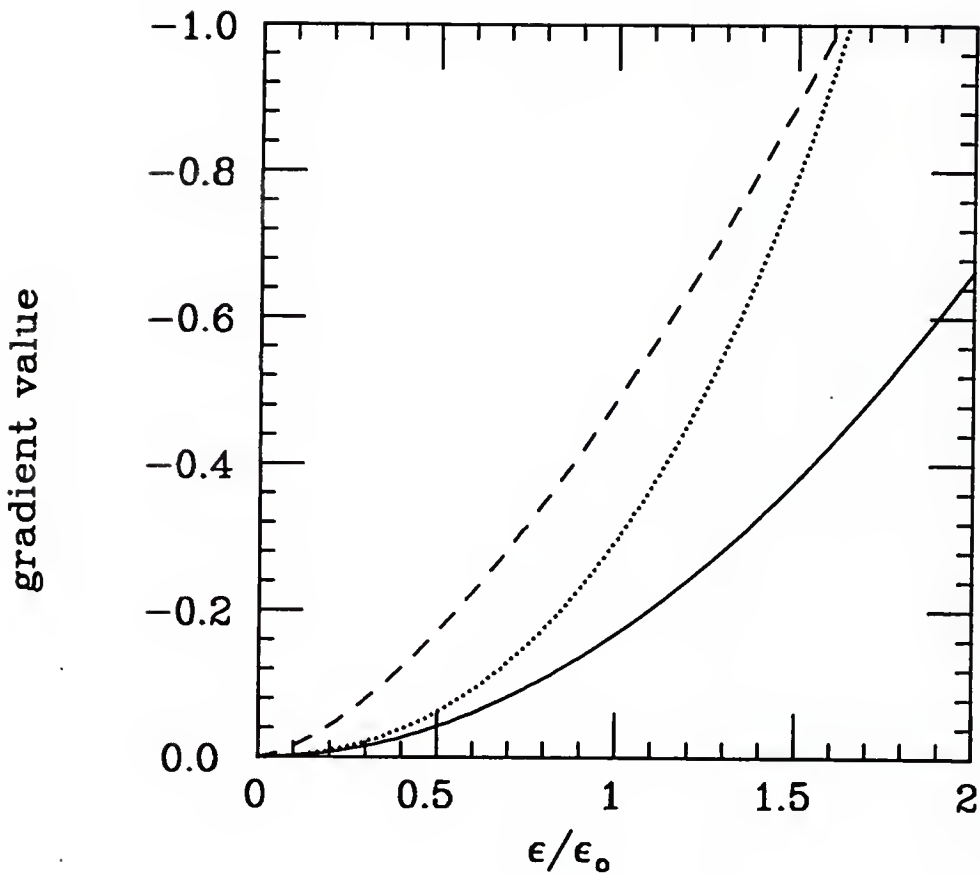


FIGURE (3.1) Field gradient term  $\langle E_{zz} \rangle_\epsilon$  as a function of the field for the APEX (—), IP (· · ·) and NN (---) models at  $n_e = 1 \times 10^{24} \text{ cm}^{-3}$  and  $kT = 800 \text{ eV}$ . The field gradient is in units of  $e/r_{o,i}^3$ . The three models are discussed at the end of section 3.1.

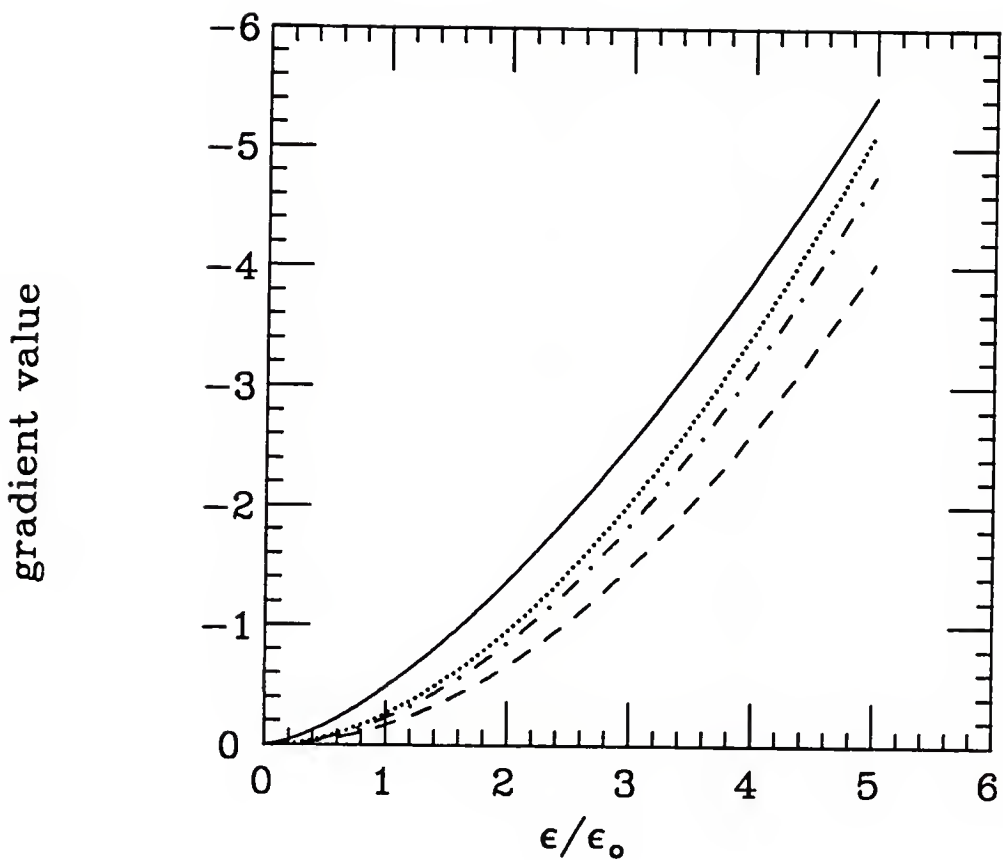


FIGURE (3.2) Approach of the constrained average field gradient term  $\langle E_{zz} \rangle_e$  to the nearest neighbor limit for increasing density. (—) refers to  $n_e = 1 \times 10^{24} \text{ cm}^{-3}$ , (---) refers to  $n_e = 5 \times 10^{24} \text{ cm}^{-3}$ , (.....) refers to  $n_e = 1 \times 10^{25} \text{ cm}^{-3}$  and (—) refers to the nearest neighbor model discussed in the text. All temperatures are  $kT = 800 \text{ eV}$ . The constrained average is evaluated using the APEX model given by Eq. (3.50).

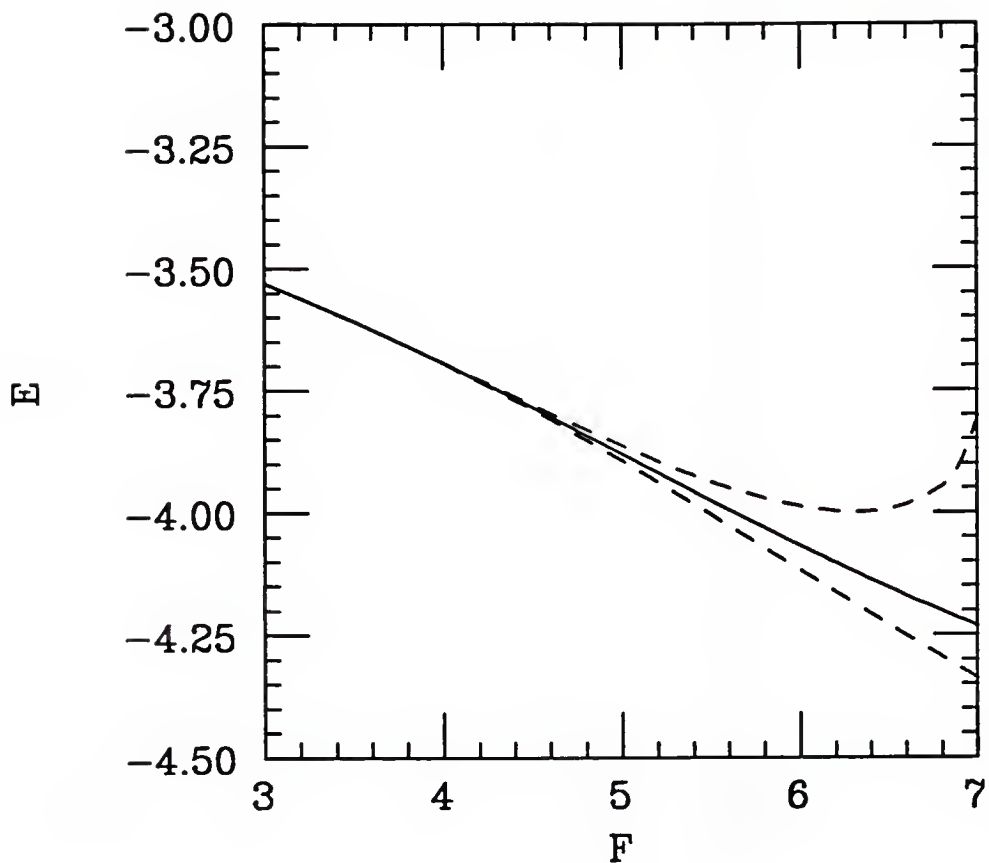


FIGURE (3.3) Example of the asymmetry of a resonant state discussed in section 3.3. This is the resonance with quantum numbers  $n, n_1, n_2, m = 4, 0, 2, 1$  or  $n, q, m = 4, -2, 1$ . The resonance center is given by (—) and the width at half maximum is given by (---). The field strength  $F$  is in units of a.u./ $1 \times 10^{-4}$  and the energy  $E$  is in units of a.u./ $1 \times 10^{-2}$ . a.u. denotes atomic units (see Appendix A).

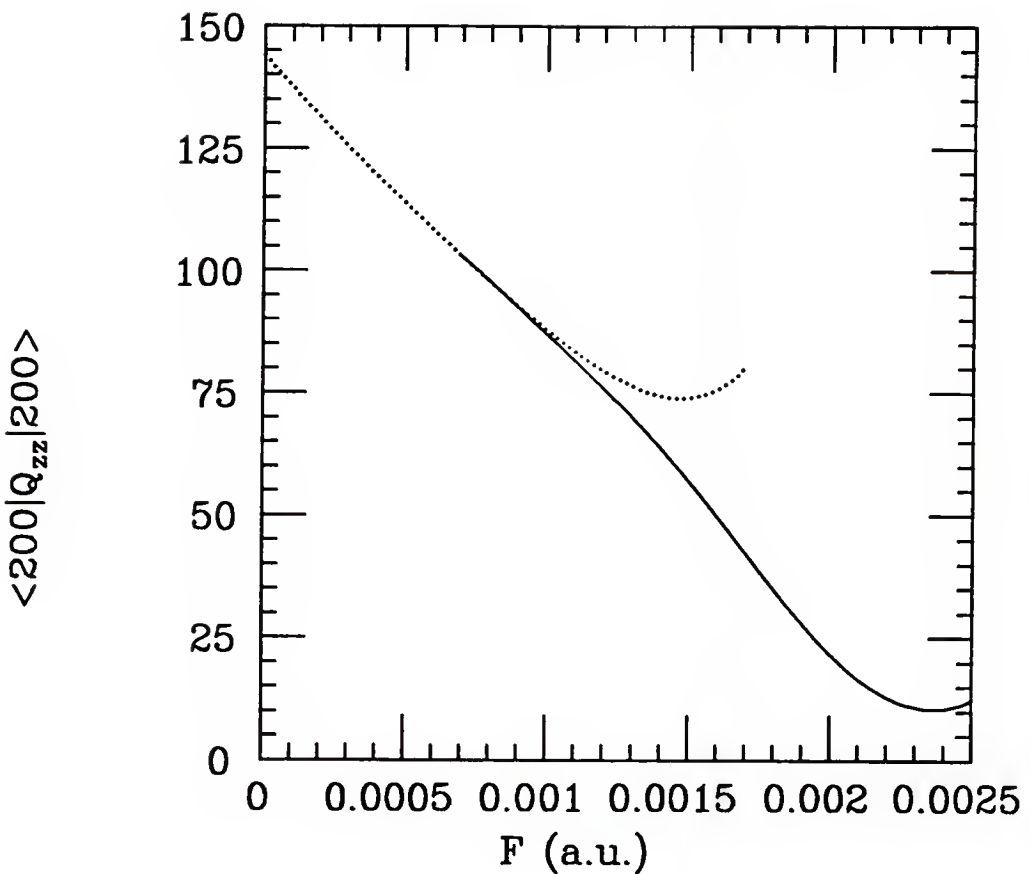


FIGURE (3.4) Comparison of numerical and perturbation theory results for the calculation of a quadrupole atomic matrix element. The example given here is a diagonal matrix element with  $n_1 = 2$ ,  $n_2 = 0$  and  $m = 0$ . The numerical solution as discussed in section 3.3 is given by (—) and the sixth order perturbation theory solution calculated from Eq. (3.129) is given by (.....). All quantities are expressed in atomic units scaled for radiator charge,  $Z = 1$ .

## CHAPTER IV RESULTS AND DISCUSSION

In the previous chapters we have formulated a general theory of plasma spectral line broadening and discussed many of the approximations used to arrive at a calculable result. The theory that we use to make these calculations has been generalized beyond previous formulations in that it includes higher-order microfield effects on: atomic matrix elements, radiator energy levels, state lifetimes, and level populations. We will now present and discuss the results of these calculations.

The presence of these higher order field effects can be expected to lead to several discernable changes in the spectral line shapes of radiators in dense plasmas. For the physical conditions we are examining the electron number density,  $n_e$ , varies from  $1 \times 10^{24}$  to  $1 \times 10^{25} \text{ cm}^{-3}$  and at a temperature,  $kT$ , of 800 eV. In this range, the lowest order corrections of the ion-quadrupole and the quadratic Stark effects will generally give rise to a blue asymmetry of the spectral line shape. This means that the intensity of the high energy (or blue) side of the spectral line will be enhanced over that of the low energy (or red) side of the line. This comes about by the preferential shifting to lower energy of components comprising the manifold of energy levels associated with a principal quantum number  $n$ . If all of the components were shifted by an equal amount, there would be no discernable change in the spectral line shape; only an overall line shift. The  $n = 1$  ground state for these transitions in highly ionized hydrogenic ions is little affected by the field because of the much stronger binding potential for the  $n = 1$  state. Additionally, the ground

state experiences no linear Stark effect. Energy levels that have been Stark shifted to the low energy side of the unperturbed upper state of the transition correspond to quasibound electrons that are found to have the maximum value of their probability amplitude on the upfield side of the radiator potential well. This corresponds to the side of the origin where the potential barrier has a maximum; the other side, the downfield side, corresponds to the potential barrier increasing without bound. The upfield electrons are more easily affected by the field and hence, their energy levels are shifted more. This preferential shifting produces a spreading out of intensity on the low energy side of the line, and thus, an increase in the peak height of the high energy side of the line. The addition of the ion-quadrupole effect enhances this trend but also generally produces a bunching, or lessening of the splitting amongst the energy levels on the blue side. This further adds to the blue asymmetry of the line. The consequences of the field dependence in the wave functions and their resulting matrix elements are harder to characterize due to less systematic results on the line shape. Therefore we study this effect only in combination with the other field effects. In this dissertation, we assume that the areas of all line shapes are normalized to one.

The possible field ionization depletion of the radiator upper level populations will lead to a lessening of intensity in the line wings. Again, the red wing should be more strongly affected due the lower potential barrier height on the upfield side of the potential well. For sufficiently strong fields, The Stark effect will cause the energy levels from states with adjacent principal quantum numbers to overlap. Inclusion of this phenomenon is important for the accurate representation of line merging.

#### 4.1 The Lyman $\alpha$ Line

The  $L_\alpha$  calculation contains the effect of the microfield on the atomic physics through field dependent matrix elements and energy levels. This gives rise to a field dependent fine structure correction to the radiator Hamiltonian (see Appendix E). The field dependence appears in the dipole matrix elements, and because we include the ion-quadrupole effect, also in the quadrupole matrix elements. We do not study the effect of possible field ionization on the levels of the  $L_\alpha$  transition because, for this case, the resonance width  $\Gamma \ll 0.1$  eV. Since for this transition the resonance nature of the states is not important, perturbation theory is adequate for the calculation of the atomic physics. At the lower end of the density-temperature range we are interested in ( $n_e = 1 \times 10^{24} \text{ cm}^{-3}$ ,  $kT = 800 \text{ eV}$ ), the Doppler effect is an important source of broadening so its inclusion is essential. For the densities and temperatures we are dealing with, the  $n = 2$  and 3 levels are well separated in energy and do not overlap for any relevant field strengths. Consequently, we will not need to consider this overlap for the  $L_\alpha$  line calculation. In Fig. (4.1) we have the  $L_\alpha$  line at  $n_e = 1 \times 10^{24} \text{ cm}^{-3}$  and  $kT = 800 \text{ eV}$ . The higher order field effects produce only a slight blue asymmetry in the line which attenuates the red peak by less than 5% in magnitude. The fine structure splitting is readily apparent with Doppler broadening being responsible for more than half the width of the peaks. We estimate the Doppler width from<sup>34</sup>  $\hbar\omega_D \sim \hbar\omega_{i,j} \sqrt{kT/m_r c^2}$ , where  $\hbar\omega_{i,j}$  is the transition energy and  $m_r$  is the radiator mass. In this case  $\hbar\omega_D \sim 3 \text{ eV}$ . As the density goes up the Stark broadening will increase and the Doppler broadening will become less important as its fraction of the total width decreases. In Fig. (4.2) the density has increased to  $n_e = 5 \times 10^{24} \text{ cm}^{-3}$ ; the

Stark broadening has increased and begun to obscure the fine structure splitting. However, the higher order field effects are still of only minor importance, accounting for changes in peak heights of less than 4%. For  $n_e = 1 \times 10^{25} \text{ cm}^{-3}$  there is still no significant attenuation of the red peak due to the higher order effects. We conclude that, for the density range of this work, the plasma microfield is not strong enough for these higher order effects to become important. As the average plasma microfield strength continues to increase due to increasing density, it will eventually become of the same order as the central Coulomb field. At that point the higher order effects will be much more likely to be manifest. If we go much beyond  $1 \times 10^{25} \text{ cm}^{-3}$ , however, the electron degeneracy will have to be incorporated into the theory as we pointed out in section 2.1.

#### 4.2 The Lyman $\beta$ Line

The  $L_\beta$  line has its excited state electron in the  $n = 3$  state. This makes it much more susceptible to the effect of the plasma microfield than in the  $L_\alpha$  case. To investigate the higher order effects on this line, we will include the ion-quadrupole effect, field dependent atomic physics, the presence of a slight resonance width,  $\Gamma$ , for each energy level, and the overlap of the levels of principal quantum number  $n = 3$  and 4.

This last process allows for atomic matrix elements connecting the two principal quantum number manifolds. It also contributes more terms to the sum over intermediate states that is performed when evaluating the electron broadening operator  $M(\Delta\omega)$ . In the field-free atomic physics calculation, this is also possible but the energy levels are widely separated at their unperturbed

energy values. Consequently, their contribution to the sum over intermediate states will be minimal. The decreasing value for large  $\Delta\omega$  of the electron broadening many-body function  $G(\Delta\omega)$  will attenuate each added term if the energy separation between levels is greater than the plasma frequency  $\omega_{p,e}$ . In the field dependent atomic physics picture, the zero-order energy levels are perturbed by the Stark effect and can overlap. When this occurs, the  $G(\Delta\omega)$  function takes its maximum value for each intermediate state and the total electron broadening term will be larger. In general, the red and blue levels of each principal quantum number manifold interact most strongly with each other, while the red levels of one principal quantum number and the blue levels corresponding to another interact hardly at all.<sup>61</sup> This quasi-selection rule causes the electron broadening of the  $n = 3$  level to be most influenced by the red levels of the  $n = 4$  level. This mechanism contributes a further blue asymmetry to the  $L_\beta$  line by way of a broader red wing caused by this additional electron broadening. These electron broadening effects are illustrated in Fig. (4.4) where we show the  $L_\beta$  line at  $n_e = 1 \times 10^{25} \text{ cm}^{-3}$  and  $kT = 800 \text{ eV}$  for the case of full field dependent atomic physics plus the ion-quadrupole effect. This is compared to the same line but with all connections to the  $n = 4$  levels excluded from the electron broadening of the  $n = 3$  to 1 transition. This is accomplished by limiting the sum over intermediate states in the evaluation of  $M(\Delta\omega)$  to dipole matrix elements connecting  $n = 3$  levels only with other  $n = 3$  levels. The sums for the  $n = 4$  to 1 transition, however, contain all  $n = 3$  and 4 levels. The  $n = 3$  to 1 line with the normal sum over all  $n = 3$  and 4 intermediate states is approximately 10% broader at half maximum intensity than the line with the restriction on the electron broadening sum.

Fine structure splitting for this line is on the order of 2 eV (see Appendix E). For  $n_e = 1 \times 10^{24} \text{ cm}^{-3}$ , the overall line width is about 40 eV. We will ignore the much smaller fine structure splitting. It has been shown<sup>83,42</sup> that this splitting introduces a slight red line asymmetry which is obscured by the blue asymmetry effects as the density increases. The overall shift of the line due to the fine structure is not insignificant but is ignored here because we are primarily interested in the line shape. At these densities it is difficult to determine exact line positions due to uncertainties in the experimental methods. We will also examine the possible influence of field induced ionization on the line shape.

Before we look at the profiles of the  $L_\beta$  line in detail, we look at some energy level diagrams for the  $n = 3$  and 4 levels as function of the field strength. Fig. (4.5) gives the energy levels as a function of the field for the case of field dependent atomic physics but no ion-quadrupole effect. The manifolds for the two levels begins to overlap at  $\tilde{\epsilon}$  values slightly greater than one. Recall that  $\tilde{\epsilon}$  is our unitless scaled field magnitude. According to the Inglis-Teller limit,<sup>84</sup> this is the point where the two spectral lines merge and become indistinct. This will only occur, however, if both lines are of equal intensity. In a spectral series the intensity of the lines generally decreases as you go up in the series (as the  $n$  value of the upper state increases). As this occurs, we will find that the  $L_\gamma$  line merges with the  $L_\beta$  line but the  $L_\beta$  line itself will still be plainly visible due to its much higher intensity. The Inglis-Teller limit is more accurately applied to lines corresponding to large values of the principal quantum number,  $n$ . For that case the intensities of adjacent lines are similar and their merger will produce an indistinguishable whole.

In Fig. (4.5) we can see the deviation from the linear Stark effect caused by the higher order corrections to the energy. This is most prominent in the  $n = 4$  levels. In Fig. (4.6) the Hamiltonian is diagonalized with the ion-quadrupole terms added. Now the levels from the two manifolds can interact strongly through the field dependent quadrupole moment matrix elements of the ion-quadrupole term. There is a downward shifting of red energy levels of both manifolds and a slight bunching together of the blue levels. When the levels approach each other between these two manifolds, there is strong interaction. Level mixing and repulsion is plainly evident. The highest energy (bluest)  $n = 3$  level experiences a strong avoided crossing with the lowest energy (reddest)  $n = 4$  level. This diagram was calculated from a direct diagonalization of the Hamiltonian for the  $n = 3$  and 4 levels using field dependent atomic physics. The previous figure is composed of the radiator energy levels calculated directly from Schrödinger's equation containing the ion-dipole term. In a plot of the line shape, the actual positions of these transition energies become somewhat blurred due to the added imaginary electron broadening and resonance width terms. Figs. (4.5) and (4.6) do give us, however, a good indication of how the levels shift and interact as a function of the field. The presence of the ion-quadrupole effect not only provides for direct energy shifts of the levels, but it also allows the levels from different principal quantum number manifolds to interact resulting in complicated level mixing and repulsion.

The  $L_\beta$  line without any higher order field effects or fine structure is an almost completely symmetric, double peaked line. The slight asymmetry is due to the frequency dependence of the electron broadening operator  $G(\Delta\omega)$ . The two levels in the center of the  $n = 3$  manifold have electric quantum number  $q = 0$  and are dipole forbidden (see Fig. (4.5)). This leaves only the

outer components which split linearly with the field thus producing the two nearly symmetric peaks. When the ion-quadrupole effect is added, the high energy levels bunch together slightly while the low energy levels are deflected downward imparting a blue asymmetry to the line. This asymmetry can be seen to increase as the density increases in Figs. (4.7), (4.8) and (4.9). In these figures the effect of the  $n = 4$  levels is also apparent. The  $L_\gamma$  line is centered at 4133 eV. In Fig. (4.7), at an electron density of  $n_e = 1 \times 10^{24} \text{ cm}^{-3}$  we see a slight increase in the intensity of the blue wing, but as the density increases a broad, flat, blue shoulder develops. At  $5 \times 10^{24} \text{ cm}^{-3}$ , the  $L_\gamma$  line is flat having merged with the  $L_\beta$  to become the prominent shoulder visible in Fig. (4.8). This illustrates the point we made earlier about the Inglis-Teller limit applying only to the less intense member of a pair of merging lines.

Having established the ion-quadrupole effect as a source of line asymmetry, we will return to it later to examine the difference in theoretical approaches to its calculation. Now, we examine the effect of the field dependent atomic physics on the  $L_\beta$  line along with the ion-quadrupole effect. From the energy level diagram, we expect the added field dependence to produce further blue asymmetry of the lineshape. In Fig. (4.10) we see this beginning for  $n_e = 1 \times 10^{24} \text{ cm}^{-3}$ . This trend continues in Fig. (4.11) at  $n_e = 5 \times 10^{24} \text{ cm}^{-3}$ . A check of these additional asymmetries against an approximate quadratic Stark effect calculation<sup>83,42</sup> shows that this asymmetry effect is due primarily to the quadratic correction to the energy. At  $1 \times 10^{25} \text{ cm}^{-3}$ , however, the added asymmetry goes beyond the quadratic correction and is due to higher order energy shifts and field dependent changes in the atomic matrix elements. This strong additional asymmetry can be seen in Fig. (4.12). In Figs. (4.13), (4.14) and (4.15) we compare the full field dependent atomic physics line shape

calculations for a range of densities, with the field independent atomic physics calculations with the quadratic Stark effect correction to the level energies. Both cases also have the ion-quadrupole effect. The quadratic Stark effect correction consists of adding the second order perturbation theory term from the treatment of an ion in a uniform electric field, to the upper state radiator energy levels. This amounts to throwing out all field dependence from the atomic physics except this diagonal energy correction second order in the field. It can be assumed that remaining differences between the two line shapes in the illustrations is due to additional field dependence of the energies, matrix elements and intensity factors. We conclude that at  $n_e = 5 \times 10^{24} \text{ cm}^{-3}$  and below, the field independent atomic physics plus the approximate quadratic Stark effect correction is a good approximation to the full field dependent results for the  $L_\beta$  line of hydrogenic argon.

In section 3.4 we discussed the effect of the possible field ionization produced when the plasma microfield becomes comparable to the strength of the Coulomb field experienced by the radiator electron. We pointed out that the real situation was probably somewhere between the extremes of field induced ionization in a uniform field and no ionization at all due to inverse processes including exchange of bound electrons between neighboring ions with quasi-molecular orbitals. We will examine the limiting case of field ionization in a uniform field to estimate the maximum possible reduction in line intensity due to population depletion. In Fig. (4.16) we see a reduction in intensity in the line wings that gives rise to a slightly sharper line with no change in the line asymmetry. As density increases we see in Fig. (4.17) a further narrowing of the line and an additional reduction in the intensity of the red wing. This follows from the fact that the lower energy states are more strongly affected

by the field and hence, ionize first. Again the peak asymmetry is not affected. This trend continues in Fig. (4.18) at  $n_e = 1 \times 10^{25} \text{ cm}^{-3}$ . This possible line narrowing, if real, could have consequences for density diagnostics. The narrower lines could be interpreted as indicative of a somewhat lower density. However, the strong asymmetries would still be present indicating the true higher density of the plasma.

The resonance widths  $\Gamma$  that are included in these calculations do not add significant width or distortion to the line shape. This is due to the resonance width becoming appreciable only where the microfield probability function becomes negligibly small. For example, for the most red  $n = 3$  level (the level most strongly affected by the field), the field dependent resonance width is  $\Gamma \sim 10^{-5} \text{ eV}$  for the field value  $\tilde{\epsilon} \approx 1$  and  $\Gamma \sim 1 \text{ eV}$  for  $\tilde{\epsilon} \approx 2$  compared to a  $L_\beta$  line width of approximately 150 eV. For our argon plasma at  $1 \times 10^{25} \text{ cm}^{-3}$  and 800 eV, when  $\tilde{\epsilon} = 2$  the microfield function  $P(\tilde{\epsilon})$  has fallen to only 25% of its peak value which occurred at  $\tilde{\epsilon} \approx 0.8$ . The resonance width, and hence resonance lifetime, has a larger possible effect on the level populations as we have seen.

Now we return to the consideration of different treatments of the ion-quadrupole effect. Previous calculations<sup>12</sup> of the ion-quadrupole effect considered only ion-radiator correlations while neglecting ion-ion correlations. We examined the importance of these correlations by comparing the results of our calculations that included such ion-ion correlations with a simple nearest neighbor approximation which did not. In Fig. (4.19) we see the results for  $n_e = 1 \times 10^{24} \text{ cm}^{-3}$ . As expected, the calculation with no correlations shows the strongest asymmetry as explained in section 3.1. This trend continues in Fig. (4.20) for  $n_e = 5 \times 10^{24} \text{ cm}^{-3}$ . At  $n_e = 1 \times 10^{25} \text{ cm}^{-3}$ , however, we see

in Fig. (4.21) that the two calculations of the ion-quadrupole term begin to approach each other. This is a reflection of the high field limit of the field gradient average as illustrated in Figs. (3.1) and (3.2).

This concludes our examination of the calculational results of our investigation of certain higher order field effects on spectral line shapes in dense plasmas.

### 4.3 Conclusions

We conclude this investigation by summarizing our findings, pointing out some of their consequences and suggesting the next steps needed to extend this work to higher densities.

For our range of physical conditions ( $n_e = 1 \times 10^{24} \text{ cm}^{-3}$  to  $1 \times 10^{25} \text{ cm}^{-3}$  at  $kT = 800 \text{ eV}$ ) and for the pure argon plasma we found that the higher order field effects begin to become important for the  $n = 3$  to 1 transition ( $L_\beta$ ). The  $n = 2$  to 1 transition ( $L_\alpha$ ) showed only very slight perturbations from the linear Stark effect with fine structure splitting and Doppler broadening. While the fine structure does show a slight field dependence, it produces no significant effect on the line splitting or shape for the  $L_\alpha$  line. The  $L_\beta$  line did show many of the additional field effects. The most pronounced was the effect of the field dependent atomic physics (matrix elements and energy levels that include an exact treatment of the ion-dipole term in the radiator Hamiltonian). This field dependence can be approximated by simply adding the quadratic correction to the level energy for densities of  $1 \times 10^{24}$  to  $5 \times 10^{24} \text{ cm}^{-3}$ . At  $n_e = 1 \times 10^{25} \text{ cm}^{-3}$ , however, the other field effects on the atomic physics becomes important and can not be ignored.

We have also seen that a more accurate treatment of the ion-ion correlations in the ion-quadrupole effect reduces the line asymmetry usually produced. At the very highest densities that we examined, a simple nearest neighbor model produces a fair approximation to the more accurate results. For densities higher than these the nearest neighbor approximation may be quite sufficient.

Our examination of possible field ionization effects has shown that this could have effects on the spectral line shape, producing a minimal narrowing of the line at high density. This point is highly speculative, however, and no firm conclusions can be drawn until a much more detailed study is carried out. This would probably entail a many-body theory treating plasma electrons and quasibound electrons on a more equal footing.

We have also seen that it is possible to carry the line shape calculation to densities beyond the Inglis-Teller merging point. We included the  $n = 4$  levels in our calculation of the  $n = 3$  to 1 transition and found that transitions from the  $n = 4$  level formed a prominent shoulder on the high energy side of the  $L_\beta$  line. We concluded, at least for this case, that the Inglis-Teller limit applies to the significantly lower intensity member of a neighboring pair of line transitions and does not indicate the complete merging of the two lines. The Inglis-Teller limit is more appropriate for higher series members where the two line intensities are nearly equal.

To carry these line shape calculations to higher densities for the same temperature range, it will be necessary to include a treatment of degenerate plasma electrons. We showed in chapter 2 that for densities of  $n_e = 1 \times 10^{26} \text{ cm}^{-3}$  the Fermi energy is of the same order as the thermal energy. When the plasma electrons become degenerate they may not be available for electron collisional broadening.<sup>85</sup> This may reduce the electron broadening at high densities. To

treat higher series members at these densities, it will be necessary to develop a more accurate way to deal with the width of the resonance state. This may be possible through the use of a line shape formalism that treats bound and continuum states on an equal footing.

At the present time the accurate experimental verification of these higher order field effects is problematical, but this may change as X-ray spectroscopic techniques improve. In conclusion, there appears to be no fundamental reason why the spectroscopy of high density plasmas can not be pushed to even more extreme conditions than are successfully dealt with today. In these regimes of ultra-high densities, we can expect to continue to find new and interesting physical phenomena in need of explanation.

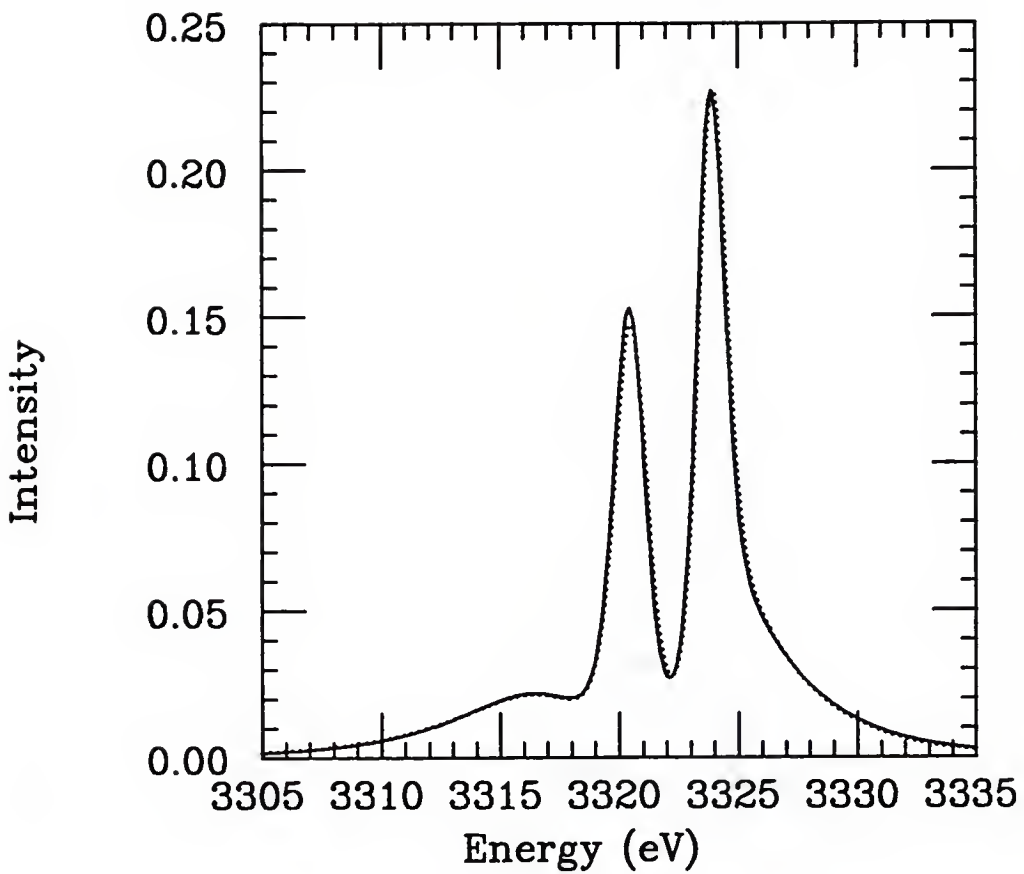


FIGURE (4.1) The  $L_\alpha$  line of hydrogenic argon for  $n_e = 1 \times 10^{24} \text{ cm}^{-3}$  and  $kT = 800 \text{ eV}$  as discussed in section 4.1. The profile with field independent atomic physics and no ion quadrupole effect is given by (—). The profile with field dependent atomic physics and the APEX ion-quadrupole effect is given by (.....). Both profiles have the fine structure and are Doppler convoluted. They are calculated from Eqs. (2.97) and (3.14).

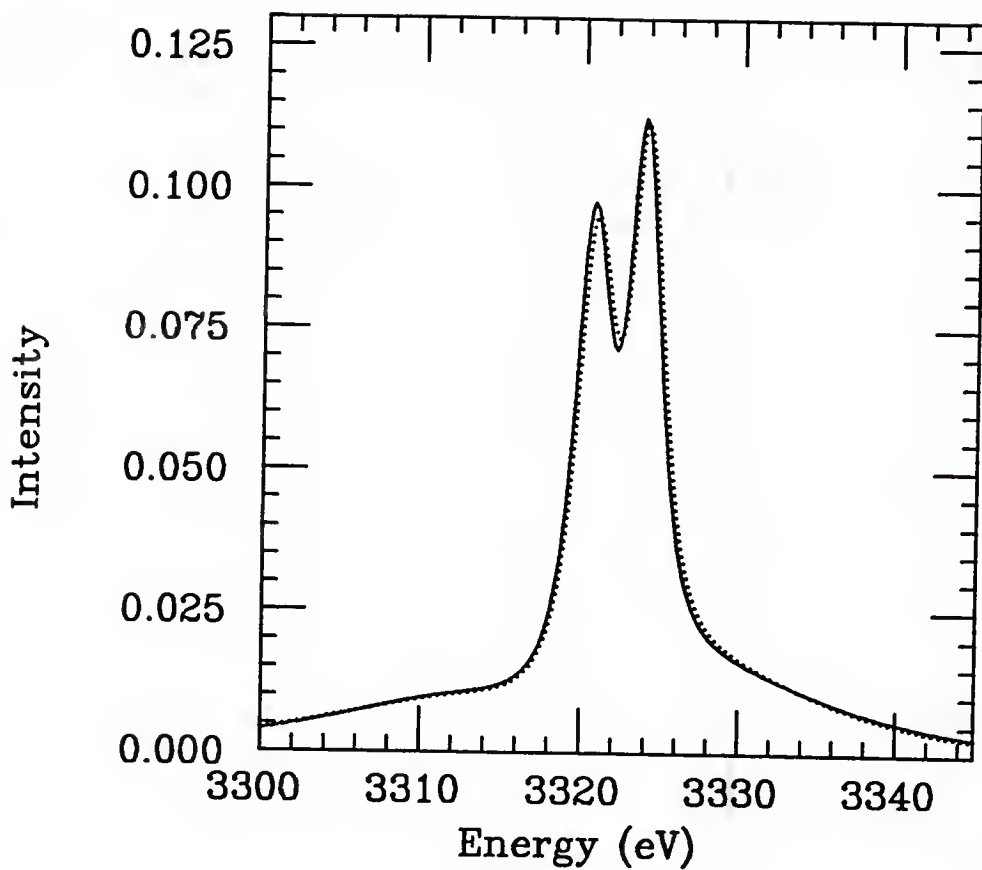


FIGURE (4.2) The  $L_\alpha$  line of hydrogenic argon for  $n_e = 5 \times 10^{24} \text{ cm}^{-3}$  and  $kT = 800 \text{ eV}$ . The profile with field independent atomic physics and no ion quadrupole effect is given by (—). The profile with field dependent atomic physics and the APEX ion-quadrupole effect is given by (.....). Both profiles have the fine structure and are Doppler convoluted.

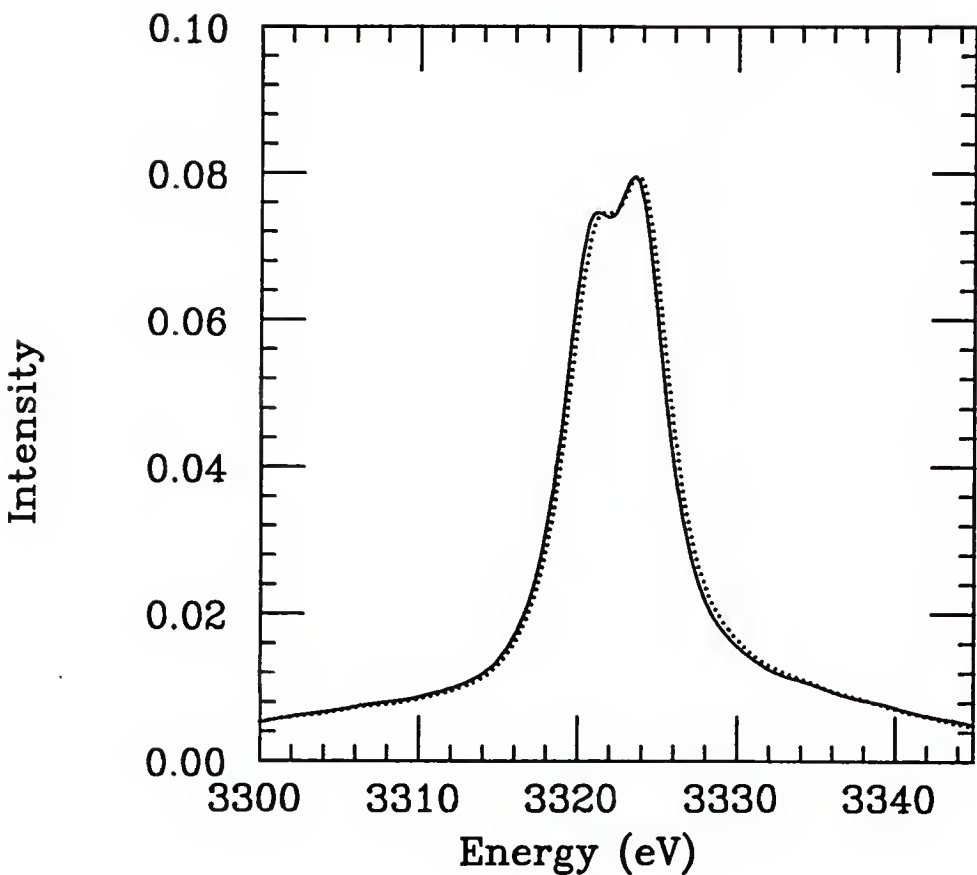


FIGURE (4.3) The  $L_\alpha$  line of hydrogenic argon for  $n_e = 1 \times 10^{25} \text{ cm}^{-3}$  and  $kT = 800 \text{ eV}$ . The profile with field independent atomic physics and no ion quadrupole effect is given by (—). The profile with field dependent atomic physics and the APEX ion-quadrupole effect is given by (.....). Both profiles have the fine structure and are Doppler convoluted.

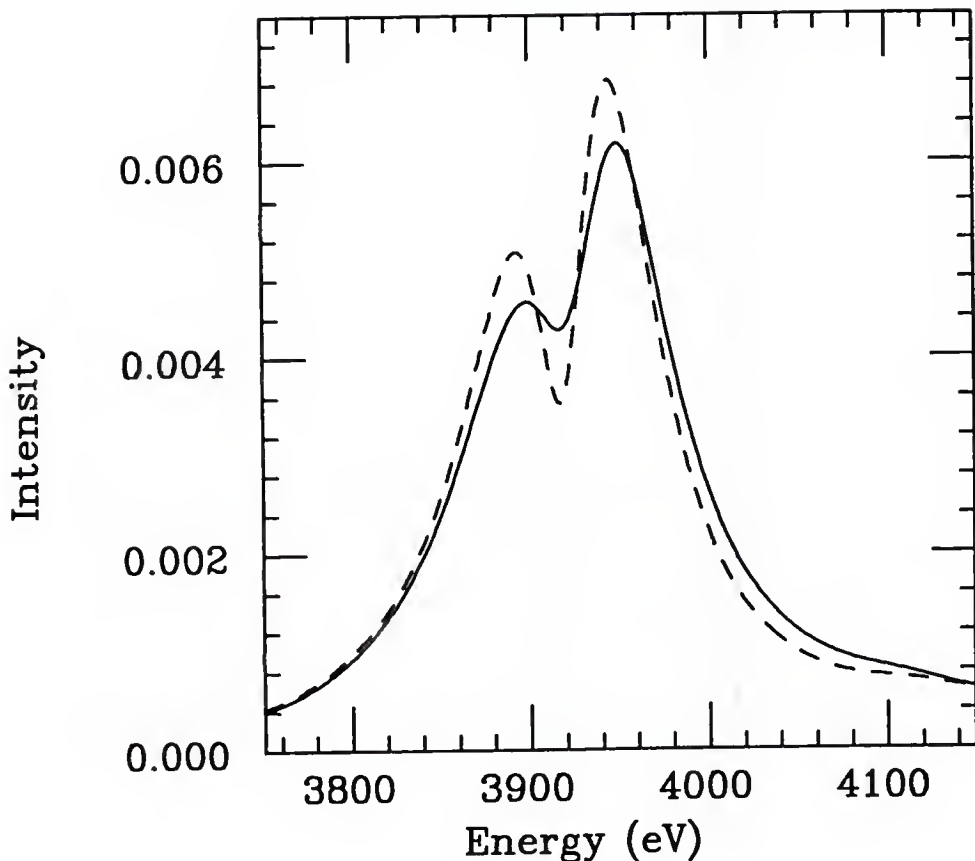


FIGURE (4.4) Comparison of the  $L_{\beta}$  line of hydrogenic argon with and without electron broadening connections to the  $n = 4$  levels. The normal line shape with field dependent atomic physics and the ion-quadrupole effect is given by (—). The same line shape but with all dipole matrix elements connecting the  $n = 3$  and 4 levels deleted from the sum in Eq. (2.96) which is used to evaluate the electron broadening operator  $M(\Delta\omega)$  is given by (---). Here  $n_e = 1 \times 10^{25} \text{ cm}^{-3}$  and  $kT = 800 \text{ eV}$ .

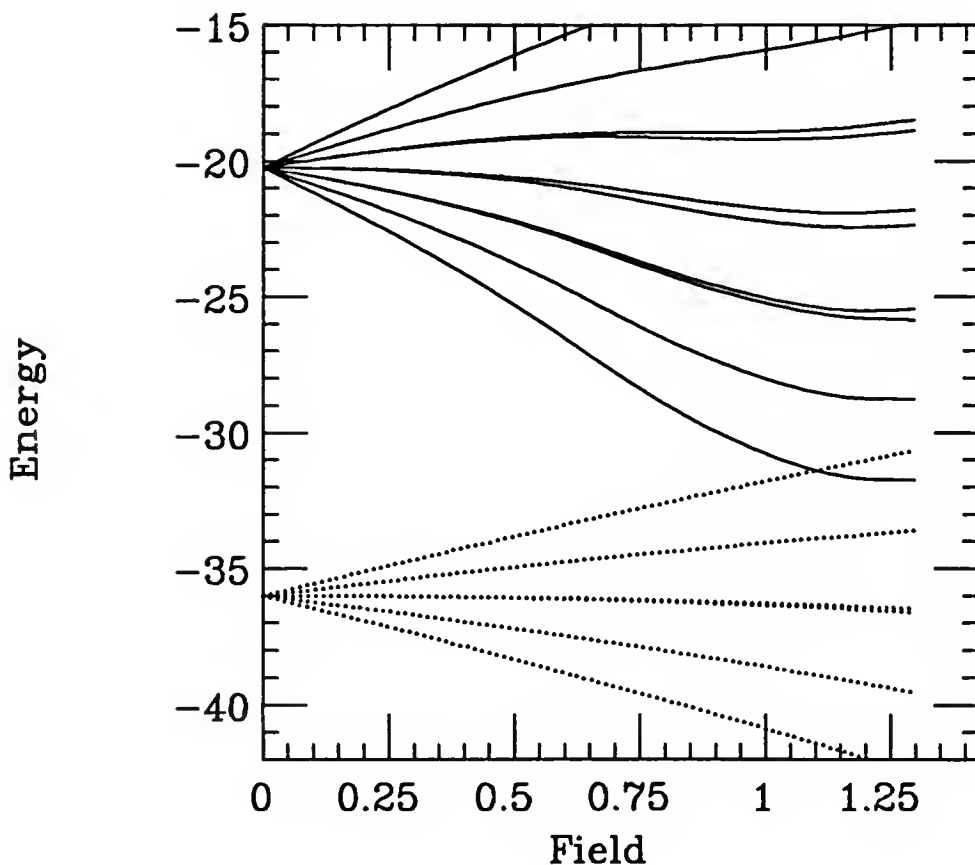


FIGURE (4.5) Energy level diagram for the  $n = 3$  and 4 manifolds of levels as a function of the plasma microfield using field dependent atomic physics but no ion-quadrupole effect. Figure discussed in section 4.2. The  $n = 3$  levels are given by (.....) and the  $n = 4$  levels are given by (—). The field is given by the unitless  $\tilde{\epsilon} = \epsilon/\epsilon_0$  and the energy is in Rydbergs.

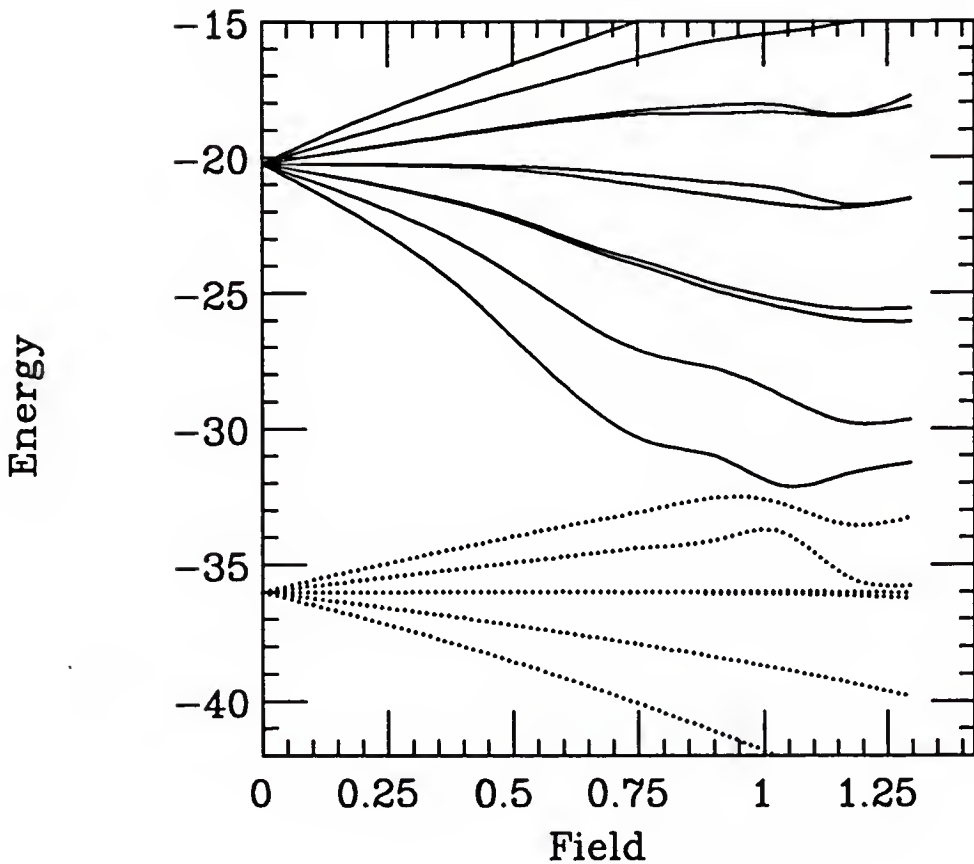


FIGURE (4.6) Energy level diagram for the  $n = 3$  and 4 manifolds of levels as a function of the plasma microfield using field dependent atomic physics and the ion-quadrupole effect. Figure discussed in section 4.2. The  $n = 3$  levels are given by (.....) and the  $n = 4$  levels are given by (—). The field is given by the unitless  $\tilde{\epsilon} = \epsilon/\epsilon_0$  and the energy is in Rydbergs. The ion-quadrupole corrections are calculated in the APEX approximation for  $n_e = 1 \times 10^{25} \text{ cm}^{-3}$  and  $kT = 800 \text{ eV}$ .

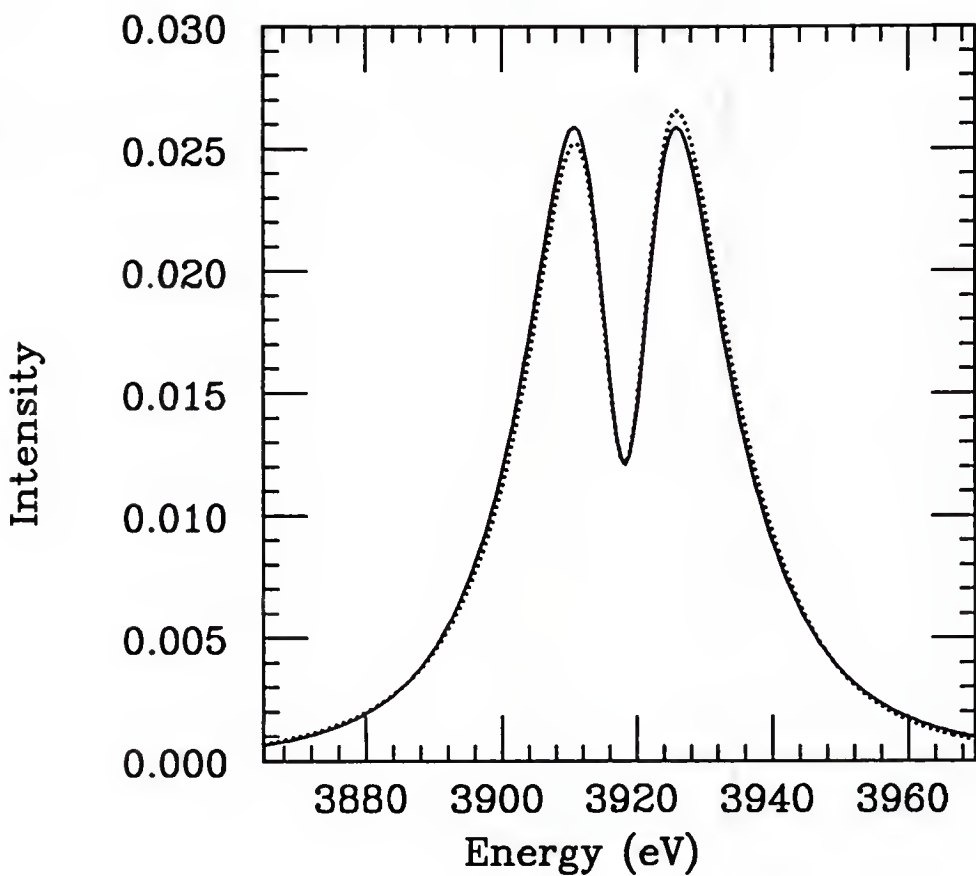


FIGURE (4.7) The  $L_\beta$  line of hydrogenic argon for  $n_e = 1 \times 10^{24} \text{ cm}^{-3}$  and  $kT = 800 \text{ eV}$ . The profile with field independent atomic physics and no ion quadrupole effect is given by (—). The profile with field independent atomic physics and the APEX ion-quadrupole effect is given by (.....). Both profiles are Doppler convoluted. They are calculated from Eqs. (2.97) and (3.14) and discussed in section 4.2.

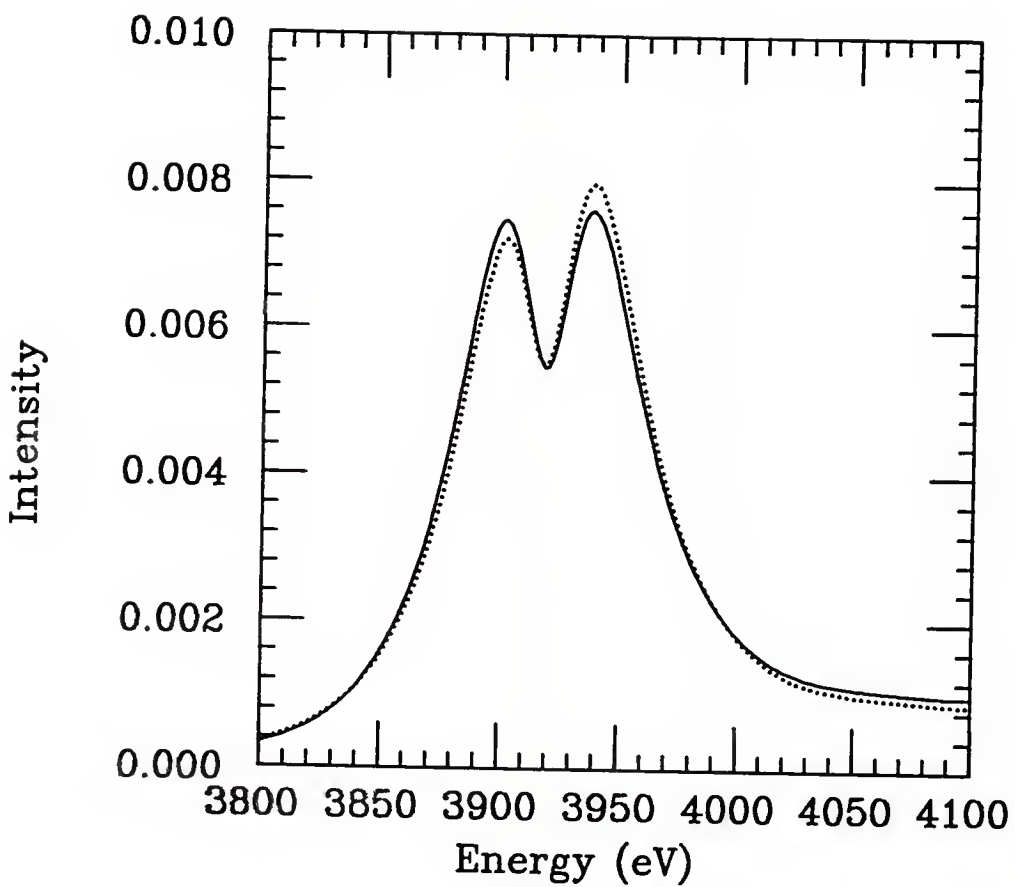


FIGURE (4.8) The  $L_\beta$  line of hydrogenic argon for  $n_e = 5 \times 10^{24} \text{ cm}^{-3}$  and  $kT = 800 \text{ eV}$ . The profile with field independent atomic physics and no ion quadrupole effect is given by (—). The profile with field independent atomic physics and the APEX ion-quadrupole effect is given by (.....). Both profiles are Doppler convoluted.

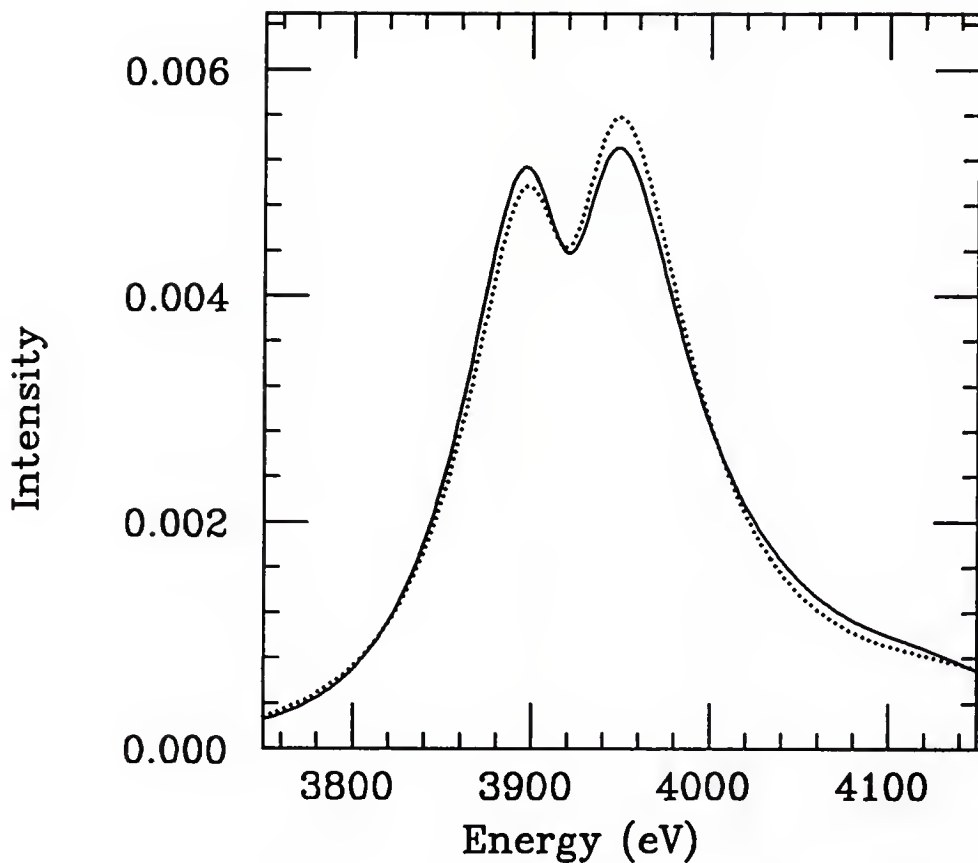


FIGURE (4.9) The  $L_\beta$  line of hydrogenic argon for  $n_e = 1 \times 10^{25} \text{ cm}^{-3}$  and  $kT = 800 \text{ eV}$ . The profile with field independent atomic physics and no ion quadrupole effect is given by (—). The profile with field independent atomic physics and the APEX ion-quadrupole effect is given by (.....). Both profiles are Doppler convoluted.

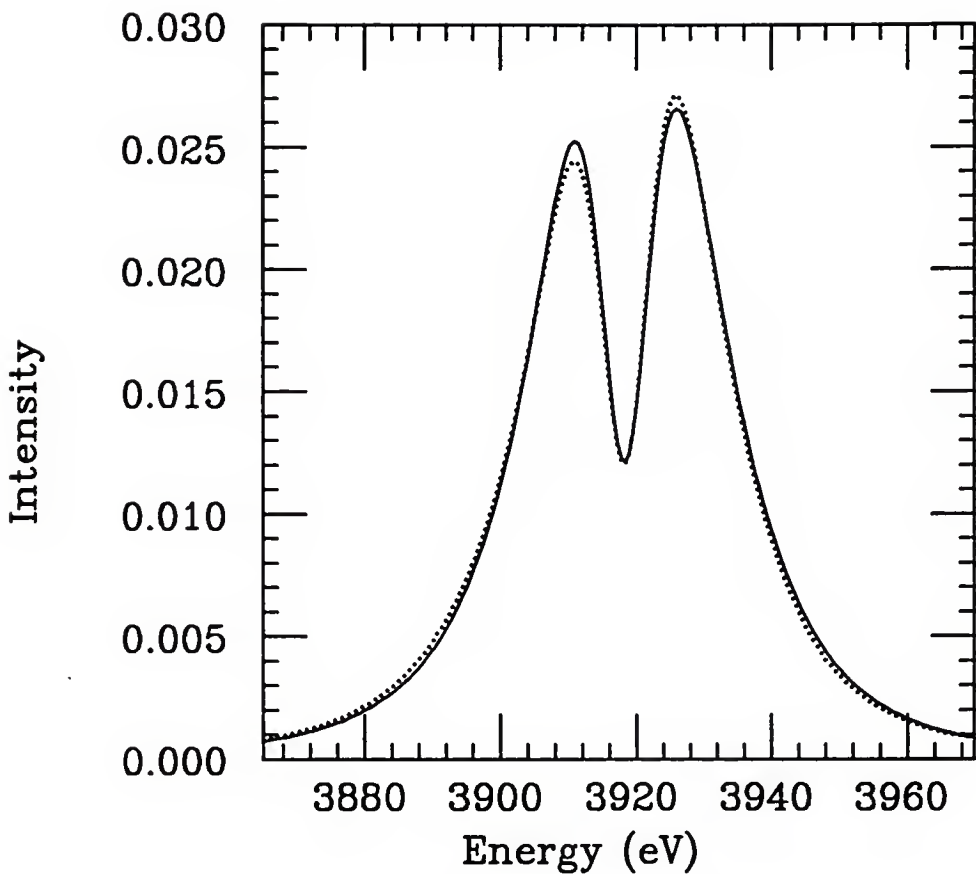


FIGURE (4.10) The  $L_\beta$  line of hydrogenic argon for  $n_e = 1 \times 10^{24} \text{ cm}^{-3}$  and  $kT = 800 \text{ eV}$ . The profile with field independent atomic physics and the APEX ion quadrupole effect is given by (—). The profile with field dependent atomic physics and the APEX ion-quadrupole effect is given by (····). Both profiles are Doppler convoluted.

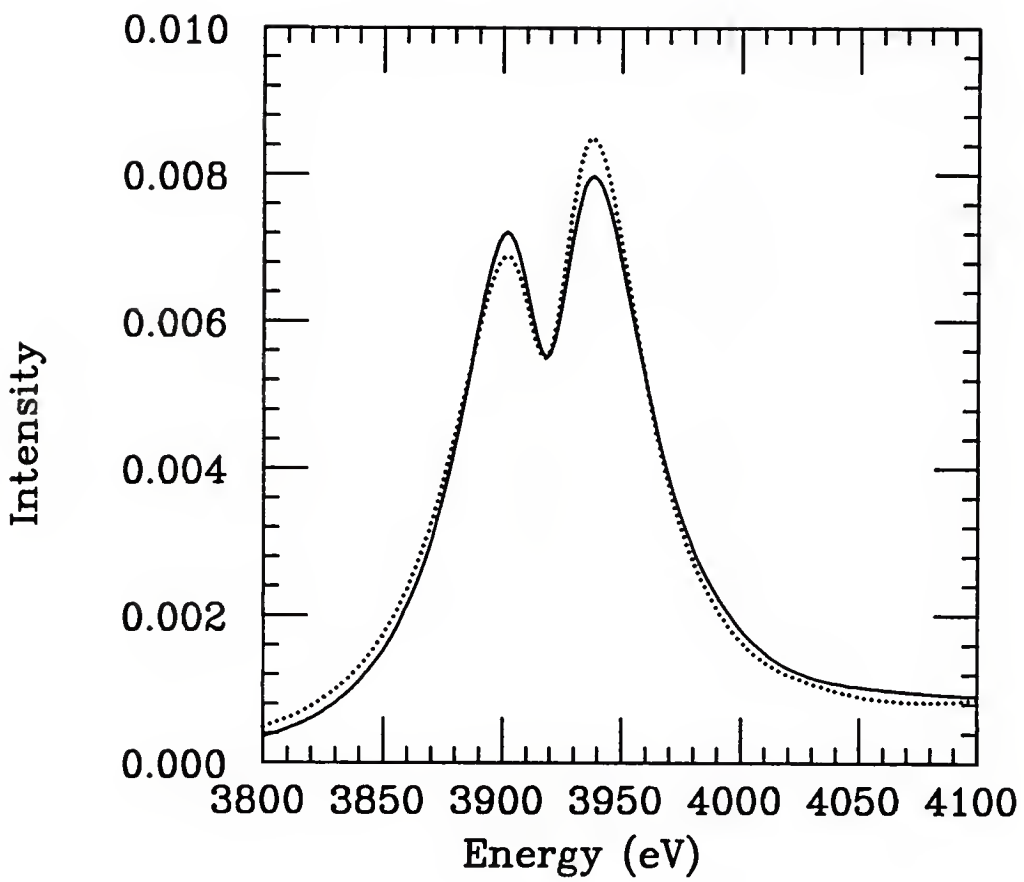


FIGURE (4.11) The  $L_\beta$  line of hydrogenic argon for  $n_e = 5 \times 10^{24} \text{ cm}^{-3}$  and  $kT = 800 \text{ eV}$ . The profile with field independent atomic physics and the APEX ion quadrupole effect is given by (—). The profile with field dependent atomic physics and the APEX ion-quadrupole effect is given by (····). Both profiles are Doppler convoluted.

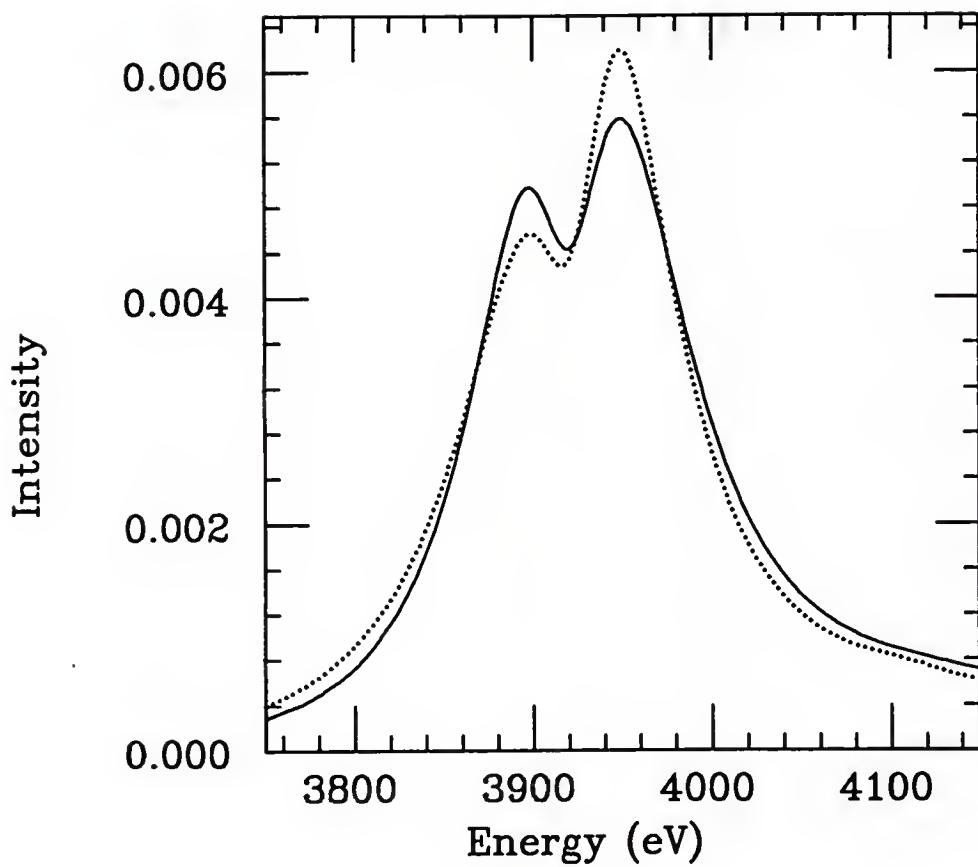


FIGURE (4.12) The  $L_\beta$  line of hydrogenic argon for  $n_e = 1 \times 10^{25} \text{ cm}^{-3}$  and  $kT = 800 \text{ eV}$ . The profile with field independent atomic physics and the APEX ion quadrupole effect is given by (—). The profile with field dependent atomic physics and the APEX ion-quadrupole effect is given by (.....). Both profiles are Doppler convoluted.

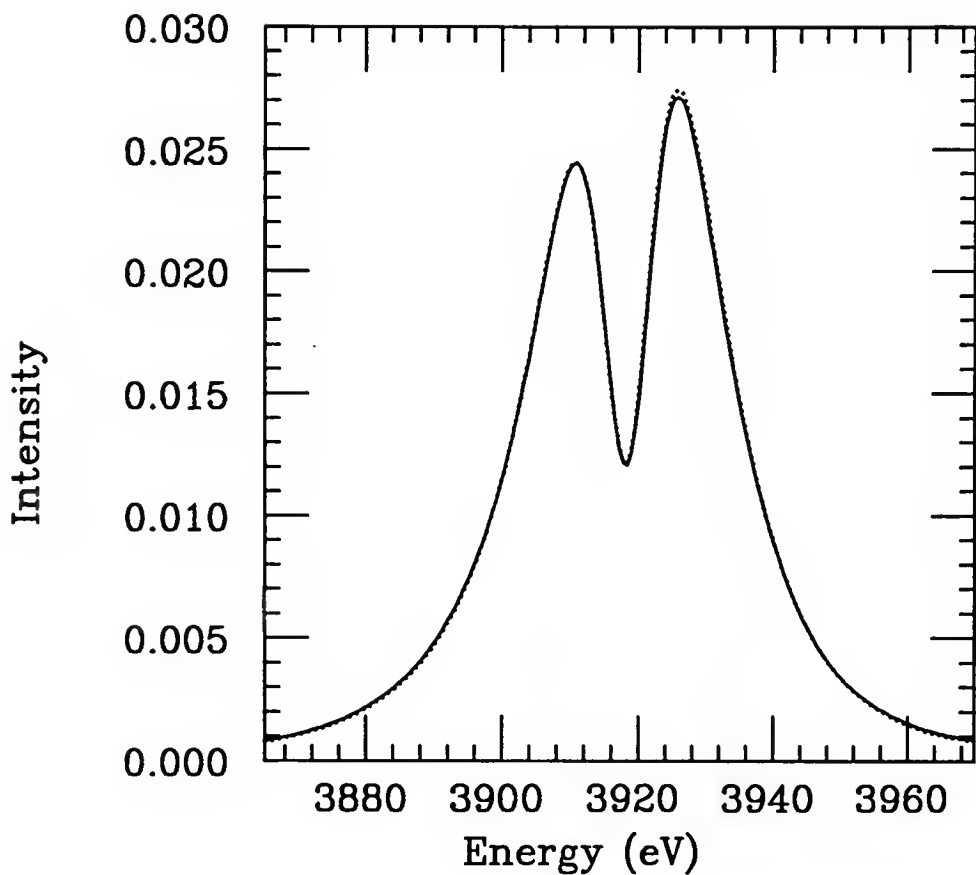


FIGURE (4.13) The  $L_{\beta}$  line of hydrogenic argon for  $n_e = 1 \times 10^{24} \text{ cm}^{-3}$  and  $kT = 800 \text{ eV}$ . The profile with field dependent atomic physics and the ion quadrupole effect is given by (—). The profile with field independent atomic physics, the ion-quadrupole effect and the quadratic energy correction is given by (.....). Both profiles are Doppler convoluted.

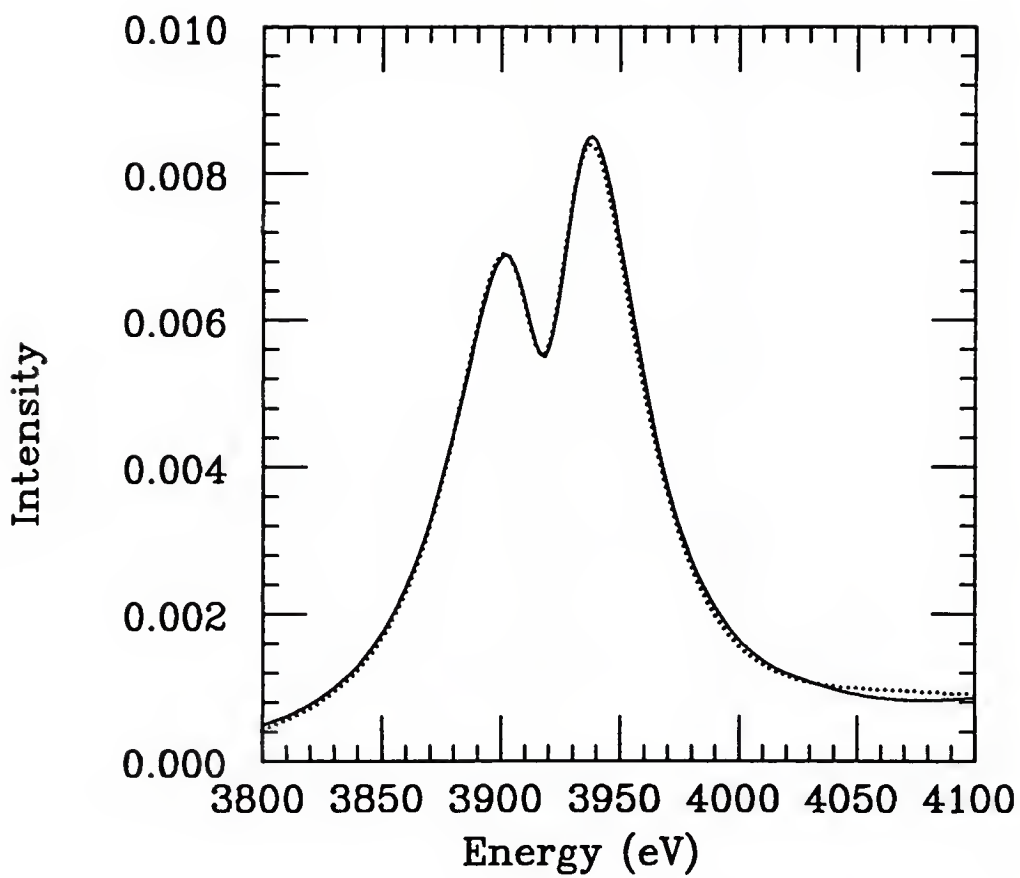


FIGURE (4.14) The  $L_\beta$  line of hydrogenic argon for  $n_e = 5 \times 10^{24} \text{ cm}^{-3}$  and  $kT = 800 \text{ eV}$ . The profile with field dependent atomic physics and the ion quadrupole effect is given by (—). The profile with field independent atomic physics, the ion-quadrupole effect and the quadratic energy correction is given by (.....). Both profiles are Doppler convoluted.

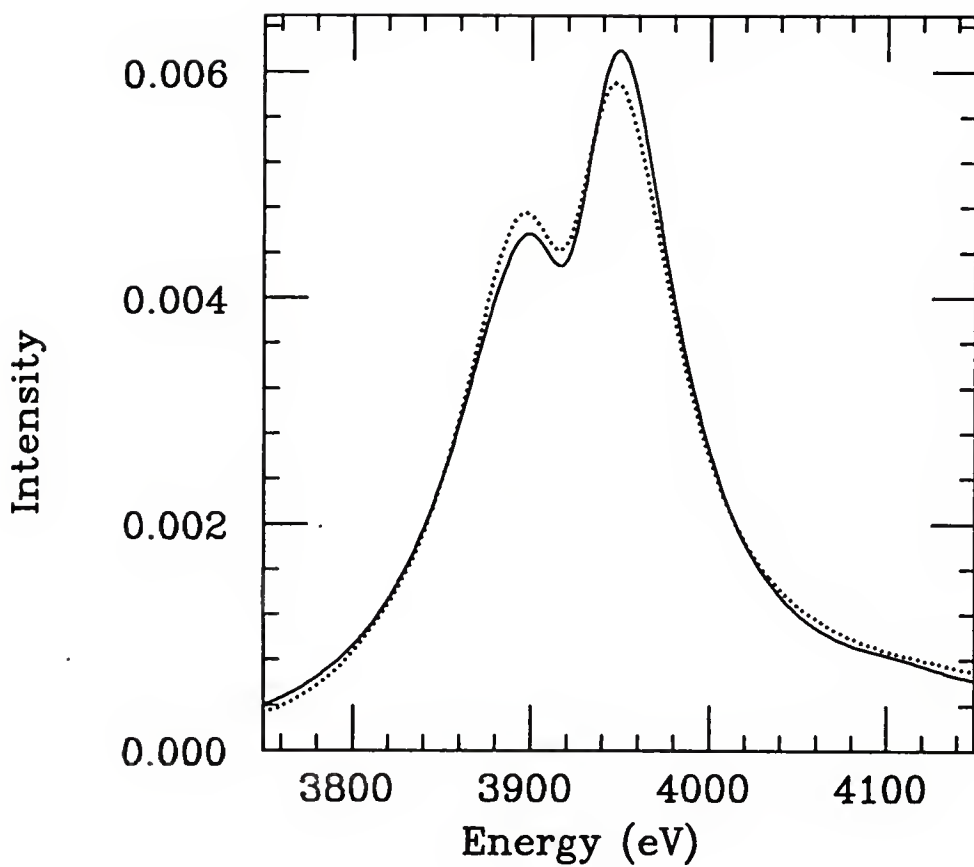


FIGURE (4.15) The  $L_\beta$  line of hydrogenic argon for  $n_e = 1 \times 10^{25} \text{ cm}^{-3}$  and  $kT = 800 \text{ eV}$ . The profile with field dependent atomic physics and the ion quadrupole effect is given by (—). The profile with field independent atomic physics, the ion-quadrupole effect and the quadratic energy correction is given by (····). Both profiles are Doppler convoluted.

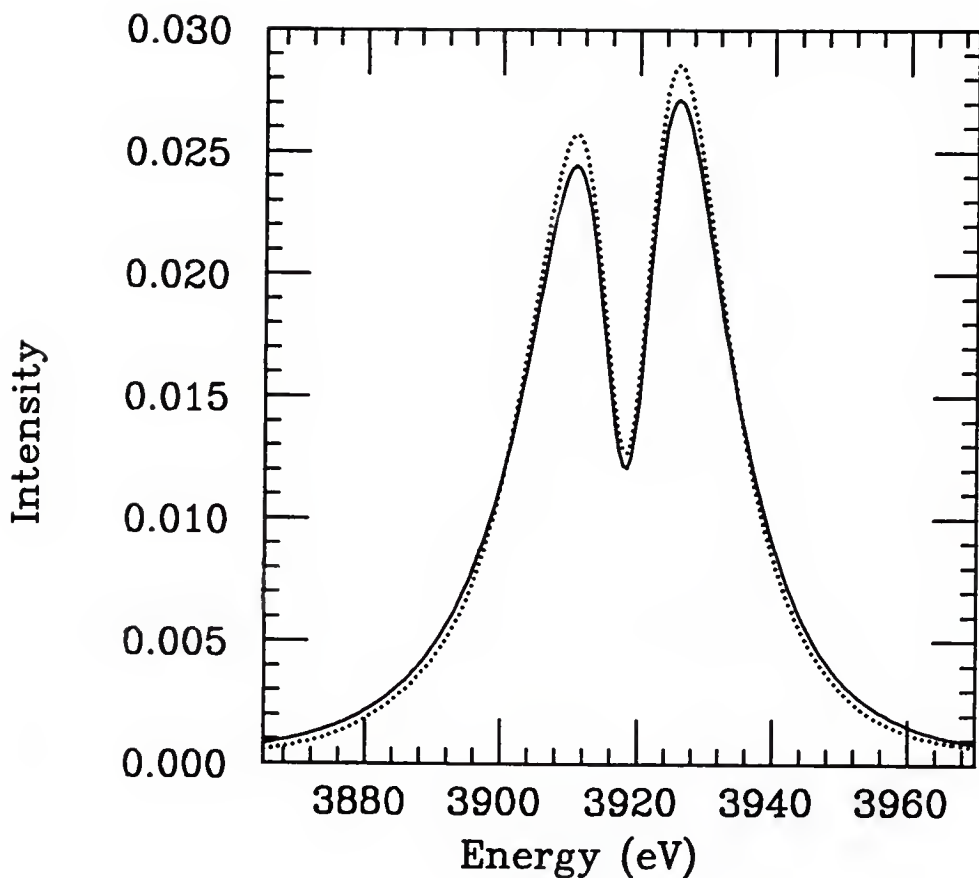


FIGURE (4.16) The  $L_\beta$  line of hydrogenic argon for  $n_e = 1 \times 10^{24} \text{ cm}^{-3}$  and  $kT = 800 \text{ eV}$ . The profile with no field ionization, field dependent atomic physics and the ion quadrupole effect is given by (—). The profile with field ionization, field dependent atomic physics and the ion-quadrupole effect is given by (· · · · ·). Both profiles are Doppler convoluted.

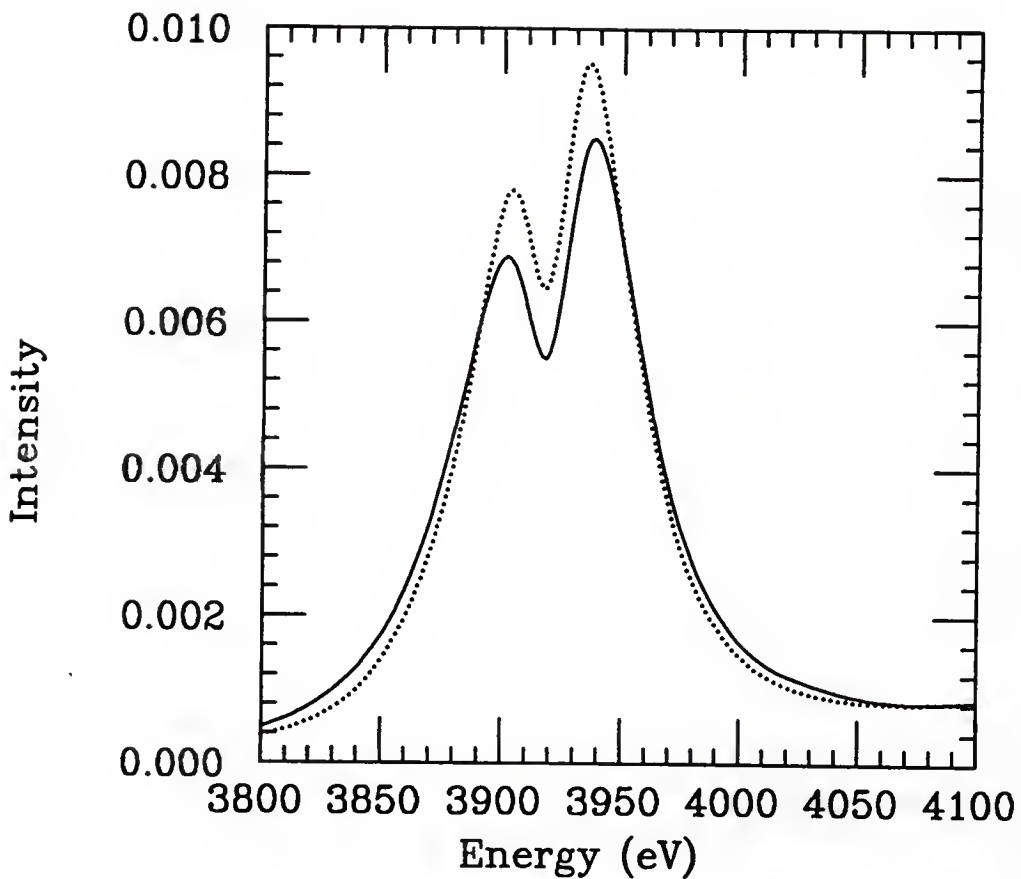


FIGURE (4.17) The  $L_\beta$  line of hydrogenic argon for  $n_e = 5 \times 10^{24} \text{ cm}^{-3}$  and  $kT = 800 \text{ eV}$ . The profile with no field ionization, field dependent atomic physics and the ion-quadrupole effect is given by (—). The profile with field ionization, field dependent atomic physics and the ion-quadrupole effect is given by (····). Both profiles are Doppler convoluted.

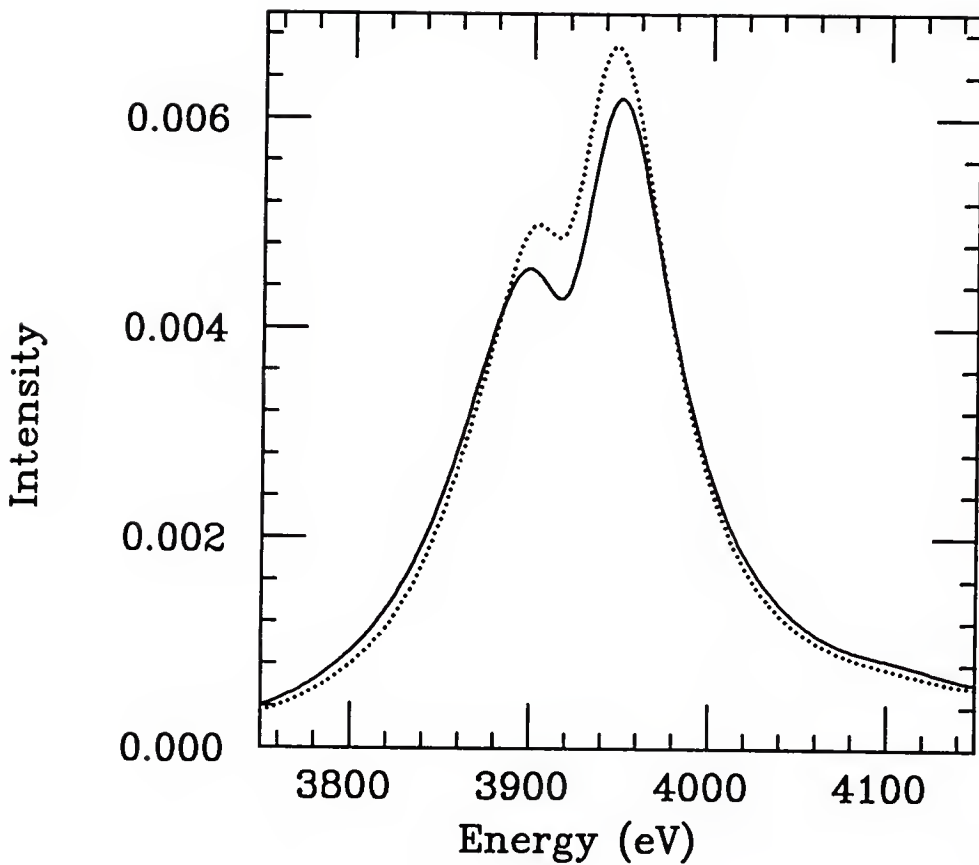


FIGURE (4.18) The  $L_\beta$  line of hydrogenic argon for  $n_e = 1 \times 10^{25} \text{ cm}^{-3}$  and  $kT = 800 \text{ eV}$ . The profile with no field ionization, field dependent atomic physics and the ion quadrupole effect is given by (—). The profile with field ionization, field dependent atomic physics and the ion-quadrupole effect is given by (.....). Both profiles are Doppler convoluted and are discussed in section 4.2.

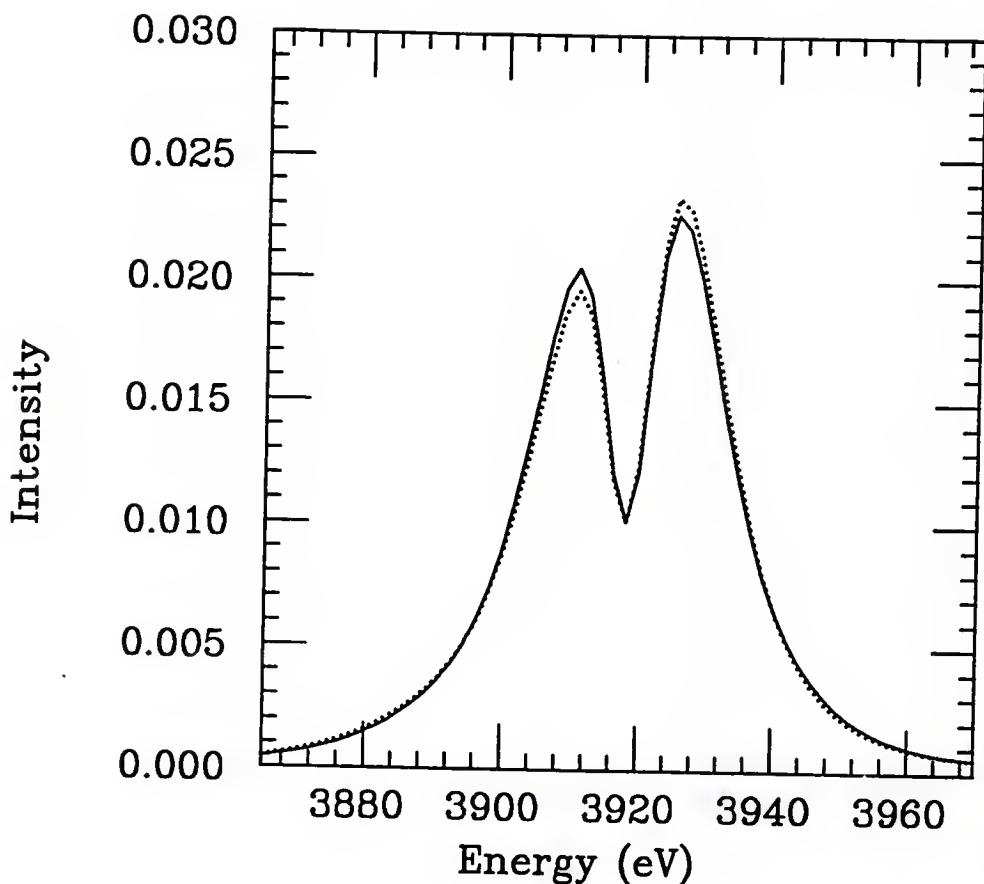


FIGURE (4.19) The  $L_\beta$  line of hydrogenic argon for  $n_e = 1 \times 10^{24} \text{ cm}^{-3}$  and  $kT = 800 \text{ eV}$ . The profile with field dependent atomic physics and the APEX ion quadrupole effect is given by (—). The profile with field dependent atomic physics and the nearest neighbor ion-quadrupole effect is given by (.....). Both profiles are Doppler convoluted.

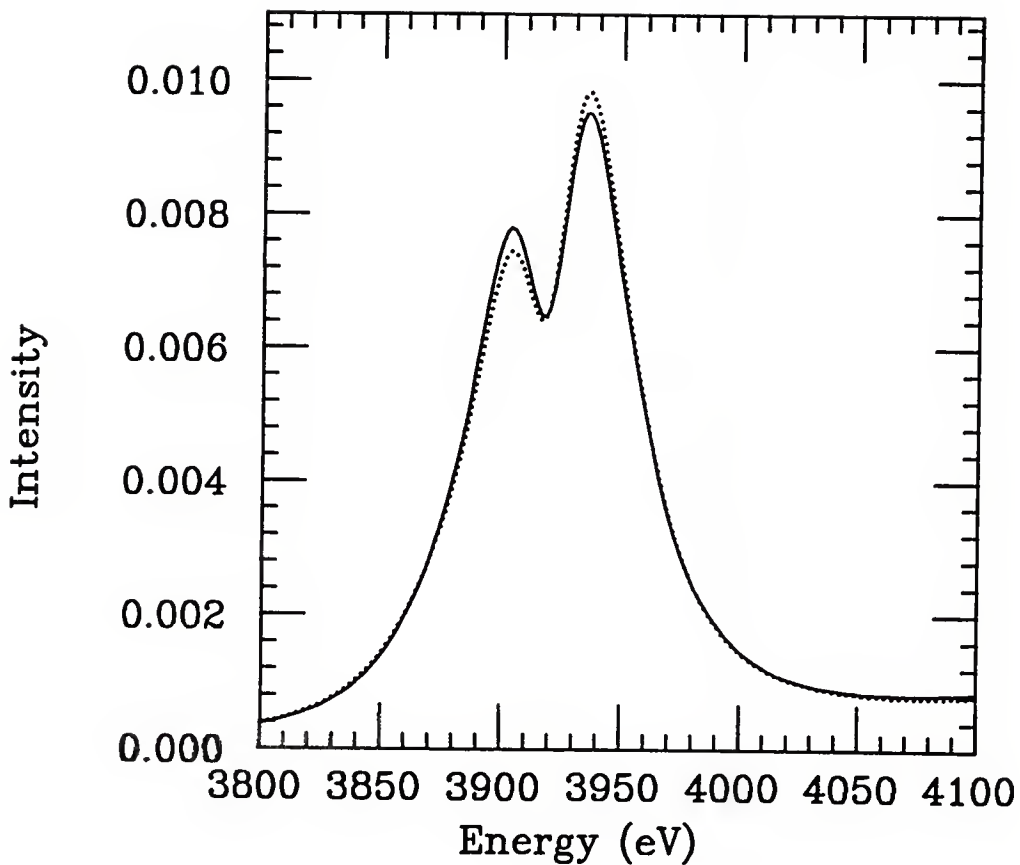


FIGURE (4.20) The  $L_\beta$  line of hydrogenic argon for  $n_e = 5 \times 10^{24} \text{ cm}^{-3}$  and  $kT = 800 \text{ eV}$ . The profile with field dependent atomic physics and the APEX ion quadrupole effect is given by (—). The profile with field dependent atomic physics and the nearest neighbor ion-quadrupole effect is given by (.....). Both profiles are Doppler convoluted.

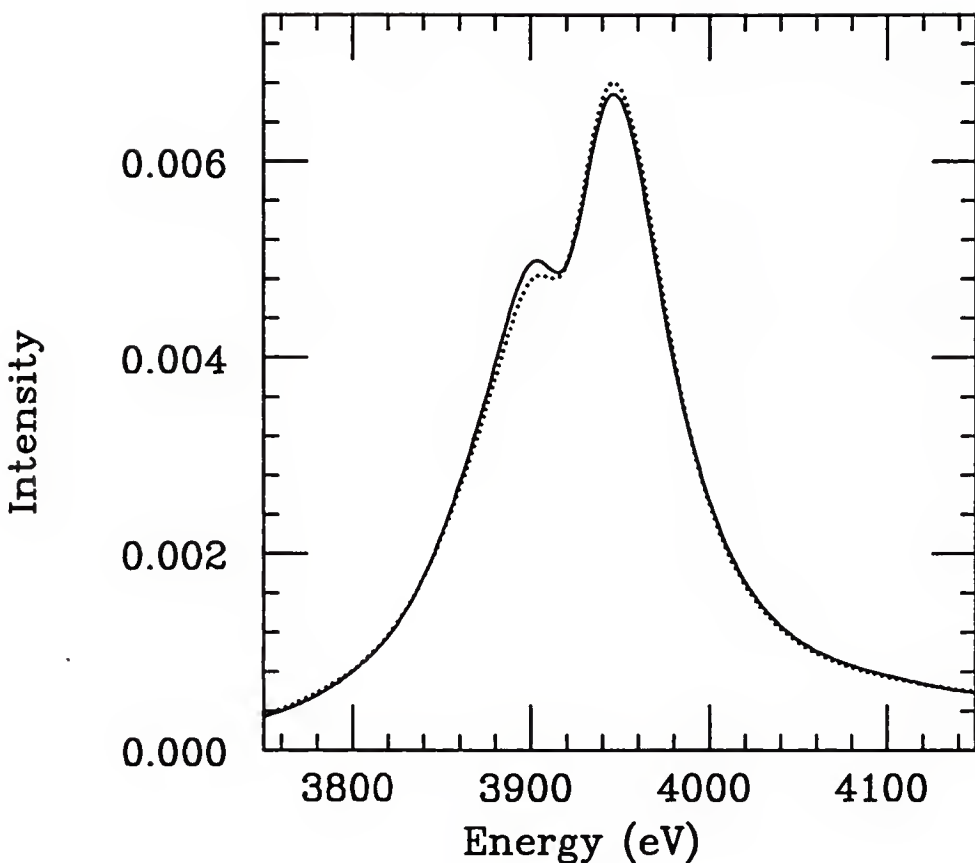


FIGURE (4.21) The  $L_\beta$  line of hydrogenic argon for  $n_e = 1 \times 10^{25} \text{ cm}^{-3}$  and  $kT = 800 \text{ eV}$ . The profile with field dependent atomic physics and the APEX ion quadrupole effect is given by (—). The profile with field dependent atomic physics and the nearest neighbor ion-quadrupole effect is given by (.....). Both profiles are Doppler convoluted.

## APPENDIX A SOME EXPRESSIONS IN USEFUL UNITS

We will present here some frequently encountered physical quantities expressed in various useful units. The reason for this is purely one of convenience. I have found that I constantly recalculate these things because I did not think it important enough to write them down where I could find them again. We will also discuss various units used in atomic physics and line broadening calculations because a long history and a mixing of several disciplines has produced a state of utter confusion in some places.

We give several useful quantities from chapter 2 in simple numerical form. In these expressions,  $n_j$  is given in  $\text{cm}^{-3}$ ,  $kT$  is given in eV and  $Z_j$  is the unit of charge for species  $j$  (i.e. for argon  $Z = 18$  and for electrons  $Z = 1$ ). We give lengths in cm but sometimes a more convenient unit for atomic scales is the Angstrom with  $1 \text{\AA} = 10^{-8} \text{ cm}$ . Also, the correspondence between energy and temperature is  $1 \text{ eV} \leftrightarrow 1.1604 \times 10^4 \text{ deg K}$  or approximately 11,000 deg K. Other relations are given in the following list.

Ion sphere radius:

$$r_{o,j} = 0.62035 n_j^{-1/3} \text{ cm} . \quad (\text{A.1})$$

Debye sphere radius:

$$\lambda_{D,j} = 1.6293 \times 10^{-2} Z_j^{-1} (kT)^{1/2} n_j^{-1/2} \text{ cm.} \quad (\text{A.2})$$

Electron thermal wavelength:

$$\Lambda_e = 6.9195 \times 10^{-8} (kT)^{-1/2} \text{ cm} . \quad (\text{A.3})$$

Atomic Bohr radius:

$$r_n = 5.2918 \times 10^{-9} Z^{-1} n^2 \text{ cm} . \quad (\text{A.4})$$

Electron plasma frequency:

$$\hbar\omega_{p,e} = 3.7133 \times 10^{-11} n_e^{1/2} \text{ eV} . \quad (\text{A.5})$$

Electron-electron coupling constant:

$$\Gamma_{e,e} = 2.3212 \times 10^{-7} (kT)^{-1} n_e^{1/3} . \quad (\text{A.6})$$

Plasma mass density:

$$\rho = 1.6605 \times 10^{-24} \frac{A_W}{Z} n_e \text{ g cm}^{-3} , \quad (\text{A.7})$$

where  $A_W$  is the ion atomic mass in atomic mass units and  $Z$  is the average effective ionic charge.

For formulae expressed in atomic units, we take  $\hbar = e = m_e = 1$  and energy is in units of Hartrees. We have 1 Rydberg = 1/2 Hartree = 13.606 eV. Common conversion factors are 1 eV =  $1.6022 \times 10^{-12}$  erg =  $8.0655 \times 10^3$  cm $^{-1}$ . To convert the electric field strength  $F$ , in atomic units with  $Z = 1$ , to the unitless electric field  $\tilde{\epsilon}$  ( $\tilde{\epsilon}$  is commonly used to give the plasma microfield function  $P(\tilde{\epsilon})$ ), we have

$$\tilde{\epsilon} = 1.37425 \times 10^{16} Z^3 n_e^{-2/3} F . \quad (\text{A.8})$$

Many other useful factors and relations can be found in Ref. 86.

## APPENDIX B THE APEX CONDITIONAL DISTRIBUTION FUNCTION

In this appendix we will derive an expression for the transform of the conditional distribution function<sup>57</sup> in the APEX approximation. We will also discuss the APEX approximation to the low frequency microfield distribution function on which the conditional distribution depends.

The conditional distribution function can be expressed as

$$\tilde{g}(\vec{r}; \vec{\lambda}) = \frac{1}{n_i} \frac{\delta(\ln \tilde{Q}(\vec{\lambda}))}{\delta(i \vec{\lambda} \cdot \vec{E}(\vec{r}))}, \quad (\text{B.1})$$

where  $n_i$  is the ion number density and  $\tilde{Q}(\vec{\lambda})$  is the Fourier-transformed microfield function. We can use a model for  $\tilde{Q}(\vec{\lambda})$  to obtain a corresponding model for  $\tilde{g}(\vec{r}; \vec{\lambda})$  which can be transformed to give the conditional distribution function  $g(\vec{r}; \vec{\epsilon})$ .

With the APEX model,<sup>54</sup>

$$\ln \tilde{Q}(\vec{\lambda}) = n_i \int d\vec{r} g(r) \frac{E(r)}{E^*(r)} \left( e^{i\vec{\lambda} \cdot \vec{E}^*(\vec{r})} - 1 \right), \quad (\text{B.2})$$

where the APEX renormalized field,  $E^*(r)$ , is

$$\vec{E}^*(\vec{r}) = Z_i e \frac{1}{r^2} (1 + \alpha r) e^{-\alpha r}, \quad (\text{B.3})$$

and the plasma-ion Debye-Hückel field is

$$\vec{E}(\vec{r}) = Z_i e \frac{1}{r^2} (1 + \kappa r) e^{-\kappa r}. \quad (\text{B.4})$$

Here,  $\alpha$  is the effective inverse screening length<sup>54</sup> and  $\kappa = 1/\lambda_{D,e}$  is the inverse Debye-Hückel screening length. These expressions are obviously related by

$$\vec{E}^*(\vec{r}) = \frac{1}{R(r)} \vec{E}(\vec{r}) , \quad (B.5)$$

where

$$R(r) \equiv \frac{(1 + \kappa r)e^{-\kappa r}}{(1 + \alpha r)e^{-\alpha r}}. \quad (B.6)$$

Thus  $\vec{E}^*(\vec{r})$  is a functional of  $\vec{E}(\vec{r})$ : i.e.  $\vec{E}^* = \vec{E}^*[\vec{E}]$ . Now we can construct the APEX version of  $\tilde{g}(\vec{r}; \vec{\lambda})$  by using Eq. (B.2) in Eq. (B.1). We obtain

$$\begin{aligned} \tilde{g}(\vec{r}; \vec{\lambda}) &= \frac{\delta}{\delta(i\vec{\lambda} \cdot \vec{E}(r))} \int d\vec{r}' g(r') \frac{i\vec{\lambda} \cdot \vec{E}(r')}{i\vec{\lambda} \cdot \vec{E}^*(r')} \left( e^{i\vec{\lambda} \cdot \vec{E}^*(r')} - 1 \right) \\ &= \int d\vec{r}' g(r') \frac{E(r')}{E^*(r')} e^{i\vec{\lambda} \cdot \vec{E}^*(r')} \frac{\delta E^*(r')}{\delta E(r)} \\ &\quad + \int d\vec{r}' \frac{g(r')}{i\vec{\lambda} \cdot \vec{E}^*(r')} \left( e^{i\vec{\lambda} \cdot \vec{E}^*(r')} - 1 \right) \left[ \frac{\delta E(r')}{\delta E(r)} - \frac{E(r')}{E^*(r')} \frac{\delta E^*(r')}{\delta E(r)} \right] . \end{aligned} \quad (B.7)$$

The second term gives zero and leaves us with the result,

$$\tilde{g}(\vec{r}; \vec{\lambda}) = \int d\vec{r}' g(r') \frac{E(r')}{E^*(r')} e^{i\vec{\lambda} \cdot \vec{E}^*(r')} \delta(\vec{r} - \vec{r}') \frac{1}{R(r')} . \quad (B.8)$$

Carrying out the integration, we obtain

$$\tilde{g}_{APEX}(\vec{r}; \vec{\lambda}) = g(r) e^{i\vec{\lambda} \cdot \vec{E}^*(\vec{r})} , \quad (B.9)$$

which is the expression we desired. In the above development, we have made use of the expression

$$\frac{\delta E(\vec{r}')}{\delta E(\vec{r})} = \delta(\vec{r} - \vec{r}') , \quad (B.10)$$

which gives us

$$\frac{\delta E^*(r')}{\delta E(r)} = \frac{\delta E^*(r')}{\delta E(r')} \frac{\delta E(r')}{\delta E(r)} = \delta(\vec{r} - \vec{r}') \frac{1}{R(r')} . \quad (\text{B.11})$$

Eq. (B.9) will allow us to calculate the constrained average  $\langle F \rangle_\epsilon$  in the simple APEX approximation.

This approximation is based on the APEX model for the low frequency microfield distribution function. We now briefly review the key features of this approximation. A simple physical picture of the APEX model consists of replacement of the usual screened-ion plasma by a plasma of noninteracting quasiparticles. Each of which will produce a field at the radiator. However, this field has an adjustable parameter  $\alpha$  which is determined by the imposition of two constraints:<sup>53,54</sup> the second moment condition and the local-field constraint. The single particle APEX electric field is given by Eq. (B.3).

The local-field constraint requires that the field produced at the radiator due to the sum of the adjustable parameter fields from the quasiparticles in a volume element  $d^3r$  at  $\vec{r}$  be equal to the field produced by the actual plasma ions interacting with the chosen inter-ion potential. In our case we choose the Debye-Hückel screened potential to describe the actual ion interactions relevant to the low frequency plasma microfield.<sup>54</sup> If we define the radial distribution function for the quasiparticles surrounding the radiator as  $G(r)$ , the local field constraint requires that

$$n_i G(r) E^*(r) d^3r = n_i g(r) E(r) d^3r , \quad (\text{B.12})$$

or

$$G(r) = g(r) \frac{E(r)}{E^*(r)} . \quad (\text{B.13})$$

The second moment condition requires that the APEX approximation to  $Q(\vec{\epsilon})$  produce the exact second moment. Specifically, that

$$\int d\vec{\epsilon} \epsilon^2 Q_{APEX}(\vec{\epsilon}) = \langle \vec{E}^2 \rangle , \quad (\text{B.14})$$

where  $\vec{E}$  is the total field produced by the ions. Again, the ions are assumed to interact with Debye-Hückel potentials.

The right-hand side of Eq. (B.14) can be rewritten as<sup>54</sup>

$$\begin{aligned} \langle \vec{E}^2 \rangle &= \frac{1}{(\chi e)^2} \langle \vec{\nabla} V \cdot \vec{\nabla} V \rangle \\ &= \frac{1}{\chi^2 e^2 \beta} \langle \nabla^2 V \rangle \\ &= \frac{4\pi}{\chi \beta} Z_i n_i \psi(\lambda_{D,e}) , \end{aligned} \quad (\text{B.15})$$

where

$$\psi(\lambda) = \frac{1}{\lambda^2} \int_0^\infty dr r g(r) e^{-r/\lambda} . \quad (\text{B.16})$$

Here  $\beta = 1/kT$  and  $\chi$  is the effective radiator charge.

The left-hand side is evaluated using the local field constraint to give

$$\begin{aligned} \int d\vec{\epsilon} \epsilon^2 Q_{APEX}(\vec{\epsilon}) &= \int d\vec{\epsilon} \epsilon^2 \langle \delta(\vec{\epsilon} - \vec{E}^*) \rangle_G \\ &= \langle E^{*2} \rangle_G \\ &= 4\pi \int_0^\infty dr r^2 G(r) E^{*2}(r) \\ &= 4\pi \int_0^\infty dr r^2 g(r) E(r) E^*(r) . \end{aligned} \quad (\text{B.17})$$

Here the subscript  $G$  on  $\langle \cdots \rangle_G$  means that we use  $G(r)$  rather than  $g(r)$  when evaluating the ensemble average of the single particle additive function  $E^*$ .

The adjustable parameter  $\alpha$  is then determined by Eqs. (B.15) and (B.17) which gives

$$\frac{Z_i n_i}{\chi} \int_0^\infty dr r g(r) e^{-r/\lambda} = \beta \lambda^2 \int_0^\infty dr r^2 g(r) E(r) E^*(\alpha, r) . \quad (\text{B.18})$$

We evaluate this equation using an HNC calculation<sup>39</sup> for  $g(r)$  and the value of  $\alpha$  calculated above. We are then free to evaluate the APEX microfield distribution function given by

$$Q_{APEX}(\vec{\epsilon}) = \int \frac{d\vec{\lambda}}{(2\pi)^3} e^{-\vec{\lambda} \cdot \vec{\epsilon}} \tilde{Q}(\vec{\lambda}), \quad (\text{B.19})$$

where the APEX approximation for  $\tilde{Q}(\vec{\lambda})$  is given by Eq. (B.2). We will use this approximation for the microfield probability function to perform the integration over field values in the expression for  $I(\omega)$  given by Eq. (3.11).

## APPENDIX C PARABOLIC COORDINATES

Parabolic coordinates<sup>61</sup> are defined in terms of the cartesian coordinates by

$$\begin{aligned} x &= \sqrt{\xi\eta} \cos \varphi \\ y &= \sqrt{\xi\eta} \sin \varphi \\ z &= \frac{1}{2}(\xi - \eta) , \end{aligned} \tag{C.1}$$

and in terms of spherical coordinates by

$$\begin{aligned} \xi &= r(1 + \cos \theta) \\ \eta &= r(1 - \cos \theta) \\ \varphi &= \varphi . \end{aligned} \tag{C.2}$$

The parabolic coordinates are defined on the domains

$$\begin{aligned} 0 &\leq \xi < \infty \\ 0 &\leq \eta < \infty \\ 0 &\leq \varphi \leq 2\pi . \end{aligned} \tag{C.3}$$

The volume element in parabolic coordinates is given by

$$d^3x = \frac{1}{4}(\xi + \eta)d\xi d\eta d\varphi , \tag{C.4}$$

and the Laplacian is given by

$$\nabla^2 = \frac{4}{(\xi + \eta)} \frac{\partial}{\partial \xi} \left( \xi \frac{\partial}{\partial \xi} \right) + \frac{4}{(\xi + \eta)} \frac{\partial}{\partial \eta} \left( \eta \frac{\partial}{\partial \eta} \right) + \frac{1}{\xi\eta} \frac{\partial^2}{\partial \varphi^2} . \tag{C.5}$$

Once the Schrödinger equation in parabolic coordinates, Eq. (3.57), is separated and solved, the solutions for the coordinates  $\xi$  and  $\eta$  have some simple characteristics.<sup>71</sup> Motion along the downfield coordinate  $\xi$  is bound since it corresponds to the part of the potential that increases without bound. By downfield we mean in the direction of the electric field vector. Likewise, upfield means the opposite direction. The separation constant  $A$  can take only discrete values related to  $n_1$  which gives the number of wavefunction nodes in the  $\xi$  direction. Motion along the upfield coordinate  $\eta$  is unbound since it corresponds to the part of the potential that forms a potential barrier. The number of wavefunction nodes in the  $\eta$  direction is given by  $n_2$  for the range between the origin and the classical turning point.

We have been using the three parabolic quantum numbers  $n_1$ ,  $n_2$  and  $m_l$  to describe the field dependent states. Another set is also in common usage; these are the electric quantum numbers<sup>62</sup>  $n$ ,  $q$  and  $m_l$  where  $q = n_2 - n_1$  and  $n$  is the usual principal quantum number given by  $n = n_1 + n_2 + |m_l| + 1$ . The electron spin can be included in this description by the addition of the spin quantum number  $m_s$  which takes the values  $\pm 1/2$ .

## APPENDIX D IMPORTANCE OF THE ION-QUADRUPOLE EFFECT

In this appendix, we present an estimate of the conditions under which the ion-quadrupole effect should become important relative to that of the ion-dipole for the case of multielectron radiators.<sup>15</sup> The ion-quadrupole effect attempts to account for the fact that perturbing plasma ions do not produce a uniform electric field at the radiator. As long as the perturbers are sufficiently far away, the uniform field approximation is not unreasonable. As the density increases, however, these perturbers, on the average, draw closer to the radiator and can produce a significant field gradient.

To help us understand when the ion-quadrupole effect will become important, we will examine in some detail a simple model system that consists of two close lying energy levels with the same principal quantum number. We will look at how the dipole and quadrupole effects cause the states associated with these two levels to mix.

Consider the radiator Hamiltonian with terms up to the quadrupole in the multipole expansion of the radiator perturbing-ion interaction:

$$H = H^0 + D + Q , \quad (D.1)$$

where  $H^0$  is the unperturbed radiator Hamiltonian and  $D$  and  $Q$  are the dipole and quadrupole corrections respectively. We assume that  $D \gg Q$  for the expansion to be valid. Both  $D$  and  $Q$  will depend on the plasma electric microfield. The parity of  $D$  is odd while that of  $Q$  is even. Because of this

fact  $D$  can have non-zero matrix elements only between states of unlike parity while  $Q$  can have non-zero matrix elements only between states of like parity. This means all diagonal matrix elements of  $D$  vanish for basis states of definite parity such as those produced by our zero-order Hamiltonian  $H^0$ . For this case, we will take the states  $a$  and  $b$  to be of different parity. This will give non-zero off diagonal matrix elements for the dipole operator  $D$  but zero off diagonal matrix elements for the quadrupole operator  $Q$ . We will represent the Hamiltonian,  $H$ , for this two state system in terms of the eigenstates of  $H^0$ ,

$$H^0 |a^0\rangle = E_a^0 |a^0\rangle . \quad (\text{D.2})$$

Thus  $D_{a,b} = \langle a^0 | D | b^0 \rangle$  and  $Q_{a,a} = \langle a^0 | Q | a^0 \rangle$  while  $D_{a,a} = D_{b,b} = 0$  and  $Q_{a,b} = Q_{b,a} = 0$  because of the parity constraint.

In matrix form, the Hamiltonian is then represented by,

$$H = \begin{pmatrix} E_a^0 + Q_{a,a} & D_{a,b} \\ D_{b,a} & E_b^0 + Q_{b,b} \end{pmatrix} . \quad (\text{D.3})$$

Construction of the secular equation for this Hamiltonian from the determinantal equation  $|H - EI| = 0$ , where  $I$  is the identity matrix, will yield the system eigenvalues:

$$E = \frac{1}{2} \left( E_a^0 + E_b^0 + Q_{a,a} + Q_{b,b} \pm \sqrt{(\Delta E_0 + \Delta Q_{a,b})^2 + 4|D_{a,b}|^2} \right) , \quad (\text{D.4})$$

where  $\Delta E_0 \equiv E_a^0 - E_b^0$  is the zero-order energy splitting between levels with the same principal quantum number and  $\Delta Q_{a,b} \equiv Q_{a,a} - Q_{b,b}$ . The energy difference, or splitting, between the two levels is then

$$\Delta E = \sqrt{(\Delta E_0 + \Delta Q_{a,b})^2 + 4|D_{a,b}|^2} , \quad (\text{D.5})$$

where  $\Delta E \equiv E_+ - E_-$ . This can be expanded to give

$$\Delta E = \sqrt{\Delta E_0^2 + \Delta Q_{a;b}^2 + 2\Delta E_0 \Delta Q_{a;b} + 4|D_{a,b}|^2}. \quad (\text{D.6})$$

We take the eigenfunctions of  $H^0$  to be real and with the assumption that

$$|D_{a,b}| \gg |\Delta Q_{a;b}|, \quad (\text{D.7})$$

we can ascertain the significance of the quadrupole term on  $\Delta E$ . The validity of this assumption can be checked for the conditions of interest with the estimates for  $D_{a,b}$  and  $\Delta Q_{a;b}$  given below. For our physical conditions of interest, it holds true but it should be checked for additional cases.

If the two eigenvalues of  $H^0$  are degenerate we will have  $\Delta E_0 = 0$ , and the dipole term will dominate. This is the case for hydrogen-like radiators. For non-hydrogenic radiators, however, this is no longer true. We then find, on inspection of Eq. (D.6), that the quadrupole term will have an appreciable effect when

$$|\Delta E_0 \Delta Q_{a;b}| \geq 2|D_{a,b}|^2. \quad (\text{D.8})$$

This is an important result that we can use to derive approximate inequalities that will tell us when to expect the ion-quadrupole effect to significantly perturb adjacent energy levels as compared to the dipole effect and hence affect spectral line shapes.

We will make approximations to evaluate Eq. (D.8) for the case of highly ionized radiators with large values of nuclear charge,  $Z$ . Consider an optical electron in the field of an effective nuclear charge,  $Z_{eff} = Z - N_b + 1$ , where  $N_b$  is the total number of bound electrons. Using hydrogenic wave functions

for this optical electron, we take for the quantum numbers in the spherical representation:

$$\begin{aligned} a \rightarrow (n, l, m) &= (n, n-1, 0) \\ b \rightarrow (n', l', m') &= (n, n-2, 0) . \end{aligned} \quad (D.9)$$

These satisfy the dipole selection rules for the  $z$  direction (i.e.  $\Delta l = \pm 1$ ,  $\Delta m = 0$ ) and correspond to eigenstates appropriate for connection to low lying ground states in resonance-like line transitions. We use the field from a particle at the average interparticle spacing  $r_i$  as an approximation for the plasma electric field:

$$F_i = \frac{eZ_i}{r_i^2} ,$$

where  $r_i$  is approximated by the ion sphere radius given by:

$$\frac{4\pi}{3}r_i^3 n_i = 1 , \quad (D.10)$$

and  $Z_i$  is the charge of the perturbing ion. Note that the ion and electron number density are related by  $n_e = Z_i n_i$ . For the dipole term in Eq. (D.8) we use:<sup>61</sup>

$$D_{a,b} = eF_i \langle a | z | b \rangle = eF_i Z_{n',l-1,m}^{n,l,m} , \quad (D.11)$$

where,

$$Z_{n',l-1,m}^{n,l,m} = \sqrt{\frac{l^2 - m^2}{(2l+1)(2l-1)}} R_{n',l-1}^{n,l} . \quad (D.12)$$

For the case of interest here, we have  $n' = n$  and the radial integral reduces to

$$R_{n,l-1}^{n,l} = \frac{3a_o}{2Z_{eff}} n \sqrt{n^2 - l^2} . \quad (D.13)$$

For the quadrupole term (again, using the field from an ion at the average interparticle spacing) we have:<sup>17</sup>

$$\begin{aligned} Q_{a,a} &= -\frac{e^2 Z_i}{r_i^3} \langle a | \frac{1}{2} r^2 (3 \cos^2 \theta - 1) | a \rangle \\ &= -\frac{e^2 Z_i}{r_i^3} \left[ \frac{1}{2} \left( \frac{n a_o}{Z_{eff}} \right)^2 [5n^2 + 1 - 3l(l+1)] \frac{l(l+1) - 3m^2}{(2l+3)(2l-1)} \right]. \end{aligned} \quad (D.14)$$

Evaluating these for our particular case gives us

$$\begin{aligned} D_{a,b} &= \frac{3}{2} n(n-1) \sqrt{\frac{2n-1}{4n^2-8n+3}} \left( \frac{4\pi}{3} \right)^{2/3} \frac{e^2 a_o}{Z_{eff}} Z_i^{1/3} n_e^{2/3} \\ &\simeq 2\sqrt{2} n^{3/2} \frac{e^2 a_o}{Z_{eff}} Z_i^{1/3} n_e^{2/3}, \end{aligned} \quad (D.15)$$

and

$$\begin{aligned} |\Delta Q_{a,b}| &= 4\pi n^2(n-1) \left[ \frac{4n^3 - 12n^2 + 4n + 5}{8n^3 - 36n^2 + 46n - 15} \right] \left( \frac{e a_o}{Z_{eff}} \right)^2 n_e \\ &\simeq 2\pi n^3 \left( \frac{e a_o}{Z_{eff}} \right)^2 n_e. \end{aligned} \quad (D.16)$$

The use of these estimates, along with Eq. (D.8), will give us a condition for the appearance of significant ion-quadrupole effects.

Upon substitution we find that the condition gives

$$\begin{aligned} |\Delta E_0| &\geq \frac{8}{\pi} e^2 Z_i^{2/3} n_e^{1/3} \\ &= 3.7 \times 10^{-7} Z_i^{2/3} n_e^{1/3} \text{ eV}, \end{aligned} \quad (D.17)$$

where  $n_e$  is in  $\text{cm}^{-3}$ . For  $Z_i = 18$  and  $n_e = 1 \times 10^{24}$  to  $1 \times 10^{25} \text{ cm}^{-3}$  we find that  $|\Delta E_0|$  must be larger than 252 eV to 547 eV respectively for the ion-quadrupole effect to dominate the dipole effect. These energy splittings are much too large to be significant for the natural splittings found in helium-like

and lithium-like argon. However, for proton perturbers where  $Z_i = 1$ , we have  $\Delta E_0 \geq 37$  eV for  $n_e = 1 \times 10^{24} \text{ cm}^{-3}$ . This is more reasonable, and the ion-quadrupole effect may be important for this case. Remember that this example is for levels with the same principal quantum number, with opposite parity and which satisfy Eq. (D.7). In conclusion, we do not expect the ion-quadrupole effect to dominate the spectra of multielectron emitters for conditions under consideration in this dissertation.

## APPENDIX E FINE STRUCTURE CORRECTIONS

The fine structure correction to the radiator Hamiltonian can be determined from a nonrelativistic expansion of the Dirac equation to order  $\alpha^2$ , where  $\alpha$  is the fine structure constant.<sup>87</sup> The correction is given by

$$H_{f.s.} = -\frac{p^4}{8m^3c^2} + \frac{e}{2m^2c^2} \frac{1}{r} \frac{\partial}{\partial r} \varphi(r) (\vec{S} \cdot \vec{L}) + \frac{\hbar^2 e}{8m^2c^2} \nabla^2 \varphi(r) + \frac{e}{2m^2c^2} F \hat{z} \cdot (\vec{S} \times \vec{p}) , \quad (\text{E.1})$$

where  $F$  is the uniform ion microfield at the radiator in the  $\hat{z}$  direction and  $\varphi(r)$  is the radiator central potential. The electron spin angular momentum operator is given by  $\vec{S}$ , the orbital angular momentum operator is given by  $\vec{L}$  and  $\vec{p}$  is the radiator electron momentum operator. Shortly, we will be interested in the total angular momentum operator given by  $\vec{J} = \vec{L} + \vec{S}$ . The first three terms lead to the usual fine structure energy shift term. The fourth term is

$$H_4 \equiv \frac{e}{2m^2c^2} F \hat{z} \cdot (\vec{S} \times \vec{p}) . \quad (\text{E.2})$$

When  $H_{f.s.}$  is evaluated in the field-free total angular momentum basis  $|nljj_z\rangle$ , the first three terms are diagonal. The fourth term can be shown to be equivalent to

$$\langle \alpha | H_4 | \beta \rangle = \frac{ie}{2mc^2} \omega_{\alpha,\beta} \hat{z} \cdot \vec{S}_{\alpha,\beta} \times \vec{r}_{\alpha,\beta} , \quad (\text{E.3})$$

where  $\alpha$  and  $\beta$  are the indices of the basis elements and  $\omega_{\alpha,\beta}$  is the energy difference between these two states. For the field-free basis, the states with the same principal quantum number are degenerate giving  $\omega_{\alpha,\beta} = 0$ . As a consequence, the matrix element will be zero. However, this is not in general the case for the field dependent basis where this degeneracy is broken and  $\omega_{\alpha,\beta} \neq 0$ . For the case of the field dependent basis,  $H_4$  can be included in the evaluation of  $H_{f.s.}$ . If we do this we find that its matrix elements only appear as off-diagonal elements of  $H_{f.s.}$ . It can be shown that

$$\langle \alpha | H_4 | \beta \rangle \sim O(Z^2 \alpha^2) , \quad (E.4)$$

which is to the same order in  $\alpha$  as the usual field independent fine structure term. In this case, however, since it only appears off-diagonally in the matrix representation of  $H_{f.s.}$ , it will only contribute corrections to the energy of order higher than  $Z^2 \alpha^2$ . This can be seen from looking at the simple example of a  $2 \times 2$  matrix eigenvalue problem with only off-diagonal corrections to an already diagonal matrix. Thus, to order  $\alpha^2$  we will ignore  $H_4$  as a field dependent addition to the fine structure term.

The remaining three terms of the fine structure Hamiltonian will give the usual fine structure energy shift<sup>61,83,88</sup> of

$$E_{n,j} = -\frac{\alpha^2 Z^4}{n^4} \left[ \frac{n}{j + 1/2} - \frac{3}{4} \right] , \quad (E.5)$$

in the total angular momentum basis. Here,  $j$  is the quantum number associated with the total angular momentum  $\vec{J}$ .

If we ignore the field dependence of the fine structure for a moment, we can look at the magnitude of the fine structure shift and splitting. For the  $L_\alpha$  case of hydrogenic argon, we find the total transition energy  $\Delta E_{2,1}^j$  to

be  $\Delta E_{2,1}^{1/2} = 3319.1$  eV for  $j = 1/2$  and  $\Delta E_{2,1}^{3/2} = 3323.8$  eV for  $j = 3/2$  compared to the value without fine structure of  $\Delta E_{2,1} = 3306.0$  eV. We see a splitting of 4.7 eV and a maximum shift of 17.8 eV. For the conditions we are considering these are easily observable. We will therefore want to examine the influence of the fine structure effect in our calculation of the  $L_\alpha$  line. For the  $L_\beta$  line the splitting will be reduced due to the  $1/n^4$  dependence of the fine structure term. Comparing splitting of the extreme components of the  $L_\beta$  transition; for  $j = 1/2$  we have  $\Delta E_{3,1}^{1/2} = 3935.1$  eV and for  $j = 5/2$  we have  $\Delta E_{3,1}^{5/2} = 3937.0$  eV. This gives a total splitting of 1.9 eV and a maximum shift of 18.5 eV. Given the relatively broad  $L_\beta$  line at these densities, it is safe to ignore its fine structure splitting. We also neglect the overall shift of the  $L_\beta$  line since we are primarily concerned only with the line shape.

In order to calculate the field dependent fine structure term for the  $L_\alpha$  case, we will transform the matrix elements of  $H_{f.s.}$  from the field free basis  $|n, l, j, j_z\rangle$ , in which it is diagonal, to the field dependent parabolic coordinate basis that we are using to calculate the other matrix elements in the line shape problem. To transform an element of one basis to that of another representation, we introduce a unitary transformation operator  $T$  such that

$$T|\psi\rangle = |\psi'\rangle, \quad (E.6)$$

where  $|\psi\rangle$  is in one representation and  $|\psi'\rangle$  is in the other. The corresponding transformation of an operator  $A$  from one representation to another is given by

$$A = T^T A' T, \quad (E.7)$$

where the matrix elements of  $T$  are given by

$$T_{i,j} = \langle \psi_i | \psi'_j \rangle, \quad (E.8)$$

and  $T^T$  is the transpose of  $T$ . In our case, we will transform  $H_{f.s.}$  from the total angular momentum basis,  $|nljz\rangle$ , to the  $|nlm_l m_s\rangle$  basis. Next, we transform to the parabolic basis  $|nqm_l m_s\rangle$ . Finally, we transform to the field dependent parabolic basis  $|nqm_l m_s(\lambda)\rangle$ . We follow this somewhat complicated route because we can compute analytic expressions for each step if we use perturbation theory for the field dependent basis.

The components of the transformation matrix for the first two transformations can be combined to give

$$\begin{aligned} \langle nljz | nqm_l m_s \rangle &= \sum_{l', m'_l, m'_s} \langle nljz | nl'm'_l m'_s \rangle \langle nl'm'_l m'_s | nqm_l m_s \rangle \\ &= (-1)^{-l+1/2-j_z+(1+m_l-q-n)/2} \sqrt{(2j+1)(2l+1)} \\ &\quad \times \begin{pmatrix} l & \frac{1}{2} & j_z \\ m_l & m_s & -j_z \end{pmatrix} \begin{pmatrix} \frac{n-1}{2} & \frac{n-1}{2} & l \\ \frac{m_l-q}{2} & \frac{m_l+q}{2} & -m_l \end{pmatrix}, \end{aligned} \quad (E.9)$$

where the notation  $(\dots)$  denotes a Wigner 3-j symbol.<sup>44,73,89</sup> The final transformation to the field dependent basis must be worked out using the perturbation theory we have explained in Chapter III. Because the method used for the calculation of these transformation matrix elements is the same as the perturbation calculation we have presented in detail in Chapter III, we will present only the final results here.

The remaining transformation matrix elements, as a function of the scaled electric field  $\lambda$ , are given by

$$\langle n, q', m'_l, m'_s(\lambda) | n, q, m_l, m_s \rangle = \sum_{p \geq 0} C_p \lambda^p, \quad (\text{E.10})$$

with

$$C_p = \frac{t_p - \sum_{i=0}^{p-1} C_i \varphi_{p-i}}{\varphi_0}, \quad (\text{E.11})$$

and

$$t_p = \frac{\sqrt{2}}{4n^2} \delta_{m,m'} \sum_{i=0}^p \left\{ f_i^{(1)} g_{p-i}^{(0)} + f_i^{(0)} g_{p-i}^{(1)} \right\}. \quad (\text{E.12})$$

Here

$$f_p^{(\alpha)} \equiv \sum_{h=\max(-n'_1, -2p)}^{2p} a_p^h I_{h,0}^{(\alpha)}, \quad (\text{E.13})$$

and

$$g_p^{(\alpha)} \equiv \sum_{h=\max(-n'_2, -2p)}^{2p} b_p^h J_{h,0}^{(\alpha)}. \quad (\text{E.14})$$

Additionally, we have

$$C_0 = \delta_{m,m'} \delta_{n_1,n'_1} \delta_{n_2,n'_2}, \quad (\text{E.15})$$

and

$$\varphi_0 = \frac{n'^2}{\sqrt{2}}. \quad (\text{E.16})$$

The remaining factors are

$$\varphi_p = \frac{N'_p - \sum_{i=0}^{p-1} \varphi_i \varphi_{p-i}}{\varphi_0}, \quad (\text{E.17})$$

with

$$N'_p = \frac{n'^3}{4} \sum_{i=0}^p \sum_{h,k} \left[ a_i^h a_{p-i}^k (x)_{h,k} + b_i^h b_{p-i}^k (y)_{h,k} \right]. \quad (\text{E.18})$$

The transformation matrix elements given by Eqs. (E.9) and (E.10) are what is required to transform the fine structure Hamiltonian from the total angular momentum basis to the field dependent parabolic coordinate basis. This transformation is used to add the fine structure correction to the  $L_\alpha$  line in our calculation. Since the  $n = 2$  levels of the radiator will be only weakly affected by the plasma microfield for the physical conditions we are examining, perturbation theory will be sufficient for treating the field effects. For the  $L_\beta$  line, however, the  $n = 3$  levels are strongly affected by the microfield and direct numerical solution of Schrödinger's equation is necessary but the fine structure is only a very weak effect and can be neglected. Consequently, only a perturbation theory calculation of the fine structure corrections are necessary for our work.

The complete representation transformation can now be carried out using

$$\begin{aligned} & \langle nq' m'_l m'_s(\lambda) | H_{f.s.} | nq''' m'''_l m'''_s(\lambda) \rangle = \\ & \sum_{\substack{q'' m''_l m''_s \\ q m_l m_s}} \sum_{\substack{l' j' j'_z \\ l j j_z}} \langle nq' m'_l m'_s(\lambda) | nq'' m''_l m''_s | n l' j' j'_z \rangle \\ & \times \langle n l' j' j'_z | H_{f.s.} | n l j j_z \rangle \langle n l j j_z | n q m_l m_s | n q''' m'''_l m'''_s(\lambda) \rangle. \end{aligned} \quad (\text{E.19})$$

This expansion gives us the perturbation theory calculation of the fine structure correction to the radiator Hamiltonian  $H_r(\vec{\epsilon})$  in the field dependent parabolic coordinate representation. As discussed in section 4.1, we find that this field dependence has no significant effect on the fine structure splittings of the  $L_\alpha$  line of hydrogenic argon at the conditions studied in this dissertation.

## APPENDIX F COMPUTER CODE DOCUMENTATION

In this appendix, we present information on the use of the computer programs developed to carry out the calculations discussed in this dissertation. We assume the reader to be familiar with the above material concerning the theory of the calculation. The codes themselves are listed in the University of Florida Plasma Physics Group Technical Report. This is available from C. F. Hooper, Jr. or R. Mancini of the Department of Physics, University of Florida, Gainesville, FL, 32611.

### Field Gradient Term Calculation

The program EZZAPEX was used to calculate the field gradient term  $\langle E_{zz} \rangle_\epsilon$  given by Eq. (3.50). This code is written in FORTRAN for the IBM 3090 mainframe computer but can easily be modified for other systems. Currently, the program runs in batch mode with a JCL file called EZZAPEX JOB. When this JCL file is submitted to the batch queue, four FORTRAN files must be included. They are EZZAPEX, XMESH, GOFR and RDF. The code is written in single precision and is run with the double precision option. The input data for a particular case consists of five quantities: the electron number density in  $\text{cm}^{-3}$ , the temperature in eV, the adjustable parameter  $\alpha$  for the radiator-ion interaction from the APEX microfield<sup>54</sup>, the radiator charge, and the perturbing ion charge. This input is read in free format from

one data line. As an example, consider the case of Li-like argon in 100% hydrogen at  $n_e = 1 \times 10^{24} \text{ cm}^{-3}$  and  $kT = 1000 \text{ eV}$  with the APEX parameter  $\alpha = 0.3734$ . This gives the input line:

1.D24 1000. .3734 15. 1. . . . (F.1)

The details of the numerical methods roughly follow the calculation of Joyce<sup>42</sup> with some modification as discussed in section 3.1 of this work and below.

The main subroutine of the code is RDF. It calculates the radial distribution function  $g(r)$  by means of solution of the HNC equation. This subroutine was developed by F. Rogers.<sup>39</sup> The main purpose of subroutine GOFR is to prepare input for and call RDF. The subroutine XMESH sets the mesh for the  $k$  integration in Eq. (3.50). This mesh can be refined if more accuracy is required for larger field values.

The output from EZZAPEX is diverted to two files. The main program output consists of the calculated values of the field gradient as a function of the field  $\tilde{\epsilon}$ . This output has three parts. The first part consists of a listing of  $\langle E_{zz} \rangle_\epsilon / \langle E_{zz} \rangle_{NN,\epsilon}$ . The second part consists of the five Padé coefficients obtained from a fit of the output from the first part to the Padé approximation employed by Joyce.<sup>42</sup> Part three consists of values of  $\langle E_{zz} \rangle_\epsilon$  as a function of  $\tilde{\epsilon}$  as generated from this Padé approximation. The Padé coefficients are used by the field dependent atomic physics line shape code FDQLINE to be discussed below. A second output file is also generated for purposes of plotting. All values of the constrained average of the field gradient are in units of  $e/r_{o,i}^3$ .

### Field Dependent Line Shape Calculation

The program FDQLINE calculates the field dependent atomic physics line shape function  $I(\omega)$  for the  $L_\beta$  line with the higher order field effects discussed in this dissertation. The different effects are turned on and off by means of numerical switches in which 0 means off and 1 or 2 means on. This code is also written in FORTRAN for the IBM 3090 but additionally uses the vector processors. The JCL file for this job is called FDQLINE JOB. It must include four FORTRAN files, five data files and a line of numerical input data. The basic input data for this code consists of two data bases of field dependent atomic physics. This consists of the file STARK-X2 DATA which contains the field dependent energies, level widths and dipole matrix elements. The data file STARQ-X2 contains the field dependent quadrupole matrix elements. Additional data files contain the field gradient Padé coefficients, the APEX microfield function and the roots of the Laguerre polynomials for Gauss-Laguerre quadrature. The main program is FDQLINEX which calls all other subroutines. The subroutines in file FIDATX2 FORTRAN reads STARK-X2 DATA, and FIDATQX FORTRAN reads STARQ-X2 DATA. When this data is read, these subroutines process it for use in the line shape calculation. All atomic physics data in files STARK-X2 and STARQ-X2 are in atomic units with  $Z = 1$ . The subroutine in POP4 FORTRAN generates the level populations from either a Boltzmann factor or the kinetics model discussed in section 3.4. The input parameter line consists of the physical conditions, the desired line shape characteristics and the numerical switches discussed above. The first three numbers are the electron number density in  $\text{cm}^{-3}$ , the temperature in eV and the nuclear charge  $Z$ . Next, comes an unused parameter set equal to zero. The next four numbers give the lower and higher end of the spectral range in

eV, the number of Doppler integration points and the number of data points in the final line shape. The next two numbers give the number of points and the step size for the microfield integration. The remaining seven numbers are the numerical switches discussed above. We will refer to them in order and by their variable names as used in the code. Switch NLTE is set equal to zero for LTE populations and one for NLTE populations calculated from the kinetic model discussed in the text. Switch IFIDAT is set to zero for field free atomic physics and one for field dependent atomic physics. Switch NOR is set to zero for an unnormalized line shape and one for a line shape area normalized to one. Switch IQD is set to zero for no quadratic Stark effect approximation and one for inclusion of the approximate quadratic Stark effect energy corrections. Switch IIQP is set to zero for no ion-quadrupole effect, one for inclusion of the APEX model for the ion-quadrupole effect and two for inclusion of the nearest neighbor model for the ion-quadrupole effect. Switch IGAMA is set to zero for no resonance width and one for inclusion of the resonance width as an imaginary component of the level energy. Switch IDOP is set to zero for no Doppler convolution and one for inclusion of the Doppler convolution of the line shape. The line shape output is in terms of intensity as a function of spectrum energy in eV. Additional input data include files with the Padé coefficients for the field gradient term and the plasma microfield function. All of these files must be included even if the data is not needed for a particular calculation. The resulting spectrum is listed in the main output file. Data for the atomic physics data base required as input is generated as discussed in sections 3.2 and 3.3.

The program for the calculation of the  $L_\alpha$  line is FDQLPERA and is very similar to the above with some minor modifications. There is only one atomic

physics data file needed. It is called STARPERA DATA and contains the perturbation coefficients for the level energy, dipole matrix elements, quadrupole matrix elements and the fine structure matrix elements discussed in appendix E. Since the electric field perturbation is relatively small for the  $L_\alpha$  cases studied in this dissertation, the entire range of field values used can be treated by perturbation theory. The level width is not included so the switch IGAMA is absent. Since fine structure is included, a new switch is added. Switch IFS is set equal to zero for no fine structure effect and one for inclusion of fine structure shift and splitting. We also specify the order of the perturbation theory to be used. Switch NPMAX gives the order of the perturbation theory. Its maximum value is six for the data used here. The main program is contained in the file FDQLPER FORTRAN. Otherwise the code is almost identical to FDQLINE.

In carrying out the line shape calculation, it is necessary to invert a complex matrix many times. This is carried out using the subroutine DLINCG from the IMSL vector subroutine library.

## REFERENCES

1. S. Ichimaru, *Basic Principles of Plasma Physics* (Benjamin Cummings Publishing, Reading, Massachusetts, 1973).
2. D. R. Nicholson *Introduction to Plasma Theory* (John Wiley and Sons, New York, 1983).
3. T. A. Heppenheimer, *The Man-made Sun: The Quest for Fusion Power* (Little Brown, Boston, 1984).
4. S. Dattagupta, *Relaxation Phenomena in Condensed Matter Physics* (Academic Press, New York, 1987).
5. H. R. Griem, *Plasma Spectroscopy* (McGraw-Hill, New York, 1964).
6. B. Yaakobi, D. Steel, E. Thorsos, A. Hauer and B. Perry, Phys. Rev. Lett. 39, 1526 (1977).
7. K. B. Mitchell, D. B. van Husteyn, G. H. McCall, P. Lee and H. R. Griem, Phys. Rev. Lett. 42, 232 (1979).
8. A. Hauer, K. G. Whitney, P. C. Kepple and J. Davis, Phys. Rev. A 28, 963 (1983).
9. C. F. Hooper, Jr., D. P. Kilcrease, R. C. Mancini, L. A. Woltz, D. K. Bradley, P. A. Jaanimagi and M. C. Richardson, Phys. Rev. Lett. 63, 267 (1989).
10. N. D. Delamater, C. F. Hooper, Jr., R. F. Joyce, L. A. Woltz, N. M. Ceglio, R. L. Kauffman, R. W. Lee and M. C. Richardson, Phys. Rev. A 31, 2460 (1985).
11. J. Nuckolls, L. Wood, A. Thiessen and G. Zimmerman, Nature 239, 139 (1972).
12. R. L. Joyce, L. A. Woltz and C. F. Hooper, Jr., Phys. Rev. A 35, 2228 (1987).
13. A. V. Demura and G. V. Sholin, J. Quant. Spectrosc. Radiat. Transfer 15, 881 (1975).
14. B. d'Etat and H. Nguyen, in: *Spectral Line Shapes*, Vol. 3 ed. F. Rostas (Walter de Gruyter and Co., Berlin, 1985)

15. I. M. Gaisinsky and E. A. Oks, *J. Quant. Spectrosc. Radiat. Transfer* 41, 235 (1989).
16. H. Griem, *Z. Physik* 137, 280 (1954).
17. H. R. Griem, *Spectral Line Broadening by Plasmas* (Academic Press, New York, 1974).
18. R. G. Breene, Jr., *Theories of Spectral Line Shape* (John Wiley and Sons, New York, 1981).
19. S. Ichimaru, *Plasma Physics* (Benjamin Cummings Publishing, Menlo Park, California, 1986).
20. L. D. Landau and E. M. Lifshitz, *Statistical Physics, Part 1*, 3rd Ed. (Pergamon Press, Oxford, 1986).
21. T. W. Hussey, J. W. Dufty and C. F. Hooper, Jr., *Phys. Rev. A* 16, 1248 (1977).
22. R. G. Breene, Jr., *The Shift and Shapes of Spectral Lines* (Pergamon Press, New York, 1961).
23. Lord Rayleigh, *Phil. Mag.* 27, 298 (1889).
24. A. A. Michelson, *Astrophys. Jour.* 2, 251 (1895).
25. C. Godfrey, *Roy. Soc. Phil. Trans.* A195, 329 (1901).
26. W. Lenz, *Z. Physik* 25, 299 (1924).
27. W. Lenz, *Z. Physik* 80, 423 (1933).
28. J. Holtsmark, *Ann. Physik* 58, 577 (1919).
29. J. Holtsmark, *Z. Physik* 20, 162 (1919).
30. J. Stark, *Spektralanalyse Chemische Atome* (S. Hirzel, Leipzig, 1914).
31. D. M. Heffernan and R. L. Liboff, *J. Quant. Spectrosc. Radiat. Transfer* 27, 55 (1982).
32. E. W. Smith, J. Cooper, W. R. Chappell and T. Dillon, *J. Quant. Spectrosc. Radiat. Transfer* 11, 1547 (1971).
33. G. Arfken, *Mathematical Methods for Physicists*, 2nd ed. (Academic Press, New York, 1970).
34. K. R. Lang, *Astrophysical Formulae* (Springer-Verlag, Berlin, 1980).

35. J. Ward, J. Cooper and E. W. Smith, *J. Quant. Spectrosc. Radiat. Transfer* 14, 555 (1974).
36. R. Stamm, B. Talin, E. L. Pollock and C. A. Iglesias, *Phys. Rev. A* 34, 4144 (1986).
37. E. W. Smith and C. F. Hooper, Jr., *Phys. Rev.* 157, 126 (1967).
38. R. Mazighi, J. P. Hansen and B. Bernu, in: *Strongly Coupled Plasma Physics* ed. F. Rogers and H. Dewitt (Plenum Publishing, New York, 1987).
39. F. J. Rogers, *Phys. Rev. A* 29, 868 (1984).
40. M. W. C. Darma-Wardana, F. Perrot and G. C. Aers, *Phys. Rev. A* 28, 344 (1983).
41. J. D. Jackson, *Classical Electrodynamics* (John Wiley and Sons, New York, 1975).
42. R. L. Joyce, Ph.D. dissertation (University of Florida, 1986).
43. E. W. Smith, Ph.D. dissertation (University of Florida, 1967).
44. R. J. Tighe, Ph.D. dissertation (University of Florida, 1977).
45. L. A. Woltz and C. F. Hooper, Jr., *Phys. Rev. A* 38, 4766 (1988).
46. R. J. Tighe and C. F. Hooper, Jr., *Phys. Rev. A* 17, 410 (1978).
47. H. R. Griem, M. Blaha and P. C. Kepple, *Phys. Rev. A* 19, 2421 (1979).
48. J. W. Dufty, *Phys. Rev.* 187, 305 (1969).
49. R. W. Lee, *J. Quant. Spectrosc. Radiat. Transfer* 40, 561 (1988).
50. R. M. More, *Phys. Rev. A* 4, 1782 (1971).
51. C. F. Hooper, Jr., R. C. Mancini, D. P. Kilcrease and L. A. Woltz, in: *Atomic Processes in Plasmas* ed. Y. K. Kim and R. C. Elton (American Physical Society, New York, 1990).
52. L. E. Reichl, *A Modern Course in Statistical Physics* (University of Texas Press, Austin, 1980).
53. C. A. Iglesias, J. L. Lebowitz and D. MacGowan, *Phys. Rev. A* 28, 1667 (1983).
54. C. A. Iglesias, H. E. DeWitt, J. L. Lebowitz, D. MacGowan and W. B. Hubbard, *Phys. Rev. A* 31, 1698 (1985).
55. J. W. Dufty, D. B. Boercker and C. A. Iglesias, *Phys. Rev. A* 31, 1681 (1985).

56. J. W. Dufty, in: *Strongly Coupled Plasma Physics* ed. F. Rogers and H. Dewitt (Plenum Publishing, New York, 1987).
57. F. Lado and J. W. Dufty, Phys. Rev. A 36, 2333 (1987).
58. H. Margenau and M. Lewis, Rev. Mod. Phys. 31, 579 (1959).
59. J. W. Dufty and L. Zogaib, in: *Strongly Coupled Plasma Physics* ed. S. Ichimaru (Elsevier Science Publishers, Amsterdam, 1990).
60. L. A. Woltz, Ph.D. dissertation (University of Florida, 1982).
61. H. A. Bethe and E. E. Salpeter, *Quantum Mechanics of One- and Two-Electron Atoms* (Plenum Publishing, New York, 1977).
62. L. D. Landau and E. M. Lifshitz, *Quantum Mechanics: Non-relativistic Theory*, 2nd Ed. (Pergamon Press, Oxford, 1965).
63. A. Messiah *Quantum Mechanics, Vols. I & II* (John Wiley and Sons, New York, 1961).
64. N. Hoe, E. Banerjea, H. W. Drawin and L. Herman, J. Quant. Spectrosc. Radiat. Transfer 5, 835 (1965).
65. N. Hoe, B. D'Etat, J. Grumberg, M. Caby, E. Leboucher and G. Coulaud, Phys. Rev. A 25, 891 (1982).
66. E. Luc-Koenig and A. Bachelier, J. Phys. B: Atom. Molec. Phys. 13, 1743 (1980).
67. E. Luc-Koenig and A. Bachelier, J. Phys. B: Atom. Molec. Phys. 13, 1769 (1980).
68. M. H. Rice and R. H. Good, J. Opt. Soc. Am. 52, 239 (1962).
69. D. A. Harmin, Phys. Rev. A 24, 2491 (1981).
70. D. A. Harmin, Phys. Rev. A 31, 2985 (1985).
71. R. Mancini and C. F. Hooper, Jr., Rev. Sci. Instrum. 59, 1512 (1988).
72. F. Herman and S. Skillman, *Atomic Structure Calculations* (Prentice-Hall, Englewood Cliffs, New Jersey, 1963).
73. R. D. Cowan, *The Theory of Atomic Structure and Spectra* (University of California Press, Berkeley, 1981).
74. S. J. Rose, Journal de Physique, suppl. au n 11, C8-159 (1983).

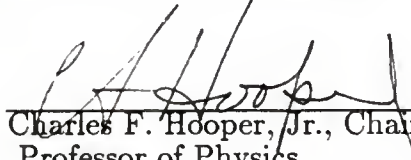
75. F. J. Rogers, in: *Spectral Line Shapes*, Vol. 3 ed. F. Rostas (Walter de Gruyter and Co., Berlin, 1985).
76. S. M. Younger, A. K. Harrison, K. Fujima and D. Griswold, *Phys. Rev. Lett.* 61, 962 (1988).
77. L. A. Collins and A. L. Merts, in: *Radiative Properties of Hot Dense Matter* ed. J. Davis, C. Hooper, R. Lee, A. Merts and B. Rozsnyai (World Scientific, Singapore, 1985).
78. J. Davis, *J. Quant. Spectrosc. Radiat. Transfer* 14, 549 (1974).
79. G. B. Rybicki and A. P. Lightman, *Radiative Processes in Astrophysics* (John Wiley and Sons, New York, 1979).
80. J. C. Weisheit, *J. Phys. B: Atom. Molec. Phys.* 8, 2556 (1975).
81. M. J. Seaton, *M. N. R. A. S.* 119, 81 (1959).
82. R. Mancini and C. F. Hooper, Jr., *J. Phys. D: Appl. Phys.* 21, 1099 (1988).
83. L. A. Woltz and C. F. Hooper, Jr., in: *Radiative Properties of Hot Dense Matter* ed. J. Davis, C. Hooper, R. Lee, A. Merts and B. Rozsnyai (World Scientific, Singapore, 1985).
84. D. R. Inglis and E. Teller *Astrophys. Jour.* 90, 439 (1939).
85. D. Boerker, Ph.D. dissertation (University of Florida, 1978).
86. D. L. Book, *Naval Research Laboratory Plasma Formulary* (Naval Research Laboratory, Washington, D.C., 1990).
87. C. Itzykson and J. Zuber, *Quantum Field Theory* (McGraw-Hill, New York, 1980).
88. R. W. Lee, *Phys. Lett.* 71A, 224 (1979).
89. A. R. Edmonds, *Angular Momentum in Quantum Mechanics* (Princeton University Press, Princeton, 1957).

## BIOGRAPHICAL SKETCH

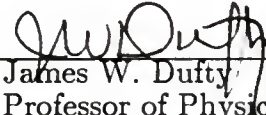
David Parker Kilcrease was born in Jacksonville, Florida, on August 7, 1952, the only child of Mary Lou and Cecil Calvert Kilcrease. He grew up and received his early education in Jacksonville, graduating from Robert E. Lee High School in 1970. After attending Florida Junior College for two years, he enrolled at the University of Florida in Gainesville to study chemistry. In 1975 he left school for financial reasons and returned to Jacksonville where he looked for work for some months during a time of national financial recession. In the afternoons and evenings he spent a great deal of time at the Jacksonville Public Library where he gave himself a liberal arts education, studying philosophy, art and literature. After a time he found employment at a factory where he worked as a machine operator for a little less than a year. He found this all to be a very educational experience about life in general. He returned to Gainesville in late 1976 to work for the university's Institute of Food and Agricultural Sciences (IFAS) and attended school part-time completing a B.S. degree in chemistry in 1978. At that time he was promoted to Chemist at IFAS and worked in that capacity until 1982 when he resigned and enrolled in graduate school at U. of F. to study physics, graduating with the degree of Ph.D. in 1991. He married Patricia Ann Flaherty in 1980.

In life he has experienced many interesting things, both ordinary and unusual and regrets very few of them. He looks forward to more of the same.

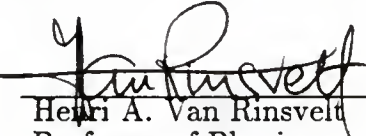
I certify that I have read this study and that in my opinion it conforms to acceptable standards of scholarly presentation and is fully adequate, in scope and quality, as a dissertation for the degree of Doctor of Philosophy.

  
Charles F. Hooper, Jr., Chairman  
Professor of Physics

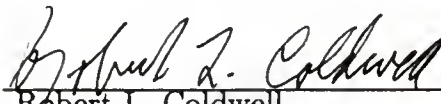
I certify that I have read this study and that in my opinion it conforms to acceptable standards of scholarly presentation and is fully adequate, in scope and quality, as a dissertation for the degree of Doctor of Philosophy.

  
James W. Duffy  
Professor of Physics

I certify that I have read this study and that in my opinion it conforms to acceptable standards of scholarly presentation and is fully adequate, in scope and quality, as a dissertation for the degree of Doctor of Philosophy.

  
Henri A. Van Rinsveld  
Professor of Physics

I certify that I have read this study and that in my opinion it conforms to acceptable standards of scholarly presentation and is fully adequate, in scope and quality, as a dissertation for the degree of Doctor of Philosophy.

  
Robert L. Coldwell  
Associate Professor of Physics

I certify that I have read this study and that in my opinion it conforms to acceptable standards of scholarly presentation and is fully adequate, in scope and quality, as a dissertation for the degree of Doctor of Philosophy.

*Kwan Chen*

Kwan Chen  
Professor of Astronomy

This dissertation was submitted to the Graduate Faculty of the Department of Physics in the College of Liberal Arts and Sciences and to the Graduate School and was accepted as partial fulfillment of the requirements for the degree of Doctor of Philosophy.

May 1991

\_\_\_\_\_  
Dean, Graduate School

UNIVERSITY OF FLORIDA



3 1262 08285 428 1